Development and Validation of an Analogue Lumbar Spine Model and its Integral Components

By

John P. Domann

Submitted to the graduate degree program in Bioengineering and the Graduate Faculty of the University of Kansas in partial fulfillment of the requirements for the degree of Master of Science.

_____

Dr. Elizabeth Friis , Chairperson

_____

Dr. Ronald Barrett, Committee Member

_____

Dr. Sara Wilson, Committee Member

Date Defended: 4/22/2011

The Thesis Committee for John P. Domann

certifies that this is the approved version of the following thesis:

Development and Validation of an Analogue Lumbar Spine Model and its Integral Components

_____

Dr. Elizabeth Friis , Chairperson

_____

Dr. Ronald Barrett, Committee Member

_____

Dr. Sara Wilson, Committee Member

Date approved: 4/22/2011

Abstract

There is a large need for an anatomically and mechanically correct model of the human lumbar spine. Such a model could have widespread use in the development of new implants and surgical procedures designed to remediate low back pain. Previous work has already been completed on such a model, and the purpose of this study is to approach release of the first generation model to the public. In order to reach this milestone significant work went into the development of a synthetic vertebral cancellous bone model, as well as analysis and development of the overall spine model itself. This work is being completed with Pacific Research Laboratories (Sawbones) who will ultimately manufacture and sell the product.

Foam theory was utilized to analyze solid materials that could serve as effective cancellous bone models. These materials were readily available to PRL, and their supply secured for the indefinite future. Following four point bend tests, one material was deemed acceptable for use in a cancellous bone model. Analysis showed that a synthetic model manufactured from this material would require 85% of human bone's relative density to obtain similar stiffness, and 111% of human bone's relative density to obtain adequate strength. Synthetic foams were prepared, mechanically characterized, and compared to the literature. Overall, the model behaved quite similarly to human bone, with mechanical properties slightly higher than the reported literature. The model had stiffness of 375 MPa, strength of 4.33 MPa, and post yield ductility of .51%.Future work will serve to further refine this model, and incorporate it into the vertebral body of the Analogue Spine Model.

At the beginning of this study, the Analogue Spine Model was behaving too stiffly, and aberrant behaviors were noticeable in axial rotation. Stiffness was approximately 1 Nm/° higher than the literature in all modes of bending. Aberrant behavior was most notable in axial

rotation. In this mode of bending, a “stair step” behavior was observed in what should have been a smooth sigmoid curve. Work was conducted on locating the source of these limitations, and altering them to improve model performance. This was conducted with the use of a systematic dissection, allowing identification of the interactions and elements responsible for the model’s behavior and stiffness. After identifications, alterations were made to the manufacturing process, and to specific soft tissues. Once completed, the model now has appropriate neutral zone stiffness in all modes of bending (flexion – 1.82 Nm/°, extension – 2.01 Nm/°, lateral bending - .85 Nm/°, axial rotation – 2.47 Nm/°), extension zone stiffness in three of four modes of bending (flexion – 3.09 Nm/°, lateral bending – 5.30 Nm/°, axial rotation – 11.25 Nm/°), but high neutral zone range of motion in all modes of bending and high extension zone stiffness in extension (9.15 Nm/°).

Future work is centered on reduction of neutral zone range of motion, and extension zone stiffness in extension. This model’s performance will be compared to cadaveric specimens tested using the experimental setup utilized in this study. Following validation, the model will be released into the market, and become accessible to researchers and companies alike.

Acknowledgements

The road to becoming a graduate student was not always an easy one, and there are several people I would like to thank for their contributions, time, patience and support.

- Dr. Elizabeth Friis for her constant guidance and support. She constantly pushed me to achieve, and opened my eyes to the opportunities surrounding me. Thanks to Professor Friis, I have no doubt I am prepared to develop and translate new technologies capable of helping those in need.
- Dr. Ronald Barrett and Dr. Sara Wilson for being members of my thesis committee, along with the time and assistance they provided on my thesis and other non-related projects.
- Departments of Bioengineering and Mechanical Engineering have been a large part of my development, education, intellect and ability to successfully analyze and solve complex problems. Furthermore, to the staff from each department for their constant help with all the problems and paperwork I encountered during my stay at KU.
- The Institute for Advancing Medical Innovation for the support and invaluable education and opportunities I was provided with while working towards my Masters.
- Rodrigo Perea, Erin Lewis, Damon Mar, Brian Good, Carlos Villanueava, Brian Blackwell, and Armand Heynes along with all my fellow lab-mates and friends. They constantly provided support, their own perspectives and much needed distractions from my work. My graduate experience would not have been the same without all of you.
- John James and Amy Johnson from Pacific Research Laboratories for their hard work and ability to implement innovative solutions to our difficult manufacturing related challenges.
- The men of The Iron Class for their constant friendship and support. Each day you provide me with motivation, remind me what we're capable of, and push me to succeed.
- My parents David and Elizabeth Domann and my sisters Katie and Annie for their love, support and guidance. I couldn't have asked for a better family.

This work was supported in part by NIH SBIR Grant 5R44 AR054289-02 and Pacific Research Laboratories, Inc.

Contents

List of Figures:

List of Tables:

List of Symbols:

P_{app} – Apparent density (g/cm^3)
Ps – Solid material density (g/cm^3)
P_{app}/ P_s – relative density (-)
ρ_{rel} – relative density (-)
σ – stress (MPa)
ε – strain (-)
E – modulus of elasticity (MPa)
σ_{yld} – Yield Stress (MPa)
ε_{yld} – Yield Strain (-)
σ_{ult} – Ultimate Stress (MPa)
ε_{ult} – Ultimate Strain (-)
ε_{ult} - ε_{yield} – Post yield ductility (-)
AD – Ash Density (g/cm^3)
α – Age (years)

A – Power law leading coefficient
B – Power law power coefficient
m – mass (g)
V_{solid} – Solid volume
V_{voids} – Void volume
R – Rate of crosshead motion (mm/min)
P – Load (N)
L – Bottom span length (mm)
w – width of specimen (mm)
d – depth of specimen (mm)
D – center of deflection (mm)
m – slope of load – deflection curve (N/mm)
θ – Angle (degrees)
M – Moment (Nm)

List of Abbreviations:

AF – Annulus Fibrosis
ALD – Adjacent Level Degeneration
ALL – Anterior Longitudinal Ligament
ANOVA – Analysis of Variance
ASM – Analogue Spine Model
ASTM – American Society for Testing and Materials
BV/TV – Bone volume divided by Total Volume
CL – Capsular Ligament
COV – Coefficient of Variance
CNC – Computer Numerical Control
CT – Computed Tomography
DD –Disc Degeneration
DDD – Degenerative Disc Disease
EZ – Extension Zone
FDA – Food and Drug Administration
FSU – Functional Spinal Unit
ISL – Interspinous ligament
IVD – Intervertebral Disc
KU – The University of Kansas
LBP – Low Back Pain
LF – Ligamentum Flavum
MTS – Material Test System
NP – Nucleus Pulposis
NZ – Neutral Zone
pQCT - peripheral Quantitative Computed Tomography

PLL – Posterior Longitudinal Ligament
PRL – Pacific Research Laboratories
PU - Polyurethane
ROM – Range of Motion
SBIR – Small Business Innovation Research
SSL – Supraspinous ligament
Std Dev – Standard Deviation
TL – Transverse Ligaments

Chapter 1. – Introduction and Significance

The purpose of the research developed in this study is to finalize the first generation of the Analogue Spine Model (ASM). In order to finalize the model two key tasks need to be completed. First is the development of open celled foam representative of human vertebral cancellous bone. Second is to demonstrate control of the soft and hard tissue properties of the ASM. This work is being conducted in an effort to develop a synthetic model which mimics the human spine's physiological response to applied loads and displacements. The ASM is designed to fulfill several unmet needs in the spine testing community. When selecting models to employ in studies, the main needs of spine researchers and the medical device industry include:

- Anatomical and mechanical accuracy
- Repeatable test platforms
- Low inter-specimen variance
- Control over a specimen's mechanical properties
- Long shelf life
- Long test life
- Readily available

This model is expected to have a large impact on the design and testing of implants and the development of new surgical procedures.

The following chapter discusses the problem of low back pain (LBP), its current treatments and their deficiencies. This includes a discussion of spinal anatomy and models currently used to evaluate new devices and procedures. Finally, it proposes a model that could facilitate design and testing of new technologies for alleviating low back pain.

1.1.Low back pain

1.1.1. A Public Burden

It is estimated that 80% of Americans will suffer from at least one severe episode of low back pain during their lifetimes [1]. This results in the American public spending more than $50 billion per year on potential treatments [1]. It is the most common cause of job related disability for people under the age of 45, and is a leading contributor to missed work [1]. Furthermore, it is the second most common neurological problem with only headaches occurring more frequently [2]. For a subset of afflicted people, surgical intervention is required. There were more than 1 million spine surgeries conducted in 2004 [3], which is more than the total number of hip and knee surgeries combined . In 2008 the "National Bill" for spinal fusion alone tallied over $32 Billion[4]. Estimates predict that by 2012, there will be more than 650,000 spinal fusions being performed each year [5]. Additionally, the number of spine surgeries is continuing to grow. With improvements in the standard of living and advancements in health care, individuals are living longer lives. The aging American population is growing at a rate of 3% every year. The probability of developing degenerative disc disease, spinal stenosis, and spondylolisthesis, all, leading causes of low back pain, have strong correlations with aging. It should come as no surprise that the number of surgeries performed each year is anticipated to grow between 3%-4% a year; an increase of nearly 100,000 surgeries over the next 4 years. [5]

1.1.2. Causes of Low Back Pain

The overall causes of low back pain are not well understood. Pain may arise from hard and soft tissues alike. This includes spinal ligaments, facet joints, vertebral periosteum, paravertebral musculature, fascia, blood vessels, the annulus fibrosis and spinal nerve roots. A discrepancy in causes and lack of proper diagnostics is one reason there is no clear best method

for the treatment of LBP. In fact, it is “possible that 85% of patients with isolated low back pain can’t be given a precise pathoanatomical diagnosis” [1]. There is a clear need for improvements to the diagnostic practices for LBP. These in turn will help guide the future of medical interventions alleviating LBP.

While no clear diagnostic exists, studies have shown where the most common sources of low back pain can be located. Musculo-ligamentous injuries may be the most common source [1]. These include:

- Disc Degeneration(DD), which shows a strong correlation with smoking [6, 7]
- Disc herniation, causing joint instability [6]
- Facet joint instability [8, 9]
- Spinal stenosis [1, 6]
- Cardiovascular illness, such as atherosclerosis [10]
- Additionally, smoking and high cholesterol have been shown to increase risk for Atherosclerosis [10], disc herniation [11]

1.2.Spinal Anatomy

Before going much further, it is necessary to acquaint oneself with the structure and function of the human spine. This will highlight the areas previously discussed, and those covered in much deeper detail further on.

1.2.1. Overall Structure

The human spine represents the most complicated element of the human musculoskeletal system and has four main functions [12, 13]. These functions are to:

- Protect the spinal cord
- Support the head, neck, and upper extremities
- Transfer loads from the head, neck, and upper extremities to the pelvis
- Permit the motion of the head, neck, and upper extremities

The human spine is segmented into four main regions, cervical, thoracic, lumbar, and sacral / coccygeal. These regions are composed of 24 singular vertebrae, the 5 complex bones that fuse together in the sacrum, and the coccyx (2-4 fused bones). The number of vertebrae present in each level is: cervical – 7, thoracic – 12 and lumbar – 5. In the coronal plane, the spine is a straight structure (abnormal curvature or rotations are referred to as scoliosis). In the sagital plane the spine has 4 main curvatures. The cervical and lumbar regions are lordotic (concave curve), while the thoracic and sacral regions are kyphotic (convex curve).

There are two key joints between adjacent vertebrae. There is an amphiarthrodial articulation formed by the connection of the superior and inferior surfaces of the intervertebral disc to the adjacent vertebrae. The apophyseal joint is formed by the facets, associated synovial capsule and articular cartilage. The primary role of these joints are to:

- Transfer loads between adjacent vertebrae
- Act as shock absorbers to dissipate energy
- Eliminate bone-on-bone contact

These joints allow wide ranges of motion; flexion and extension, lateral bending, and axial rotation, and to a much lesser extent translation (shear) in the remaining directions (Figure 1). While some stability is provided by the intrinsic soft and hard tissues (ligaments, intervertebral disc, facets), a large part of spinal stability is controlled through the extrinsic stabilizers of the neuromuscular system [14]

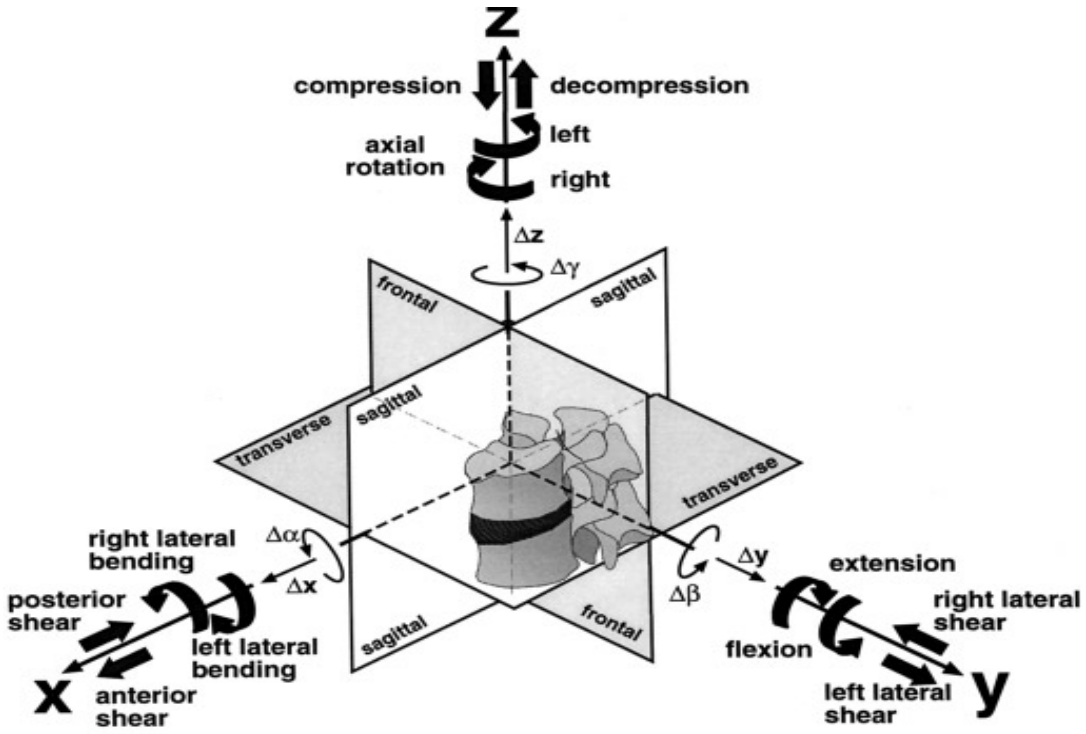

Figure 1: Three dimensional coordinate system of the spine, demonstrating clinically relevant translations and rotations [15]. (Image reprinted with permission of Springer©)

1.2.2. Lumbar Spine

As stated above, the lumbar spine is composed of 5 vertebrae and the associated ligaments, tendons, muscles, and intervertebral discs. It has a lordotic (concave) curvature. Furthermore, the size of each vertebra increases when moving from the first lumbar vertebra (L1) inferiorly to the fifth lumbar vertebra (L5) [16]. This occurs as lumbar vertebrae are designed to carry a large portion of the bodies weight[13], and this load increases when moving caudally through the spinal column. Additional segmental changes include the orientation of the facet joints (Figure 2). Progression from superior to inferior vertebrae leads to increased facet rotation from the midline in the sagital plane. This in turn leads towards greater resistance to axial rotation and less overall resistance to extension and translation.

Overall, the lumbar spine has ranges of motion greater the thoracic region, as it lacks the additional support of the rib cage, yet less motion than the highly mobile cervical region.

Furthermore, the lumbar spine is the most commonly occurring location of back pain. Reasons for this will be discussed in detail in Section 1.2.2 – The Lumbar Spine.

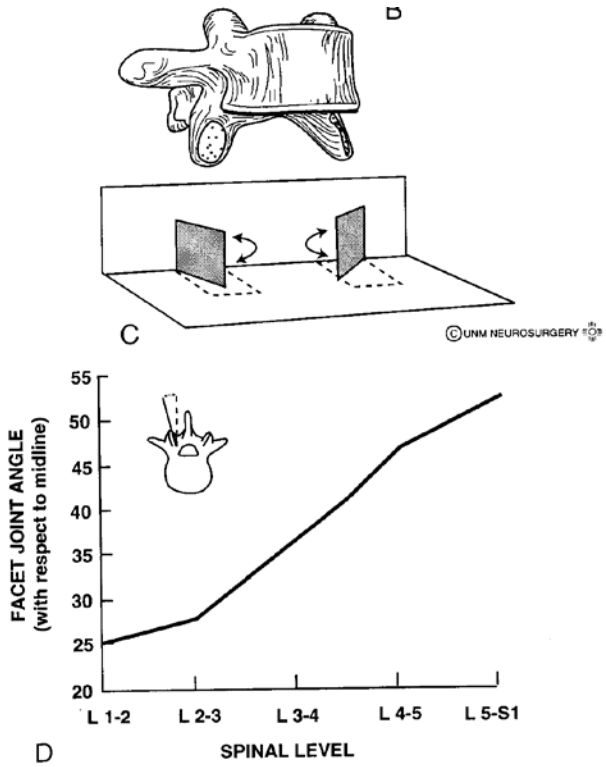

Figure 2: Lumbar facet orientation changes with vertebral level. Caudal vertebrae are more resistant to axial rotation [16]. (Reprinted with permission of The British Library Board©)

1.2.3. Hard Tissue

The primary hard tissue of the human spine is the vertebral body. It forms the main load bearing unit of the spine, and is the location of ligament and muscle attachments [17]. The vertebral body is comprised of two key regions. The centrum is the main body of the vertebra, and therefore responsible for resisting most of the compressive load transmitted through the spine. The vertebral body has a very thin cortical shell (averaging .4 mm [18]) covering an interior of cancellous (spongy) bone. The vertebral body (centrum) is connected to the neural arch (posterior aspects) by the pedicles. The neural arch is a key structure, forming the spinal canal and shielding the spinal cord. The facets (articular processes) branch out from the

pedicles, and form one of the key joints resisting vertebral motion. As mentioned above, they are key in resisting axial rotation and extension in the lumbar spine. Each vertebra has a pair of superior and inferior facets which pair with facets from the adjacent vertebrae in a synovial joint capsule. Furthermore, each vertebra has several spinous processes. The spinous process arises from the posterior portion of the neural arch. It provides attachment sites for the inter-spinous and supra-spinous ligaments, which are crucial to extensor muscle attachment. The transverse processes form from the lateral portions of the neural arch. They are sites of attachment for the transverse ligaments, key sites for lateral bending muscle attachments. Each vertebrae has a superior and inferior endplates [19]. Endplates form the boundary between the intervertebral disc and the cancellous core. Endplates are approximately .5 mm thick, and covered by a layer of cartilage of nearly the same thickness. Finally, the endplates are responsible for resisting disc herniation into the vertebral body [16].

1.2.4. Soft Tissue

Although there is a singular hard tissue in the lumbar spine, there are several different soft tissues. Ligaments are key elements in the passive stability of the lumbar spine. Ligaments exhibit non-linear behavior and primarily act in tension. Initially they have low stiffness that gradually increases as they are strained [20]. The inter-spinous ligament (ISL) is a thin membrane that typically degenerates to a similar degree as the IVD [21]. It attaches to the spinous process and has a relatively large moment arm; yet it is believed to contribute very little to the stability of adult spines. The supra-spinous ligament (SSL) plays a critical role in segmental stability. It is also attached to the spinous process, and forms an integral structure with the ISL. The transverse ligament (TL) connects the transverse processes of adjacent vertebrae. It is a weak structure in all but the lumbar region. The ligamentum flavum (LF) connects the laminae of adjacent vertebrae. It is a thick, wide structure which possesses high elasticity and contracts the

vertebrae, keeping them together and aligned. The LF primarily resists flexion and lateral bending. The facet capsular ligament (CL) connects the inferior and superior facets of adjacent vertebrae. The CL forms a capsule to enclose and protect the synovial joint. This ligament provides significant contributions to stability in flexion and torsion [20]. The Posterior longitudinal ligament (PLL) is meshed into the collagenous fibers of the posterior annulus, yet not attached to the vertebrae. It primarily resists flexion. The anterior longitudinal ligament (ALL) attaches anteriorly to the surface of the vertebrae. Similar to the PLL, it meshes to the intervertebral disc (anteriorly) and the margins of the endplate on the vertebrae. It is not rigidly connected to the surface of the vertebral body. The PLL primarily influences behavior in extension, as well as resisting bulging of the IVD (and therefore stiffening the disc).

The intervertebral disc provides mobility to the spine, absorbs and dissipates shock, and is responsible for restraining excessive motion [16]. Furthermore, the disc evenly distributes load to each vertebrae[19]. This is due to its unique structure (Figure 3). The nucleus pulposis (NP) is a gel like amorphous hydrogel surrounded by the highly structured annulus fibrosis (AF). The AF is a highly anisotropic structure. The AF is composed of concentric layers that alternate fiber orientation at 30° angles with respect to one another. Hydrostatic pressure develops in healthy NPs, and is contained by the generation of hoop stress in the AF. The NP has a high concentration of hydrophilic proteoglycans which enabling it to retain water [17]. This leads to its isotropic nature, allowing it to evenly distribute loads across the vertebral endplate [22].

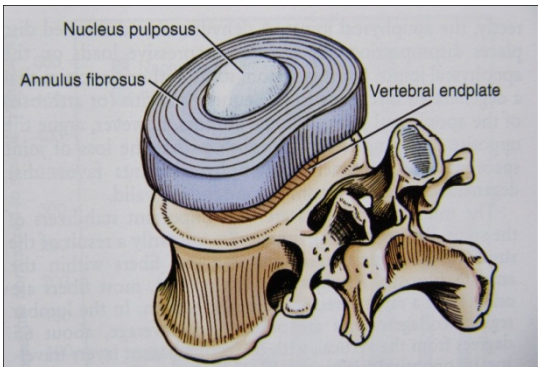

Figure 3: Typical anatomy of the human lumbar intervertebral disc. The annulus fibrosis (AF) is composed of concentric layers similar to a fiber composite, while the nucleus pulposis is an isotropic gel capable of evenly distributing loads to the vertebral endplates and AF [23]. (Image reprinted with permission of Elsevier©)

1.3.Current surgical treatments for LBP

There are several non-surgical treatments to alleviate low back pain. These typically involve some form of core strengthening exercises, stretches, supplements and medication. However, for over 1 million patients each year, these treatments are not sufficient, so they undergo surgical intervention. The following section describes commonly used procedures which this model will be useful in evaluating and improving.

1.3.1. Spinal fusion

Spinal fusion was originally used to treat spinal infections; however it soon expanded to deal with vertebral fractures and tumors. Afterwards surgeons began using it to treat spinal deformities (scoliosis) [24]. More recent uses employ fusion to relieve joint pain caused by degenerative disc disease (DDD). The intent of spinal fusion is to restore disc height, segmental stability and appropriate alignment of the vertebral column. Fusion relies on assumption that pain at the afflicted level is caused by motion, and that halting motion will stop the pain. This is achieved by using instrumentation to rigidly connect adjacent vertebrae, and then stimulating bone growth to fuse the vertebrae together. There are several methods of accomplishing this; one of the most common entails the use of pedicle screws (Figure 4), while others use fusion

cages and spacers. Patients can expect an expensive procedure requiring a lengthy hospital stays and follow-up visits [24]. The average cost for fusion was $133,000 in 2008, with mean values ranging from $45,000 to $255,000 depending on the specific operation and incidence of complications [4]. Incidentally, there is a high rate of complications and morbidity. While the average hospital stay ranges from 2-4 days, most patients require long recovery times of 6-12 months before relief of pain, and return to normal behavior [4, 24].

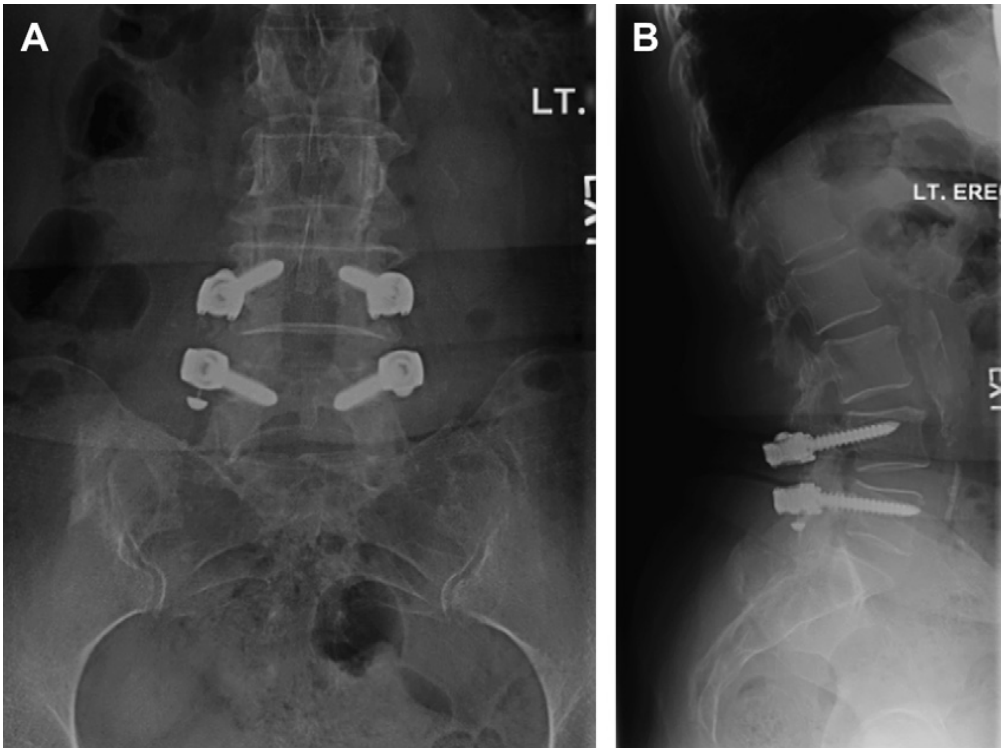

Figure 4: Anterior-posterior and lateral radiographs of lumbar spinal fusion (L4-L5) using pedicle screws with PEEK rods. PEEK is a radiolucent material, and as such the majority of the rod does not show up on the radiograph [25]. (Image reprinted with permission of Elsevier©)

Even though fusion has been widely used for years, it still has a high risk of failure, resulting in a nonunion (pseudoarthrosis). Reported failure rates are widely varied, and depend on patient criteria, device, approach and several other factors. One study by Turner et al. is consistent with other reports, and presents a 14% failure rate [26]. High failure rates are due to several shortcomings with the procedure. One widely reported shortcoming is adjacent level

degeneration (ALD). This effect is found in 92% of patients, at long term follow-up (>5yr), in cervical fusion patients [27], and 34% of lumbar fusion patients [28]. ALD is the deterioration of segments above and below the fused level. Degeneration occurs as a result of the higher stress and strain imposed on these segments due to the restricted mobility of the fused level. However, researchers are currently divided on whether ALD actually affects clinical outcomes (whether or not the fusion was successful, and alleviates pain).

1.3.2. Intervertebral Disc Replacement (Non-fusion)

Intervertebral disc replacement is one alternative to spinal fusion. During this procedure the IVD is excised from the patient and replaced with an artificial disc. This procedure is intended to restore function to a degenerated IVD, restore disc height, maintain mobility and deter adjacent level degeneration [29]. It is important to realize that this procedure relies on the assumption that pain is generated by the soft tissue of the IVD (and that removing those tissues eliminates pain). Patients undergoing this procedure can expect a quick return to mobility [24]; no brace is required, patients can return home after 3-4 days and then return to work after 3-4 weeks. This is much shorter than the down time expected for spinal fusion patients.

In theory at least, disc replacement should be a superior alternative to spinal fusion. However, as it is very difficult to diagnose the IVD as the sole pain generator. Due to this fact, pain relief may not occur, even after a successful surgery is performed [29]. If the source of pain is not the IVD, it is unlikely that this treatment will alleviate the pain. Instead it is likely the treatment will destabilize the spine, and place added stresses on it. IVD replacement has yet to demonstrate improved outcomes over fusion, yet is currently more costly and dangerous [30, 31]. As such, this procedure is not eligible for reimbursement through insurance agencies.

1.3.3. Laminotomy / Laminectomy

Laminotomies and laminectomies are similar techniques used to alleviate LBP. They are conducted by either partial or total removal of the lamina as a form of spinal decompression surgery [32]. These surgical treatments are primarily used to correct ankylosing spondylitis, degenerative disc disease, herniated discs, sciatica, spinal stenosis and spondylosis (osteoarthritis). Furthermore, they can be coupled with partial discectomy if need be.

The Intent of these procedures is to reduce pressure on spinal nerves and the spinal cord. It is feasible to have this performed at several levels and for the spine to still be structurally stable. Patients can expect an average 3.5 days in the hospital [4]. Roughly 100,000 people received this treatment in 2008, at an average cost $35,000. This procedure is used most often for older patients in the 65-84 year old age bracket (47.59% of procedures).

This can be a very successful procedure that has minimal effect on spinal biomechanics while still relieving pain. However, while the facet joints and musculature remain, it does leave the spinal cord slightly more prone to injury. Furthermore, it mainly relieves pain caused by nerve or spinal cord compression, not inflamed tissue. Finally, it has excellent short term results, but long term follow up (5.5 years) demonstrates failure rates near 25% [33].

1.3.4. Kyphoplasty/ Vertebroplasty

Kyphoplasty and vertebroplasy are used to correct spinal compression fractures [34]. These fractures occur mainly as a result of osteoporosis which degrades bone strength over time. Oftentimes the first symptom of osteoporosis is a broken bone, making it difficult to prevent. Fractures results in severe pain, deformity, loss of disc height and possibly even nerve compression. Until recently, these fractures had no suitable treatment, patients mainly used medication, bed rest, bracing, or invasive surgeries such as spinal fusion. Vertebroplasty is a

minimally invasive method intended to repair the fractured vertebral body. Bone cement is injected into the vertebral body to prevent further degradation. In kyphoplasty, doctors can relieve pain, restore height, stabilize the fracture, and reduce deformity. This is done by inflating a balloon inside the vertebrae until proper height has been restored. The cavity left by the balloon is then filled with bone cement.

Both of these procedures can even be used to halt possible injuries resulting from osteoporosis, if successfully detected in time. Vertebral fractures occur in more than 700,000 patients per year. The patients that undergo these procedures can expect short surgical times, requiring only general or local anesthesia. Most patients leave the same day and return to normal activities shortly, no bracing is required, and pain relief can occur almost immediately. This treats the symptoms of osteoporosis, but not the cause. While it can be used preemptively, most people typically don't have a reason check for osteoporosis, let alone have either of these surgeries until the first fracture. Furthermore, cement can leak from the vertebrae into the surrounding tissue and circulatory system, causing nerve root compression or the creation of emboli. In fact, estimates predict this can occur in up to 65% of vertebroplasties [35].

1.4.Analysis of current test models for LBP treatments

As previously stated, non-surgical solutions exist. However for surgical intervention, doctors and engineers need models on which to test new techniques and implants, and aide in their design. There are several different types of models currently in use. The most popular of these models can be broken down into four main categories: biologic, computer models, anatomically correct physical models, and mechanically correct physical models. As previously mentioned, the ideal model possesses the following qualities:

- Anatomical and mechanical accuracy
- Repeatable test platforms
- Low inter-specimen variance
- Control over a specimen's mechanical properties
- Long shelf life
- Long test life
- Needs to be readily available

1.4.1. Biologic - Human Cadaveric Spines

Human cadavers currently represent the gold standard for models. They are anatomically and mechanically correct, and can be used to perform basic tests analyzing stiffness, range of motion, non-linear behavior, and the effect of implants or surgical operations on these values. Furthermore, they can provide medical students and surgeons with a hands-on method of becoming familiar with spinal anatomy, and learning new techniques.

However, even though human cadavers represent the current gold standard, their use is accompanied by a host of drawbacks and complications. Cadavers can be difficult to obtain, with problems facing overall supply, and long lead times to actually obtain specimens [36]. Researchers must go through agencies that collect the specimens post mortem. Depending on what the allowable criteria are (intact bones, no history of drug use, no bone spurs or osteoporosis, etc.), it can take several months to a year to obtain viable specimens. Furthermore, if accurate soft tissue properties are a necessity, researchers only have a 20 hour window in which to test thawed material. After this window, the soft tissue is substantially degraded, and the results become unreliable [37]. Along with this, cadavers require specialized storage (<-20°C) in order to preserve their properties [38]. Coupled with the required time frame and storage requirements, specimens can't be embalmed to preserve the tissue as it

affects mechanical performance [15]. Tests on multiple freeze-thaw cycles have determined that up to three cycles may be used before degradation of soft tissue mechanical properties occurs [39]. Additionally, since they can only be used for 20 hours, and are viscoelastic, their ability to be used in endurance testing is limited. It is also worth noting that researchers typically wish to employ sensors to measure interesting parameters such as intradiscal pressure, facet load, and facet strain. It can be very difficult to rigidly attach transducers to slick cadaveric tissue, and it is often time consuming, taking up large portions of the 20 hour testing window. Finally, there is no guarantee you will obtain an 'average' spine. There is a large inter-specimen variability among spines, with the standard errors of mechanical stiffness of 100% or more between specimens [40, 41]. Intradiscal pressure has been shown to vary as much as five-fold from specimen to specimen[42]. These variances can make it difficult to understand what effects are derived from the specimen and what effects are due to the test setup and designed surgical interventions. This is especially true when using small samples sizes, which tend to be quite common as a result of prohibitive costs and availabilities.

1.4.2. Biologic - Animal Cadaveric Spines

Since the availability of human cadavers is limited, researchers have often utilized animal cadavers as more cost effective solution. A benefit of using animal cadavers is that they have been shown to have more uniform geometry and properties, reducing the effects of inter-specimen variability. While it's true that properties do not exactly match human spines, they do exhibit the same trends. If carefully selected, animal spines can be used for specific applications with high levels of accuracy. Sheep can be used for studying disc surgery or bone healing processes [43]. Canine spines have been used in-vivo and in-vitro in studies examining stabilization and fusion techniques [44-46]. Bovine spines are biomechanically similar to humans, but above T6 they begin to differ widely from human anatomy [47]. Porcine spines are

the best models of human anatomy, especially once consideration of facet orientation is taken into account [41, 48].

Even with all these advantages, large variation still exist between geometries of human and animal spines [41]. These models can provide useful early stage results, however testing on a model that represents human anatomy and mechanical behavior is critical for devices that will eventually go to use inside the human body, as required by the Food and Drug Administration (FDA). Finally, all of the testing issues inherent to human cadaveric specimens are also present in their animal counterparts.

1.4.3. Computer Models

Similar to animal cadavers, computer models can be very useful in early stage testing and the design of implants. With computer models, researchers can control the anatomy, tissue properties and interactions between elements, enabling customization, and the ability to test on 'average' specimens, as well as potential outliers and pathologies at will. Additionally, computer models can be used to analyze much more than just mechanical properties. They can simulate living systems, providing insight into complex processes like bone remodeling. A large benefit of using computer models is they last as long as the lab ensures their compatibility with the latest software package they are using. This can continue almost indefinitely, and models can be upgraded to new packages. Models can also be created allowing an introduction to surgical techniques, mainly guiding students through the anatomy and potential operations they will encounter.

While computer models are versatile, and capable of studying complex processes, there are some inherent limitations. First off, most models are developed within labs, and aren't commercially available. This leads to a large amount of variation between models, limiting potential multi-lab comparisons. Additionally, as useful as they are for early stage design work,

computer models can't be used to test physical devices. FDA approval requires testing on physical models before devices can be marketed. Likewise, at a certain point, surgical training requires hands on experience, not just a visual guide to the body. Finally, computer models require an expert in order to utilize them. To obtain accurate results, the user must be well versed at the software package they run on, as well as the assumptions built into the model, which can limit the range accuracy.

1.4.4. Physical Models – Anatomically Correct

Anatomically correct models are typically used for show only. They provide varying levels of anatomical accuracy, typically including vertebrae with intervertebral discs. It is also possible to obtain models including various ligaments and possibly the surrounding musculature. These models last indefinitely, and can be utilized where mechanical properties may not be of critical importance. For the most part, these models are strictly for show. No attempt is made to accurately model mechanical properties, let alone non-linear behavior. Initial training can be completed on them, however if a researchers wish to test the effects of surgical intervention, or new devices, they must use a different type of model.

1.4.5. Physical Models – Mechanically Correct

Mechanically correct models are widely used by device manufacturers to test new devices. These models are especially useful to conduct fatigue testing, which are not reasonable on cadavers due to time constraints. Mechanical models have even been standardized by the American Society for Testing and Materials (ASTM). Standard ASTM 2077: Test Methods for Intervertebral Body Fusion Devices lays out the design of a common model (Figure 5) [49].

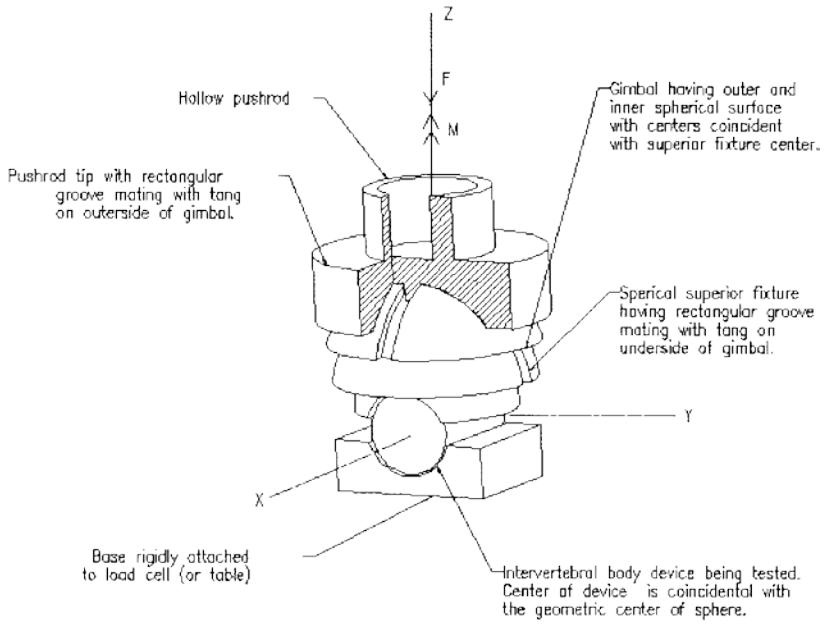

Figure 5: Depiction of the axial rotation fatigue testing model recommended by ASTM F2077-03. Note the complete lack of anatomical accuracy, and how motion is constrained by grooves in the bearing surfaces [49]. (Image reprinted with permission of ASTM International©)

Among these models, minimal attempt is made to replicate correct anatomy, or non-linear behavior. These models are typically composed of rigid bodies (blocks) that slide over one another or are connected by springs. They can be mechanically accurate but may vary from lab to lab, as they are typically assembled by the labs utilizing them. This property can be quite useful as researchers may switch out components that break or are damaged. However, this also means there is no uniform model. Furthermore, there is a large disadvantage in using rigid blocks to represent vertebrae. They don't accurately reflect the properties of cancellous bone. A large failure mechanism during fatigue testing is screw toggling which is more likely to occur in cancellous bone than the models being used. If this mode of failure is ignored, potential complications could arise with the in-vivo use of an implant.

1.5.Solution: The Analogue Spine Model

1.5.1. Description

The Analogue Spine Model (ASM) is designed to be the first anatomically and mechanically correct model of the human lumbar spine. Each component has been designed to mimic its human counterpart, and assembled in a way to ensure the model behaves like an average cadaveric spine, even following surgical intervention. By analyzing the strengths and weaknesses of current alternatives, the ASM has been created to fulfill the key requirements of such models.

1.5.2. Comparison to current technologies

The ASM is a mechanically and anatomically correct model which can be repeatedly tested over long periods of time, is capable of use in endurance tests, is easily adaptable by its users, and readily available. The ASM is the only model that possesses all of these qualities. As such, it has been designed to provide a successful alternative to the use of the current gold standard, human cadaveric spines.

A key limitation to this model is its lack of accounting for the active components of the spine which largely control its stability. This includes but is not limited to the neuromuscular system [14]. However, it should be mentioned that none of the previously mentioned models take this into account either, and that only computer models are reasonably suited to handle the situation. While this is a simplified model, it still provides extremely useful information, and can represent worst case scenarios for compromised, unstable spines.

Furthermore, future plans will elevate this model further beyond the alternatives. Work is currently being conducted to integrate sensors for measuring various parameters of interest (facet contact force, intradiscal pressure) into the manufacturing. This will allow direct

comparison between models, and reduce potential experimental errors. One key use of this model will be to facilitate comparison between differing experimental test setups. There is no widely agreed upon standard test method, and most researchers use custom built machines to perform their testing. By utilizing a repeatable model between test setups it will be possible to compare results obtained in different labs. These differences will be explored in more detail later on.

1.5.3. Previous work on the ASM

Substantial work has already been completed in the development of the Analogue Spine Model, including the creation of anatomically and mechanically correct hard and soft tissues [50]. This work has been carried out at The University of Kansas and Pacific Research Laboratories.

The cortical bone used to construct each vertebra has already undergone substantial development. It is manufactured by Pacific Research Laboratories (Sawbones). This short fiber epoxy composite is now in its fourth generation. The first generation was released in the early 90's, and has since undergone significant testing and improvements. The fourth generation was developed by early 2007. In addition to testing its basic material properties (stress/strain behavior), its behavior has been quantified in crack propagation, and fatigue testing, ensuring its accurate mechanical properties can be utilized during endurance testing [51].

An appropriate model for cancellous bone is also required to make realistic vertebra. Closed-cell foams are already utilized in many of the models that Sawbones sells. However for the Analogue Spine Model, open-celled foam is desirable. This would allow for the effects of cement intrusion on implant fixation to be studied. Further, it would provide realistic dynamic and fatigue failure mechanisms [52, 53]. However, the rigid open-cell foams currently available

do not have mechanical properties that are strong enough to simulate young healthy cancellous bone [54]. The researchers on this project have developed the manufacturing techniques necessary to create an open-cell foam with the desired properties [55]. A key part of this research was determining which of PRL's available materials would be best suited to create this model. This involved the testing of solid materials, and the utilization of foam theory to estimate the properties of the foams they would make (see: Chapter 2 – Cancellous Bone). A portion of the Phase II SBIR Grant funding this research is dedicated towards the creation of an open-cell synthetic foam, and its incorporation into a cortical shell with accurate vertebral morphology and mechanical properties

An NIH SBIR Phase I grant was previously funded supporting work developing the soft tissues used in this model[56]. One student developed and characterized the ligaments, another worked on the intervertebral disc. Work was completed ensuring the analogue ligaments had dimensions and mechanical properties similar to those reported in the literature [50, 57]. Most of the initial work was carried out on the anterior longitudinal ligament (ALL) and posterior longitudinal ligament (PLL), and demonstrating that changes in their properties effectively control the mechanical behavior of the ASM. The analogue ALL has an initial stiffness of approximately 35 MPa at .8% strain, and a secondary of 65 MPa. The analogue PLL has an initial stiffness of approximately 153 MPa at 2% strain, and a secondary stiffness of 250 MPa.

The intervertebral disc (IVD) has a shape customized for each level of the spine. This was completed by creating lost-wax molds of human IVD's. These components are now readily created using injection molding techniques. Initial work on the IVD attempted to recreate the alternating 30° fibrous morphology, of the annulus fibrosus (AF). This was carried out by embedding polyester fibers in a polyurethane (PU) matrix. However, manufacturing hurdles were encountered; involving rapid degradation, and failure of the AF along the fiber boundaries.

In order to overcome these hurdles, a simplified design was chosen. Instead of embedding fibers in the AF (which are designed to provide its non-linear behavior), a single woven sheet of polyester fibers was attached to the vertebrae around the entire disc. This approach successfully contains the disc, while still imparting non-linear behavior to the structure. Furthermore, by bonding directly to the vertebrae, it increases the durability of the model. The nucleus is composed of low durometer isotropic PU. A gel-like isotropic material was chosen in order to evenly transfer hydrostatic pressure across the adjacent endplates. Compressive testing was performed on the discs to ensure that they compared favorably with the reported literature of Hirsch and Markolf [58, 59].

The facet capsule has also undergone significant development. It was initially composed of silicone adhesive impregnated with a fabric mesh. Articular cartilage was simulated with pure silicon. Later models utilized a "reverse synovial joint." This is created by using wax to cover each of the opposing facets, which were then covered in a low durometer PU. When compressed, the wax should shear out of the way (synovial fluid), while a strip of PU between the opposing facets acts as the articular cartilage. Injection molds have been developed to facilitate rapid, repeatable creation of the facet capsule. This is a marked improvement over earlier methods of painting PU over the joint.

1.5.4. Study Objectives

As mentioned, PRL already manufactures a cortical bone with mechanical properties similar to human tissue. However, there is still a need to develop accurate open-cell foam for use as a cancellous bone model. This foam will be integrated into the manufacturing of the ASM, providing realistic vertebrae, composed of a thin cortical shell filled with cancellous bone. Objectives for the cancellous bone study are:

- Rapidly test a variety of materials for potential use in an open-cell foam
- Predict which materials will yield the optimal foam
- Manufacture open-cell foam from the selected materials
- Quantify the mechanical properties of the new cancellous bone model, and assess manufacturing related variability

The mechanical properties of the spine model's soft tissues have already been quantified, and deemed similar to human properties. However, during manufacture of the spine model, the various components interact with each other, stiffening the model, or causing unwanted behavior (see: section 3.3.1 - Initial Status of the Analogue Spine Model). These interactions need to be located and dealt with in order to ensure proper model behavior. The objectives for studying overall model performance are:

- Determine the interactions responsible for aberrant behavior encountered during preliminary tests
- Identify the soft tissues that contribute the most to neutral zone stiffness
- Reduce neutral zone stiffness
- Compare model performance to human data found in the literature

Chapter 2. – Cancellous Bone

The following chapter discusses the development of a synthetic vertebral cancellous bone model. The composition and structure of human vertebral bone are looked at, followed by a description of cancellous bone's primary functions. Following this, the mechanical properties of human bone are described as reported in the literature. Discussion of the new model is preceded with an introduction to Foam Theory, which proved valuable during its development. Following this introduction, two different types of testing (four point bending, unconfined compression) are reported on, and then compared to the literature.

2.1.Form and function

2.1.1. Composition and structure

Bone is the primary hard tissue of the human spine. Bone differs from soft tissues in both rigidity and hardness [60]. These properties are derived from inorganic salts that impregnate the surrounding matrix. This matrix is composed primarily of collagen fibers, non-collagenous proteins and mineral. Vertebrae are components of the axial skeletal system. As such, they are primarily composed of cancellous bone, surrounded by a highly porous thin shell of cortical bone. [19, 60]

Cancellous bone is widely recognized as a cellular solid composed of a network of rod and plate-like trabeculae [61]. Cancellous bone is easily characterized by a hierarchical structure [62]. At its first level (macroscopic, >3000 μm), cancellous bone is a highly porous interconnected network similar to open-cell foams. Its bone volume fraction (relative density) ranges from 5%-60% throughout various anatomical sites. The structural unit at this level is the trabeculae. These come in the form of rod or plate like elements, depending on age, anatomic site, and mechanical loading, among other factors. Trabeculae typically range from 200 μm -

1000 µm long. As opposed to the osteons that compose cortical bone, trabeculae typically do not have a central canal through which a blood vessel may flow.

The second level (microstructure) of cancellous bone is similar to that of cortical bone. At this level, single trabeculae exist. Trabeculae are composed of lamellae, lacunae, canaliculi and cement lines. In cancellous bone the lamellar packets are longitudinally organized and 3-7 µm thick. Cancellous bone lacks the osteonal structure of cortical bone. Instead the lamellae are arranges in angular segments of parallel sheets, preferentially aligned with the longitudinal axis of the trabeculae [60]. Lamellae are separated by cement lines, regions of amorphous substance that lack collagen.

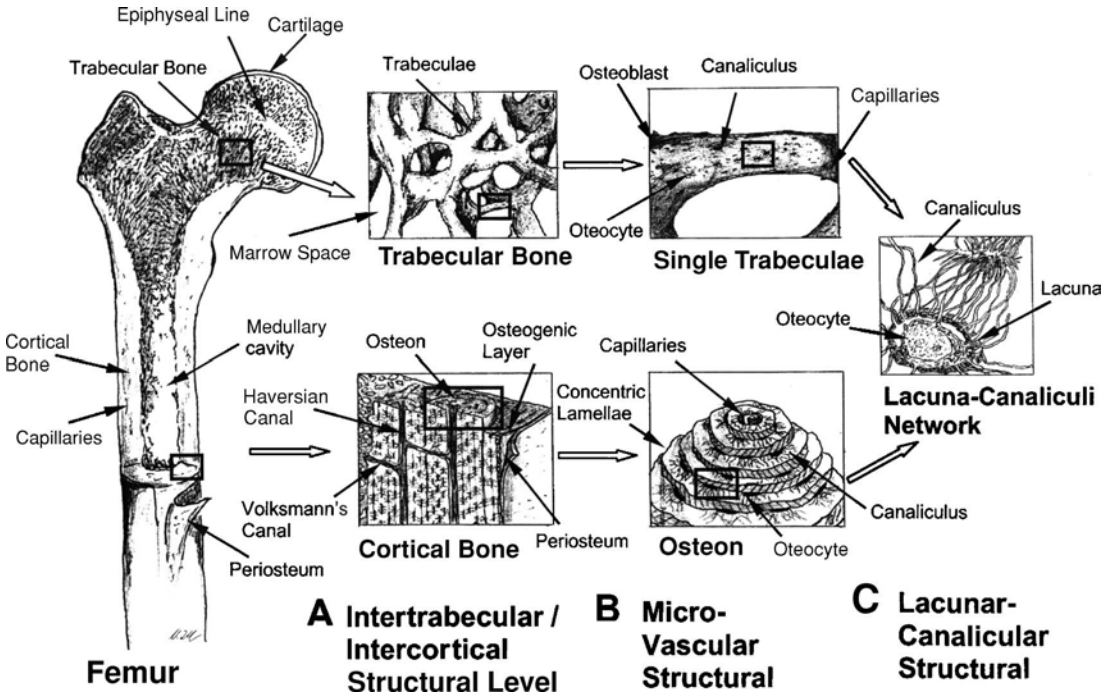

Figure 6: Bone is a material possessing a hierarchical structure. Trabecular and cortical bone differ at the macro and microscopic level, but are fundamentally similar at the lamellar level [63]. (Image reprinted with permission of Springer©)

The third level (sub-microstructure) of cancellous bone is composed of the same entities as cortical bone. This is the level at which lamellae exist. The main constituents are collagen fibrils and interstitial mineral composites. Looking at the nanostructure of lamellae reveals highly organized arrangement of the collagen fibrils and an interspersed mineral phase. The collagenous scaffold (90% fibril type I) is interspersed with the mineral hydroxyapatite [64] (Figure 7). In a lamellar packet, collagen fibers are aligned parallel to each other, with overlapping ends that are staggered by one quarter of the fiber length. This staggered arrangement stabilizes the fibers through molecular cross linking, and provides gaps for minerals to form (nucleate). The collagenous scaffold provides tensile strength, while the mineral phase provides compressive stiffness. The amount of cross-linking effects the final mechanical properties [64].

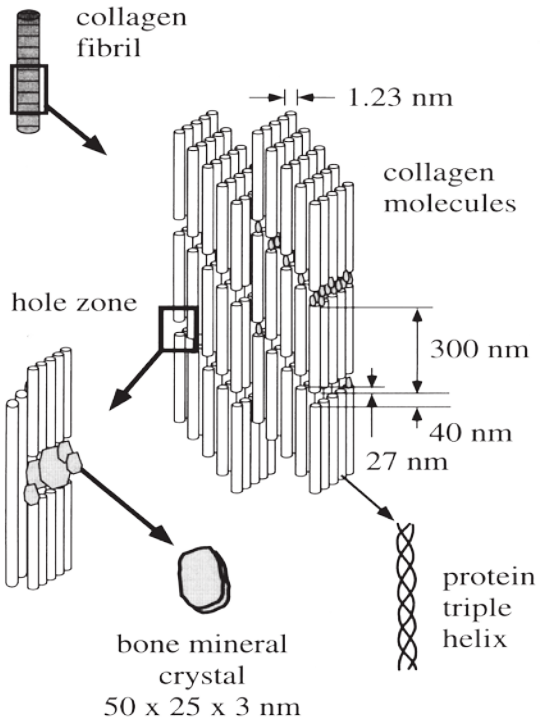

Figure 7: The lamellar nanostructure of bone is composed of staggered overlapping collagen packets with interstitial mineral crystals [65]. (Image reprinted with permission of Elsevier©)

On the macroscopic level, cancellous bone is spatially variant throughout the vertebral body. Near the endplates, more dense, rod-like trabeculae, with horizontal connections exists [19, 66]. Far from the endplates, less dense, plate-like trabeculae are dominant [19]. Furthermore, areas of dense bone exist near the base of each pedicle [66]. This architecture suggests that the primary forces exerted on the vertebrae are axial compressive in nature, except near the pedicles, where large bending moments are generated [66, 67]. This agrees with the findings of other studies, which show mechanical properties are dependent on anatomical site and direction of loading [68-70]. Additionally, this demonstrates that cancellous bone is a heterogeneous and anisotropic material. Not only is its structure dependent on anatomic site, but it is also varies temporally with age (Figure 8).

a) b)

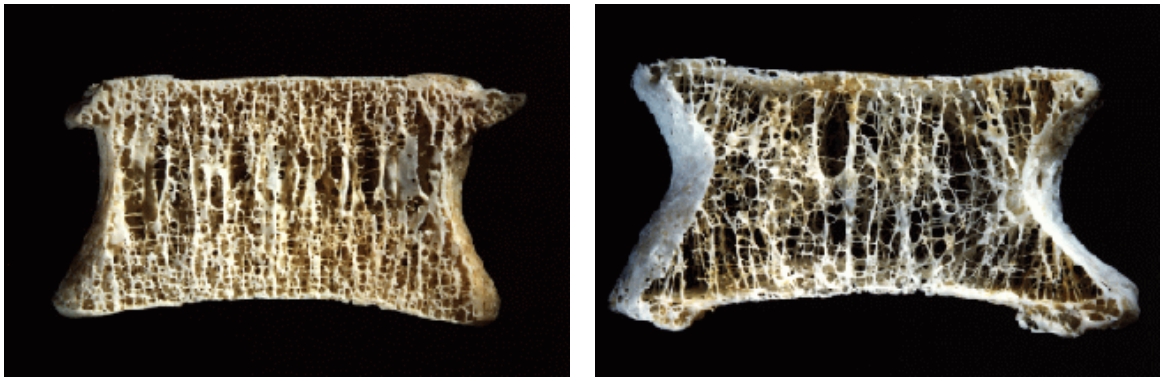

Figure 8: Vertebral body from a) young and b) elderly specimens respectively. Notice the difference in trabecular bone density between images [71]. (Image reprinted with permission of Springer©)

Younger bone typically has thick vertically oriented plate-like morphology, horizontally connected with rod-like trabeculae. During aging, gaps in the plates are generated through tissue remodeling, and the horizontal supports decrease, and eventually disappear [72]. This is one reason apparent bone density shows great variation between individuals(.05 g/cm^3 - .35 g/cm^3), and has been shown to exist as a function of age [19, 73].

2.1.2. Function – Mechanical

The vertebral body is the key bony structure of the human spine. It is critical to the mechanical stability of the spine, as it provides a rigid body for the attachment of ligaments, tendons and muscles.

As mentioned and shown above, the vertebral shell consists of a thin layer of cortical bone. The shell is mechanically important as it provides key insertion sites for the various soft tissues surrounding each vertebra. The cortical shell is a slightly porous structure, so even though it contains the hematopoietic marrow residing within each vertebra, it also allows some fluid transfer. This structural feature of the core has led many researchers to hypothesize that vertebrae are hydraulically stiffened by this slightly porous network. While this work has primarily concluded that at physiologic strain rates, fluid flow plays a minimal role, at high (traumatic) strain rates, the vertebral body can be stiffened and strengthened through this mechanism [63, 74-77].

The cancellous core is the primary bone tissue of the human spine. While its primary function is metabolic, it also provides the majority of each vertebrae's strength [60]. Even though the cancellous core isn't the key attachment site for soft tissues, it strengthens the outer shell, and is the key hard tissue responsible for energy absorption. The mechanical role of cancellous bone can easily be highlighted by analyzing the risk of vertebral fracture with respect to aging. The majority of vertebral bone loss occurs in the cancellous core, a result of its high surface to volume ratio, and subsequent contact with bone marrow. This bone loss makes patients highly susceptible to fractures, and the thoracolumbar spine is one of the most prone areas of the body due to this bone loss [78]. Studies have even shown that slight increases in

the bone mineral density of cancellous bone can be responsible for 50-60% reductions in vertebral fracture incidence [79].

2.1.3. Function – Metabolic

Vertebrae in young individuals are filled with hematopoietic (red) bone marrow. As a result, vertebrae serve as key sites for the creation of blood cells. In adults vertebrae are primary locations of hematopoiesis, along with the pelvis, cranium and sternum. Researchers have shown that the microenvironment surrounding cancellous bone facilitates the creation of mature blood cells [80]. These cells are derived from the hematopoietic stem cell line inherent to red marrow. Interactions between these cells and their surrounding chemical and mechanical environment guide their development.

Another critical function of cancellous bone is its role in mineral storage. Cancellous bone is critical to maintaining mineral homeostasis [78, 80]. Vertebral cancellous bone is well is well suited to meet this challenge. Its high surface to volume ratio means that the majority of each trabecula comes into contact with the surrounding bone marrow and large quantities of blood output from the heart. This direct interface facilitates the chemical reactions necessary to ensure proper mineral storage and regulation. Cancellous bone is able to store and distribute calcium and phosphate when needed. Bone also contains 95% of the body's supply of sodium, and 50% of its magnesium. This supply of minerals in conjunction with its direct interface with red bone marrow allows cancellous bone to respond to changes in mineral concentration within the blood supply. These stored ions are utilized in various chemical reactions, and regulate the composition of the extracellular fluid. Calcium alone is vital to neuromuscular activity, blood clotting, and intracellular signal transduction. Finally, cancellous bone is also capable of absorbing toxins and heavy metals in order to minimize their potential effects on the

surrounding tissues Due to its high surface area, and direct tie into the circulatory system, vertebral cancellous bone effectively monitors and regulates the composition of blood and minerals throughout the body

2.1.4. Function – Sensory

While most researchers easily recognize the roll of ligaments and soft tissues as sensory structures [82-84], it is worth noting that human vertebrae are also innervated with nerves. Several nerve endings (fine free fiber and complex un-encapsulated type fibers) are present in the periosteum surrounding each vertebra. Fibers are also present around the vascular sinusoids of the cartilaginous endplate [84-86]. Periosteal nerves tend to be sensory in nature, some of which are nociceptive (pain) receptors [87]. It is often assumed that unencapsulated fibers play a crucial role in sensing pain [88]. Nerves have been found to enter the vertebra via the

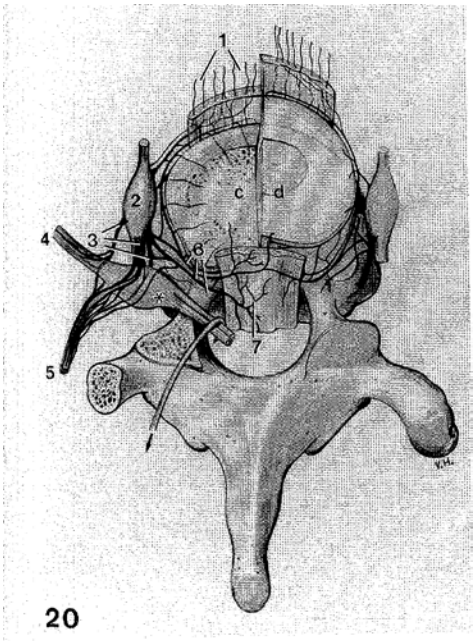

Figure 9: Drawing of nerves surrounding and innervating the vertebral body. Of key importance are nerves in the surrounding periosteum, and those entering the vertebral body with the bassivertebral vessels [81]. (Image reprinted with permission of Wiley-Liss, Inc. ©)

posterior vascular foramen with the basivertebral vessels. Furthermore, nerves also enter through the anterior cortex into the marrow [89]. As a result, both the cortical and cancellous structures are innervated with nerves. These fibers provide the body with a means of tracking the various forces at play in the vertebrae, and as such, are potential sources of low back pain.

2.2.Mechanical Properties of Human Vertebral Cancellous Bone

The structure and mechanical properties of bone are closely related. As an example, trabeculae tend to align with the axes of principal stress to better resist tension and compression [66]. This optimal structural orientation of trabeculae offers maximal stiffness and strength with minimal mass. Most attribute this structure to adaptive remodeling (Wolff's Law), which resorbs unloaded bone, and generates new bone in areas of high stress. Researchers initially hypothesized that cortical and cancellous bone were made of the same components, and therefore had the same mechanical properties at the continuum level. However, studies have since shown that the two types of bone have dissimilar properties, correlating to their differing structural elements [90]. Estimates conclude that shell accounts for less than 15% of the vertebral body's strength, with the remainder accounted for by the cancellous core [19, 91, 92].

2.2.1. Mechanical Characterization

Cancellous bone is analogous to porous engineering materials. This is due to its cellular structure, dynamic, and energy absorption characteristics [68].The most common test method is the use of axial compression tests. During these tests, cancellous bone exhibits a typical cellular stress-strain relationship, with linear zone, followed by yielding, a flat plastic collapse zone and finally, a densification zone (Figure 10) [93]. The plastic collapse zone yields high displacements at near constant stress. It occurs as a result of yielding by individual trabeculae. If displaced far

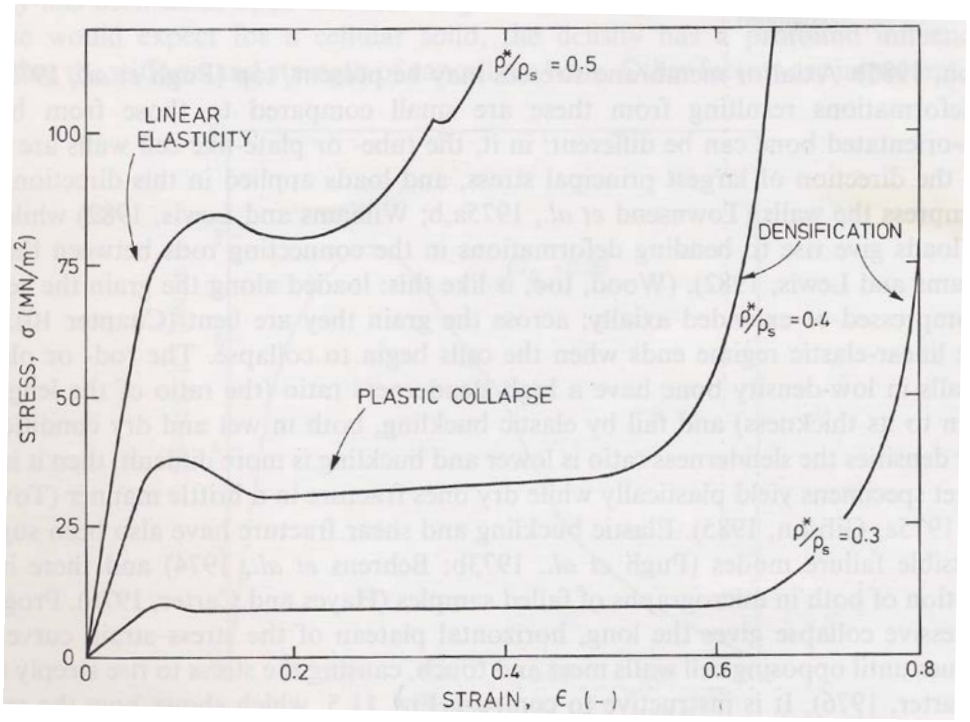

Figure 10: Stress-strain behavior of cancellous bone at various relative densities. Increasing relative density results in performance similar to typical solid engineering materials. Low density materials exhibit prolonged plastic collapse regions [96]. (Image reprinted with permission of Elsevier©)

enough, this region will be followed by a stiff linear region (densification). This occurs as a result of the trabeculae collapsing far enough to load upon one another.

There has been debate over whether cancellous bone exhibits an initial non-linear region. Initial studies seemed to support this idea, however researchers later utilized extensometers, instead of recording axial displacement of the loading platen. That change allowed researchers to conclude the nonlinear zone was merely an artifact of the test setup [61, 94, 95].

2.2.2. Test Methods

There are a wide variety of test methods utilized to study human cancellous bone. These methods can effectively be broken down into two categories, those studying the properties of individual trabeculae, and those studying the properties of the porous structure. Studies on

individual trabeculae have proven useful in developing analytical models. These models are concerned with analyzing the properties of bone tissue, and combining that information with structural models to predict macroscopic bone behavior. The most direct methods for analyzing the macroscopic properties of cancellous bone however, are compressive and tensile tests. These tests are regularly conducted on large bone specimens. Furthermore, these methods are analogous to those used characterizing common engineering materials. When additional properties such as apparent density and morphology are collected, these studies can develop powerful predictive models estimating the strength and stiffness of a patient's bones.

There are a large number of reported test methods put to use on cellular solids. The following provides a summary of what has been determined to be the current best practices for the testing of cancellous bone. Unconfined compression tests between parallel platens are possibly the most commonly used method for testing the mechanical properties of cancellous bone. Not only are the tests simple to set up and perform, but comparison across multiple studies shows that they are reliable, with multiple labs producing similar figures [97]. Keaveny et al. have performed several studies outlining a widely used test setup, that minimizes possible sources of variation and improves inter-lab repeatability [69].

The mechanical test setup is fairly simple, and produces accurate repeatable results. Specimens are obtained by using a circular core to extract 8mm diameter cylinders from the vertebral centrum (Figure 11). Specimen ends are then potted in quick drying epoxy to avoid the confounding effects caused by friction on the free trabeculae (end artifacts) [95, 98]. Previous research has shown that not potting specimens causes over-estimation of the modulus and yield strain. This can result in inaccuracies as large as 40% for measured bone stiffness [97]. The majority of early literature in this field did not consider the effect of end artifacts. As such, the

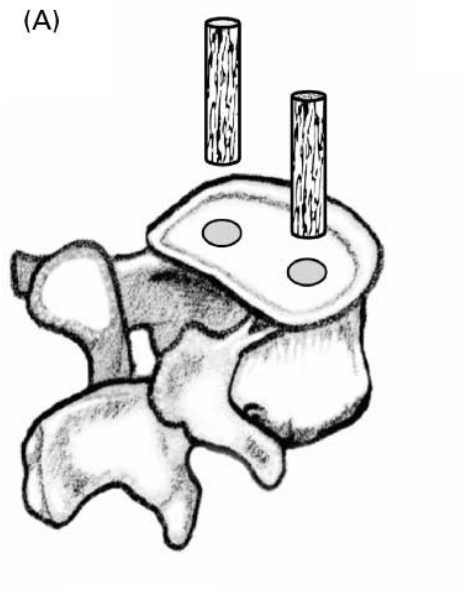

Figure 11: Illustrating the removal of core specimens from human vertebra. These specimens are removed with the use of circular coring tools to reduce interspecimen variability resulting from specimen processing [69]. (Image reprinted with permission of Elsevier©)

absolute values from these studies are skewed, and should not be used as accurate measures of mechanical performance. That said, they still provide useful qualitative validation of trends inherent to the specimens. Testing is usually carried out with 3-5 conditioning cycles to a low strain value (e.g. .1%). Then specimens are loaded to failure at low strain rates (e.g. .5% strain /sec). Specimen gage length is equal to the length of bone exposed between the end caps, plus half the embedded length. While compressing to failure, axial force and specimen strain are recorded with the use of specimen mounted extensometers and a load cell. If researchers are worried of specimen failure due to incorrect preparation, they should use two extensometers, one spanning the middle (5mm), one spanning he entire specimen. This can be used to determine if failure occurs near the end caps, or in the middle of the specimen. Failure near the end caps can be a result of end effects, and poorly reflect the actual specimen properties.

Following testing, several material properties are calculated from the collected data. Yield stress and strain are calculated with the traditional .2% offset technique common to engineering materials. The apparent modulus of elasticity is commonly defined as the slope of the stress-strain curve in the linear region. Several studies have shown measured properties to be influenced by anatomical site, specimen geometry and test methods [61, 97, 99, 100]. Researchers utilize a statistical analysis of variance (ANOVA) to compare specimens across anatomical sites, loading modalities (tension vs. compression), specimen geometry, and other applicable variables.

2.2.3. Morphological and Mechanical Properties

Several different properties taking account of specimen morphology have been collected over the years. As improved imaging and computational power has emerged, so has a new set of variables, previously inaccessible to the researcher.

Apparent bone density is perhaps the easiest variable to collect, and yet has shown the most predictive power in the generation of models. It is simply the apparent volume of the specimen, divided by its mass. It is the 'apparent density' as it is a measure of the structural density, not that of the tissue. Apparent density commonly varies from.05 g/cm^3 to .35 g/cm^3 [64, 69, 93]. Apparent density varies between individuals, anatomic locations, and as a function of age [19]. This parameter can also be collected with the use of peripheral quantitative computed tomography (pQCT), as used by Banse et al [64]. This method can provide increased accuracy over using calipers, due to its more accurate measurement of bone within a specified volume.

Ash density is a similarly related parameter. It is calculated by incinerating specimens following testing. The mass of the resultant ash is recorded, and divided by the original specimen's apparent volume. While this parameter is more time consuming to collect, it reduces

the variation in attempting to record the mass of specimens that are inherently saturated in bone marrow and other fluids. This provides a measure of strictly the bone tissue, and is minimally influenced by associated fluids.

Grote et al., and Hou et al. calculate a useful ratio that is analogous to relative density, bone volume divided by total volume (BV/TV%) [101, 102]. This parameter provides a measure of bone density that has been normalized with respect to tissue density. This parameter is often used by theoreticians in the field, as it is the key controlling variable used in foam theory (also called "relative density"). Grote et al. used an automatic computer program to analyze this property. It was shown that there are large changes of BV/TV in the cervical and superior thoracic regions, followed by primarily constant behavior in the lower levels (Figure 12).

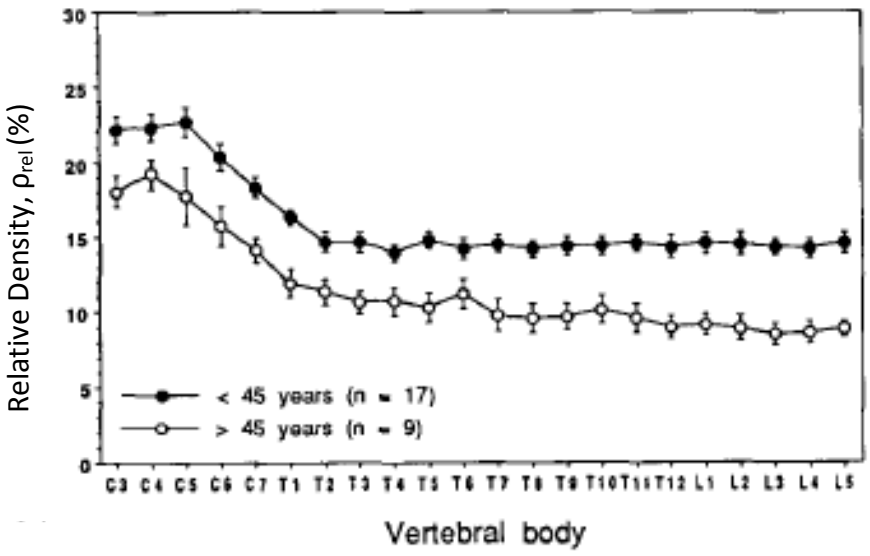

Figure 12: Dependence of the relative density (ρ_{rel}, %) of cancellous bone on vertebral level and its decrease with age [101]. (Image reprinted with permission of Elsevier©)

The modulus of elasticity of cancellous bone has been reported to vary from under 100 MPa to over 700 MPa [102, 103]. Part of this variation is due in part to how the modulus is calculated, of which there is no clear consensus. Keaveny et al. have calculated the modulus of

elasticity as the slope of the best fit straight line to the stress – strain data between .02% - .24% strain [98]. Banse et al calculate similarly, but use endpoints of .0001% 0 .2% strain. Others calculate stiffness as the maximum slope of the stress - strain curve [102]. Finally, misalignment of the specimen from its primary axis can lead to a reduction in modulus of more than 30% [69, 98].

It can be seen in Table 1 that there is a wide range of reported values for the stiffness of vertebral cancellous bone. The study by Moseklide et al. clearly demonstrates the anisotropy of cancellous bone, with the longitudinal direction being at least three times stiffer than the transverse. The work performed in Banse, and Keaveny's labs follow the same experimental setup, and have produced results consistent with each other. Furthermore, their approach takes care to minimize all possible sources of experimental error. As such, it is likely that the actual

Table 1: Literature values for the compressive modulus of vertebral cancellous bone

Apparent Stiffness, E (MPa)							
Author	Year	Direction	Boundary Condition	Ave	Std Dev	Min	Max
Banse [64]	2002	Longitudinal	Capped	352	145	127	725
Morgan / Keaveny [69]	2002	Longitudinal	Capped	344	148	-	-
Kopperdahl / Keaveny [98]	1998	Longitudinal	Capped	291	113	90	536
Moseklide [72]	1987	Longitudinal	Platen	67	7	-	-
Moseklide [72]	1987	Transverse	Platen	20	3	-	-
Hou [102]	1998	Longitudinal	Platen	316	226	10.6	975.6
Lindahl [104]	1976	Longitudinal	Platen	55.6	0.7	1.1	139

mean values for the stiffness of vertebral cancellous bone are in the range of 290 – 352 MPa. It is also likely that bone routinely possesses stiffness from 90 – 725 MPa, depending heavily on density and specimen age.

For vertebral cancellous bone, yield stress ranges from less than 1 MPa, to 5 MPa. Yield properties depend on anatomic site, extrapolation of best fit models to other sites, even at the same densities, are not applicable. Keaveny et al use the .2% offset method common to most engineering materials to calculate specimen yield [98]. Keaveny et al. have shown that yield stress is dependent on the direction of testing, and that using a platen without embedding the ends tends to overestimate the yield stress. This is evident in Table 2, when comparing the work of Kopperdahl / Keaveny to that of Lindahl's earlier study. Based on the results by Keaveny et al, the yield stress of vertebral cancellous bone is approximately 2 MPa, but routinely ranges from .5 – 4 MPa in human specimens.

Table 2: Literature values for the yield stress of vertebral cancellous bone

Yield Stress, σ_{yld} (MPa)							
Author	Year	Direction	Boundary Condition	Ave	Std Dev	Min	Max
Morgan / Keaveny [69]	2002	Longitudinal	Capped	2.02	0.92	-	-
Kopperdahl / Keaveny [98]	1998	Longitudinal	Capped	1.92	0.84	0.56	3.71
Lindahl [104]	1976	Longitudinal	Platen	4	0.1	0.1	9.7

The effect of capped specimens is just as pronounced when analyzing reported yield strains (Table 3). Free trabeculae at the ends of each specimen are capable of large deformations when not contained by epoxy. This leads to deceptively high strain values, and failure near the end caps, instead of in the middle of the gage length. Furthermore, early studies

did not account for this effect [104], and relied on platen displacement as an accurate measure of specimen strain. The use of strain gauges allows researchers to determine when specimens are yielding in the gage length, or due to testing artifacts (end effects). Based on the studies by Keaveny et al, the yield strain of trabecular bone averages approximately .8%, and routinely ranges between .75% - .95%. Yield strain appears to have minimal dependence on density, and theoretically should be constant across different densities and anatomic locations [69]. This is discussed in further detail in the section 2.3.1 - Foam theory.

Table 3: Literature values for the yield strain of vertebral cancellous bone

Yield Strain, ε_{yld} (-)							
Author	Year	Direction	Boundary Condition	Ave	Std Dev	Min	Max
Morgan / Keaveny [69]	2002	Longitudinal	Capped	0.77 %	0.06 %	-	-
Kopperdahl / Keaveny [98]	1998	Longitudinal	Capped	0.84 %	0.06 %	0.75 %	0.95 %
Lindahl [104]	1976	Longitudinal	Platen	6.7 %	0.2 %	4.1 %	8.6 %

Ultimate stress is defined as the maximum stress achieved, with ultimate strain being the corresponding strain at maximum stress. Similar to modulus of elasticity and yield stress, ultimate stress is dependent on the test setup. Leaving specimen ends un-capped leads to artifacts which produce unnaturally high values (Table 4). Once again, the similar protocols of Banse and Keaveny allow for repeatable results between labs, and an accurate look at expected properties. The mean value of vertebral yield stress appears to be between 2.2 MPa and 2.4 MPa. The reported range of values is from .6 to 6.17 MPa, demonstrating a large range that is dependent on specimen density and age.

Table 4: Literature values for the ultimate stress of vertebral cancellous bone

Ultimate Stress, σ_{ult} (MPa)							
Author	Year	Direction	Boundary Condition	Ave	Std Dev	Min	Max
Banse [64]	2002	Longitudinal	Capped	2.37	1.14	0.6	6.17
Kopperdahl / Keaveny [98]	1998	Longitudinal	Capped	2.23	0.95	0.7	4.33
Moseklide [72]	1987	Longitudinal	Platen	2.45	0.24	-	-
Moseklide [72]	1987	Transverse	Platen	0.88	0.12	-	-
Hou [102]	1998	Longitudinal	Platen	3.29	2.34	-	-
Lindahl [104]	1976	Longitudinal	Platen	4.6	0.3	0.2	10.5

Table 5: Literature values for the ultimate strain of vertebral cancellous bone

Ultimate Strain, ε_{ult} (-)							
Author	Year	Direction	Boundary Condition	Ave	Std Dev	Min	Max
Banse [64]	2002	Longitudinal	Capped	1.19 %	0.26 %	0.72%	2.01%
Kopperdahl / Keaveny [98]	1998	Longitudinal	Capped	1.45 %	0.33 %	0.96%	2.30%
Moseklide [72]	1987	Longitudinal	Platen	7.4 %	0.2 %	-	-
Moseklide [72]	1987	Transverse	Platen	8.5 %	0.3 %	-	-
Hou [102]	1998	Longitudinal	Platen	-	-	-	-
Lindahl [104]	1976	Longitudinal	Platen	9.5 %	0.4 %	5.30%	1.44%

Banse and Keaveny also present similar values for ultimate strain. The mean value is likely between 1.19% and 1.45% as reported by these authors. The range of physiologic values reported in their studies is from .72% to 2.30% strain (Table 5).

Relationships with Age:

Age has been shown to affect several morphological and mechanical factors. A relationship between ash density (AD) and age(α) was developed by Mosekilde [72]. Equation 1 is valid for samples between 20 to 80 years of age, and results in a decline of 48%-50% across the range. This equation was experimentally determined, and has a correlation factor of r2=0.72 (Figure 13).

$$AD = -.0017 \times \alpha + .23 \quad [\frac{g}{cm^3}]$$

Equation 1: Relationship between ash density (AD) and age (α) [72]

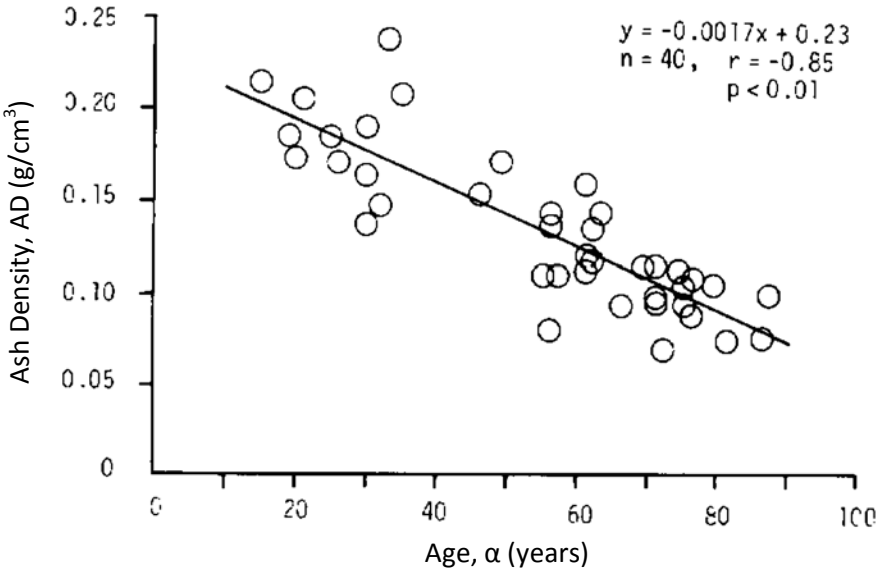

Figure 13: Experimentally determined relationship between age and ash density. The ash density decreased by approximately 50% from age 20 to 80 [72]. (Reprinted with permission of Elsevier©)

Relationships between mechanical properties and age have been determined in several older studies. However as these studies don't take into account the effects of end artifacts, and other experimental errors, the absolute values of these relationships aren't applicable. The trends developed by these relationships should still hold true, regardless of the absolute value.

Mosekilde et al. have demonstrated a dependence of the modulus of elasticity upon age [72]. As mentioned above, the absolute values aren't accurate due to the test setup, however the trend should hold true. The experimental relationship was determined for specimens between 20 and 80 years old (Equation 2). This results in an 80% loss between these ages, a 14% reduction in stiffness each decade (Figure 14).

$$E = -1.7 \times \alpha + 160 \quad [MPa]$$

Equation 2: Dependence of the modulus of elasticity, E (MPa), on age (α) [72]

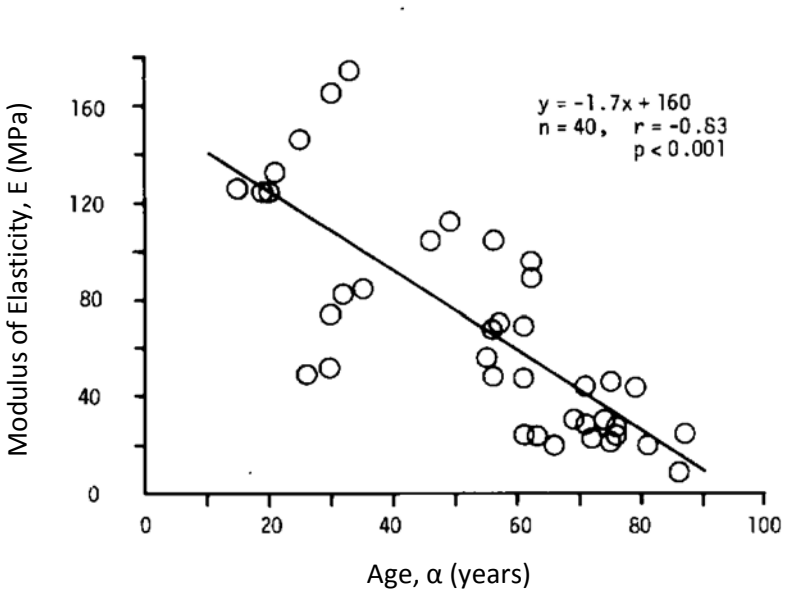

Figure 14: Experimentally determined relationship between age and modulus of elasticity. The modulus of elasticity drops 80% from age 20 to 80 [72]. (Reprinted with permission of Elsevier©)

Trends have not been reported, for yield properties, however they should hold similar to those of a specimen's ultimate properties. Mosekilde et al. have shown a degradation in ultimate stress of 75%-80% from age 20 to 80 [72]. This decrease is extremely similar to that of the modulus of elasticity. As will be discussed in more detail below, these two properties are closely correlated, and both have the same relationship with relative density. The decrease in strength is even more pronounced in the transverse direction, with decreases of 90%-96% occurring. In contrast with ultimate strength, the ultimate strain actually increases 17%-28% over this same interval.

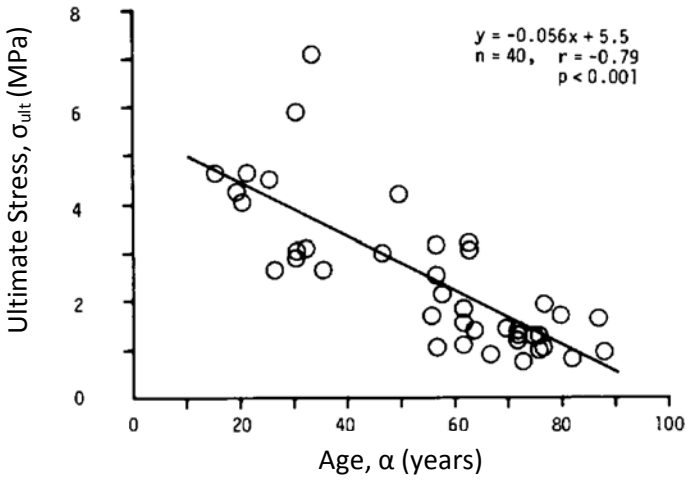

Figure 15: Experimentally determined relationship between age and maximum stress. The ultimate strength decreases 80% over the 60 year interval studied [72]. (Reprinted with permission of Elsevier©)

Relationships with Density:

Correlations to measures of density are perhaps the most widely used variables in predictive modeling [61]. Several researchers have shown that apparent density can account for over 80% of the variability in cancellous bones performance. It is widely agreed upon that increasing bone density increases the modulus of elasticity, yield strength and failure strength.

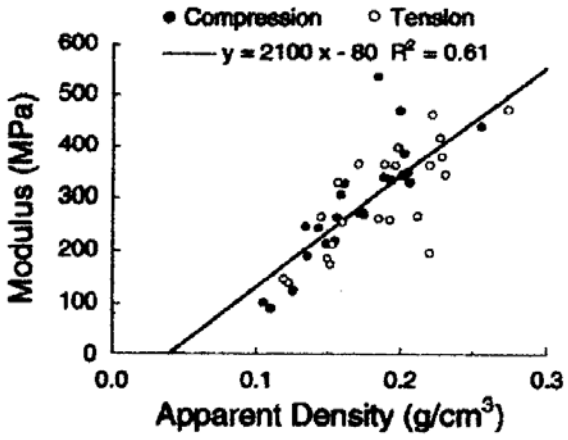

Figure 16: Experimentally determined relationship between apparent density and modulus of elasticity. The relationship was shown constant regardless of the direction of loading [98]. (Reprinted with permission of Elsevier©)

Table 6: Experimentally determined equations relating the modulus of elasticity (MPa) with the apparent density (g/cm^3) of human vertebral cancellous bone

Modulus of Elasticity (MPa) $E=A\,\rho^B$				
Author	Year	A	B	r^2
Morgan / Keaveny [69]	2001	37.1 (1.30)	1.74 (0.15)	0.8
Carter and Hayes [94]	1977	3790	3	-
Keaveny, Gibson ,Hayes [105]	1993	3380	2.21	0.85
Rice [90]	1988	820	2	0.78
Keller [106]	1994	757	1.94	0.702
Linde [97]	1992	2654	1.81	0.533

Several researchers have independently studied the relationship between density and cancellous bone's stiffness. Kopperdahl and Keaveny propose a linear fit between stiffness and apparent density. This relationship was recorded over a small range of apparent densities [98]. Their work showed that the modulus is independent of loading direction, with tension and

compression producing the same results (Figure 16). Other studies over wider ranges of apparent density have shown power law relationships of the form $E=A\rho^B$ (Table 6).While relationships are typically reported between the first (B=1) and third order(B=3), most authors acknowledge that they are theoretically and experimentally close to second order (B=2) (Table 6).

Morgan and Keaveny have experimentally shown that yield stress depends on anatomic site, and loading modality [69]. For the vertebral body in compression, a power law regression line was generated that correlated well to the results (r^2 = .80) (Figure 17 A). Kopperdahl and Keaveny have further shown that the relation between yield stress and apparent density is dependent on the direction of testing [98]. As will be discussed in the section on Foam Theory (Section 2.3), if buckling dominates failure, the relationship will be second order, as in compression. However, as buckling cannot occur in tension, yield stress is subject to a linear relationship with apparent density (Figure 17 B).

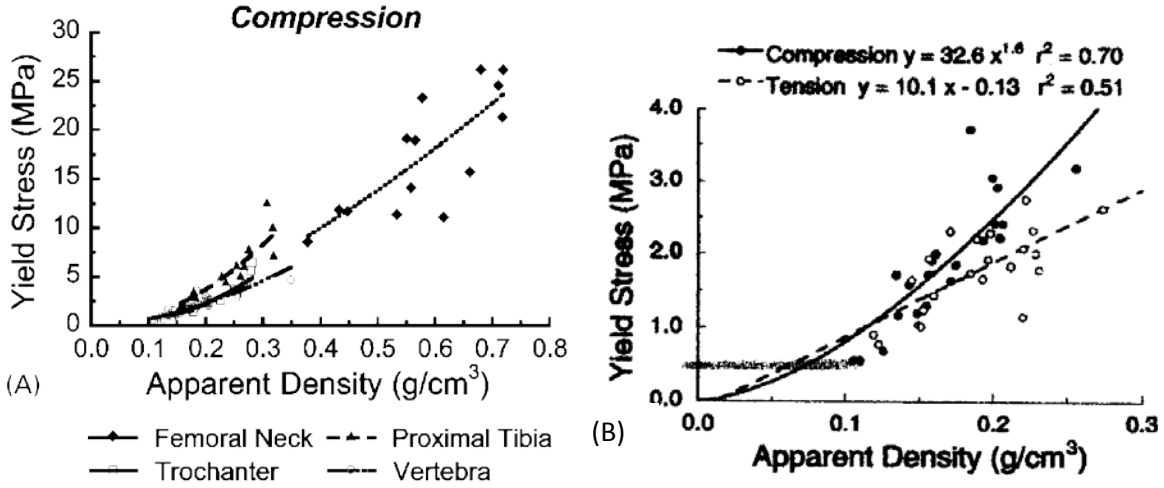

Figure 17: Experimentally determined relationship between yield stress and apparent density for human vertebral cancellous bone subjected to compression and tension. (A) Relationships are dependent on anatomic location. (B) Furthermore, compression typically exhibits a power law relationship, while tension shows linear performance. [69, 98]. (Reprinted with permission of Elsevier©)

Table 8: Experimentally determined equations relating the yield stress (MPa) with the apparent density (g/cm^3) of human vertebral cancellous bone in compression

Yield Stress (MPa) $\sigma_{yld} = A\,\rho^B$				
Author	Year	A	B	r^2
Morgan / Keaveny [69]	2002	37.1	1.74	0.8
Kopperdahl / Keaveny [98]	1998	32.6	1.6	0.7

Similar to yield stress, a second order relationship best describes the behavior of strength as a function of apparent density [90]. This result has been experimentally validated by several researchers (Table 8).

Table 7: Experimentally determined equations relating the ultimate strength (MPa) with the apparent density (g/cm^3) of human vertebral cancellous bone in compression.

Ultimate Stress (MPa) $\sigma_{ult} = A\,\rho^B$				
Author	Year	A	B	r^2
Carter and Hayes [94]	1977	68	2	-
Keaveny, Gibson and Hayes [105]	1993	40	1.98	0.90
Hansson [107]	1987	85.3	2.24	0.76
McCalden [108]	1997	0.024	1.78	0.94
Rice[90]	1988	-3.04	2	0.73
Rice [90]	1988	-	3	0.68
Keller [106]	1994	40.5	1.92	0.93
Keller[106]	1994	97.9	2.30	0.79
Linde[97]	1992	32.4	1.87	0.64

Disagreement exists on whether failure strains are dependent on apparent density. Some researchers have found little to no correlation with apparent density (or therefore modulus, yield stress or ultimate stress) [61]. While others have demonstrated moderate dependence (r=.41)[64]. As will be discussed in Section 2.3.1 - Foam theory, failure strain should be constant if the modulus of elasticity and ultimate stress share the same relationship to relative density.

Relationships with Anatomic Location:

Another source of variation arises from the specimen's anatomic location. Keaveny et al. have performed several studies on cancellous bone analyzing the dependence of properties on anatomic site, and overall yield strain behavior [69, 98]. Between anatomic sites, yield stress differed by a factor of 8, and modulus of elasticity by a factor of 10. Since the coefficient of variation within anatomic sites was low, this means values may be considered different across sites, but somewhat uniform within them [64]. Furthermore, there is limited certainty that cancellous bone from different anatomic locations or specimens will exhibit the same morphology (rod vs. plate-like), even at the same density. As a result, there is large variation in the mechanical properties of bone, even at the same relative density. For this reason, it is crucial to specify anatomic location, specimen age, apparent density, and test methods when reporting mechanical values.

Relationships with the Specimen's History:

Outside of what can be explained by dependence on apparent density and age, there is a large amount of variability in the reported literature. Some of this variability can be attributed to the personal history of the specimen. Key sources of variation due to specimen history are:

- Inter-specimen variation due to the subject's physical history [104, 109, 110]
- Biological composition [64]

Variation due to a subject's history occurs mainly as a result of bone remodeling. It is expected that individuals who subject their bones to higher levels of loading (i.e. athletes), will have stronger, stiffer bone. This occurs as higher loading will induce net bone growth, and result in high apparent densities. This behavior can also increase the rate of remodeling, and result in higher trabecular orientation, increasing mechanical properties. Conversely, specimens with sedentary behavior, or with repeated injuries resulting in immobilization will, on average, possess lower mechanical properties. This is a result of bone remodeling resulting in net bone resorption due to inactivity.

Some of this variability can also be explained with a biochemical analysis of the bone. The amount of cross-linking between collagenous fibers was shown to correlate with mechanical properties [64]. It is expected that the amount of cross linking ties back into the subject's physical and metabolic history. Specimens deficient in calcium, or the other building blocks of bone will have decreased abilities to grow new bone, and therefore molecular cross-linking.

Relationships with Experimental Factors:

There are several experimental factors that have been shown to affect perceived mechanical performance. The remaining inter-specimen variability up to this point has been mainly described by several factors [61]. Key among these factors are:

- Geometry
- Size and aspect ratio
- End effects
- Measurement method
- Storage methods
- Machine compliance
- Rate of testing

Specimen geometry has been studied in several publications. Cylindrical and cubic specimens are statistically similar when analyzing most mechanical parameters [105]. These results hold true for specimens with similar cross sectional areas and aspect ratios.

Increasing the specimen size and aspect ratio (length/diameter) causes the modulus to approach a second order relationship with apparent density. As this is its theoretical relation, it is assumed that an aspect ratio of 2:1 is more accurate than 1:1 specimens. Furthermore, correlation between variables becomes more accurate when a 2:1 L:D ratio is used [105]. These results have also been closely validated by Linde et al. [97].

As mentioned above, further variation also occurs as a result of the test methods used. It is critical to take end effects into account, as well as overall specimen preparation [111, 112]. Studies by Keaveny et al. have demonstrated that potting the inferior and superior ends of each specimen in an epoxy prior to testing reduces testing artifacts related to uneven edges and specimen friction with the loading platens. Furthermore, when end caps are not used, specimens tend to preferentially fail prematurely at the specimen/platen interface.

Most early studies on cancellous bone used platen displacement as a measure of specimen strain. Keaveny et al. have shown that this method results in increased specimen strain, due to slight specimen irregularities inherent to the preparation and testing process [95,

112]. Instead, if extensometers are mounted to each specimen, accurate performance can be collected, as well as a determination if specimens failed in their gauge length, or prematurely at the specimen/machine interface. Furthermore, studies recording platen displacement report an initial nonlinear behavior to their specimens, while those using extensometers have revealed that bone is actually a linear material [95, 111].

Specimen handling and storage are also critical factors in the measured material properties. For instance, Lindahl et al. tested dried defatted cancellous bone, and observed much stiffer and more brittle characteristics than is typically seen in wet bone [104]. Most researchers store their specimens below 20°C, with bone marrow still intact. Then specimens are allowed to thaw to room temperature prior to testing. This protocol has shown to preserve the mechanical properties of freshly deceased samples [15, 113].

According to Linde, one of the major potential errors involved in strain measurements on cancellous bone is machine compliance [97]. That said, this factor can be easily dealt with by pre or post-hoc. Platen on platen testing will reveal the test setup's load deformation response, which can then be filtered out of the collected results.

Significant work has also been conducted determining cancellous bone's viscoelastic behavior. Under physiologic loading conditions, strain rate was found to have limited impact on the mechanical properties of cancellous bone. Bone is often regarded as having properties proportional to strain rate raised to the .06 power [68]. This limited influence means that bone can be tested at most physiologic rates of motion with limited change in recorded properties. It is not until fast impact / traumatic loading occurs that strain rate becomes an extremely important variable.

The above discussion illustrates there are several critical variables that need to be controlled when testing human cancellous bone. Few studies have been provided that carefully account for these variables. The ones that do, however, show strong inter-lab agreement on most mechanical characteristics (Table 9). Banse and Keaveny et al. use the most widely published experimental setups and the results from their studies will be used to guide the development of the open-cell foam created in this study.

Table 9: Comparison of recent cancellous bone studies that account for specimen variability due to preparation and experimental test setup

		Banse [64]		Morgan / Keaveny [69]		Kopperdahl / Keaveny [98]	
$P_{apparent}$ (g/cm^3)	Ave (Std)	0.17	(0.05)	0.18	(0.05)	0.17	(0.04)
E (MPa)	Ave (Std)	352	(145)	344	(148)	291	(113)
	Range	127 –	725	-		90 –	536
σ_{yld} (MPa)	Ave (Std)	-		2.02	(0.92)	1.92	(0.84)
	Range	-		-		0.56 –	3.71
ε_{yld}	Ave (Std)	-		0.77 %	(0.06%)	0.84 %	(0.06 %)
	Range	-		-		0.75 % –	0.95 %
σ_{ult} (MPa)	Ave (Std)	2.37	(1.14)	-		2.23	(0.95)
	Range	0.60 –	6.17	-		0.7 –	4.33
ε_{ult}	Ave (Std)	1.19 %	(0.30 %)	-		1.45 %	(0.33 %)
	Range	0.72% –	2.01%	-		0.96% –	2.30%

2.3. Testing and Development of a Synthetic Cancellous Bone

2.3.1. Foam theory

As previously mentioned, cancellous bone can effectively be modeled as a porous engineering material. Pioneering work in the field was delivered by Gibson and Ashby, outlining a theoretical analysis of the mechanical properties of cancellous bone based on its structure [93, 96, 114]. These initial models structurally analyzed the unit cell of open and closed cell foams in order to determine their mechanical properties.

As these authors highlight, an understanding of how the structure of bone affects its mechanical properties can be indispensible in monitoring and preventing bone related pathologies and potential injuries. In the elderly, loss of bone mass in the hip, wrist, and vertebra increase risk of fracture. Non-invasive techniques can be used to measure parameters such as bone density and structure. An understanding of the relationship between these factors and strength will allow the clinician to understand if their patient is at risk for fracture. Furthermore, this understanding is critical for the design of bone interfacing implants. Mechanically incompatible implants can cause problems such as stress shielding, leading to eventual implant loosening and possibly failure. The majority of the human vertebra is comprised of cancellous bone. As a key use of the Analogue Lumbar Spine Model will be in the testing and development of implants, the creation and implementation of a mechanically correct cancellous core is integral to its potential success.

Following the initial structural analysis of the unit cell, researchers used a dimensional analysis to model deformation and failure. Even without knowing the shape of the unit cell (triangular, square, octahedral, etc.), if the shape is consistent at different relative densities, the dependence of the properties on relative density can be calculated and understood.

Relative density is apparent density of the foam, divided by the density of the solid it is composed of. Apparent density is the mass of the cellular solid, divided by the volume of the solid material, and voids in the material combined (apparent volume).

The primary mode of deformation in compressing cancellous bone is dominated by bending of individual trabeculae. As such, the modulus of elasticity varies as a function of relative density squared [93]. Deformation via bending (as opposed to axial straining or torsion) was confirmed by stepwise micro CT studies [115, 116]. Changes in architecture result in changes the C_1 constant in Equation 5.

$$\rho_{apparent} = \frac{m}{V_{solid} + V_{voids}} = \frac{m}{V_{apparent}}$$

Equation 3: Apparent density of a cellular solid

$$\rho_{relative} = \frac{\rho_{apparent}}{\rho_{solid}}$$

Equation 4: Relative density of a cellular solid

$$\frac{E_{apparent}}{E_{solid}} = C_1 \left(\frac{\rho_{apparent}}{\rho_{solid}}\right)^2 = C_1(\rho_{relative})^2$$

Equation 5: Apparent modulus of elasticity when the primary mode of deformation is bending of individual trabeculae

If the structure drastically changes to resemble vertical plates supported by horizontal rods, then the relationship becomes cubic or linear depending on whether it is loaded transversely, or longitudinally (in the plane of the plates) (Figure 18). Therefore it is likely that the dependence between mechanical properties and relative density gradually change as density increases. They exhibit quadratic relationships at low to moderate densities, and linear

to cubic relationship (depending on the direction of loading) once high densities, and therefore plate-like morphologies are reached. This has been experimentally observed (see section 2.2).

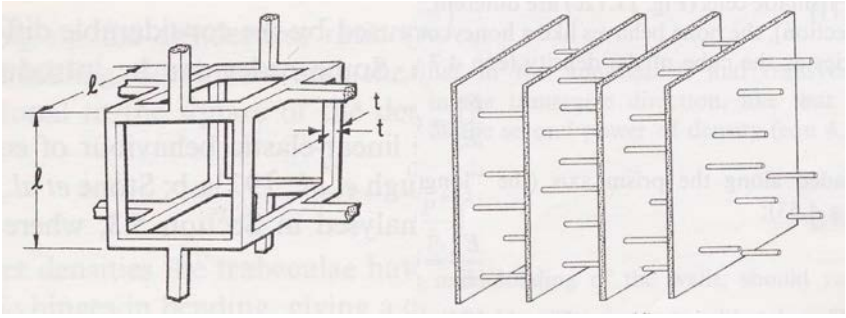

Figure 18: Simplified models simulating rod-like, and plate-like morphology models used to analyze open-cell engineering materials, and human cancellous bone [96]. (Reprinted with permission from Elsevier©)

A similar power relationship holds for estimating the compressive strength of cancellous bone. This relationship has been validated experimentally, and leads researchers to believe the primary mode of failure is trabecular elastic buckling, not, plastic yield, or brittle crushing [90].

Models predict that strength should transform from a function of density squared at low densities (with rod-like architecture) to a linear function of density or density cubed at high density (with plate-like morphology) depending on the direction of loading [96, 114, 117]. This explains some scatter in perceived relationships. If one author tests low density specimens, and the other high, they shouldn't be expected to generate the same relationships. This also holds

$$\sigma_{ult} = C_2 \left(\frac{\rho_{apparent}}{\rho_{solid}} \right)^2$$

Equation 6: Relationship between compressive strength and relative density

true if authors don't carefully monitor and control the orientation of their specimens when

loading. Reported correlation to experimentally derived models typically range from r^2 =.4 to .8 [118].

It has been noted that for low to intermediate densities, the modulus and failure strength both share the same density dependence. A result of this is that the failure strain is not a function of relative density , and instead is likely constant [98]. A quick check will show that in order to maintain dimensional accuracy, strain cannot be a function of relative density.

$$\sigma\left(\frac{\rho_{apparent}}{\rho_{solid}}\right)^2 = E\left(\frac{\rho_{apparent}}{\rho_{solid}}\right)^2 * \varepsilon$$

Equation 7: Hooke's law illustrating strain (ε) cannot be a function of relative density if strength (σ) and modulus (E) already are. If this occurred, dimensional accuracy of the equation would be lost.

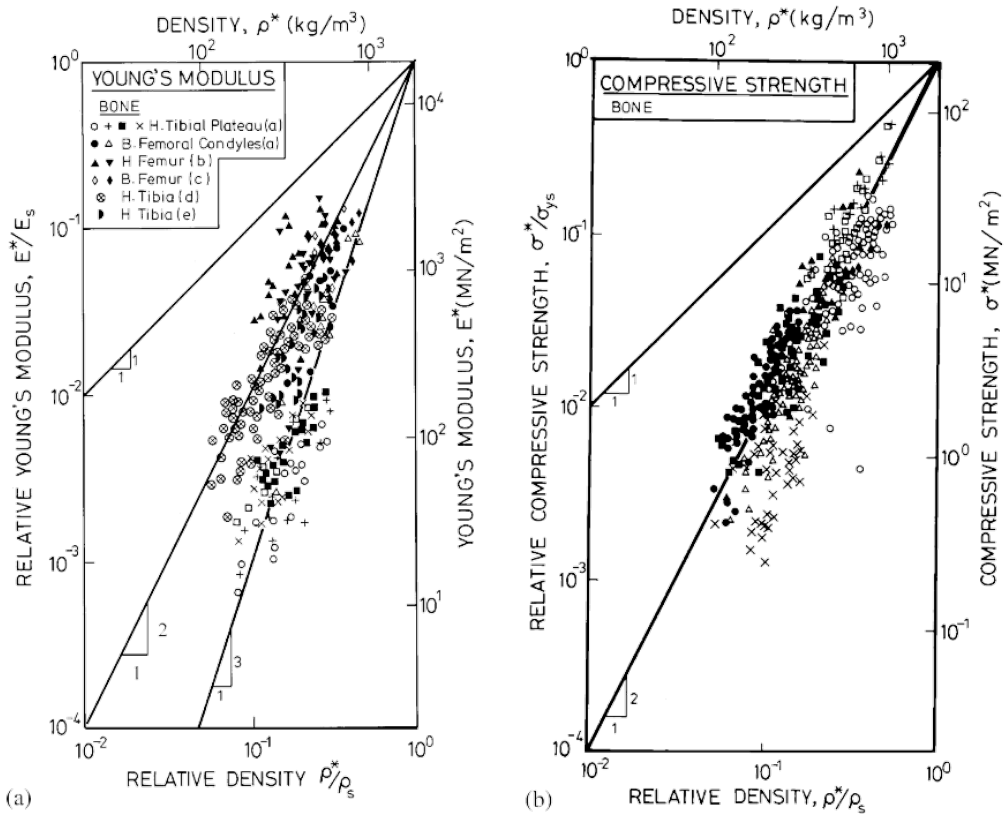

Figure 19: Relation of Modulus and Compressive Strength with Relative Density for human cancellous bone from multiple anatomic sites [93, 96]. (Reprinted with permission from Elsevier©)

2.3.2. Experimental Protocol- Mechanical Test Methods

A key element in the product development of the Analogue Spine Model is the ability to rapidly and accurately develop and test materials. The test setup for foam specimens is time consuming, a result of the necessity to secure the ends in epoxy. Instead of testing and modifying foam specimens, it would be beneficial to utilize a basic, yet accurate test setup with minimal specimen preparation.

It has been illustrated that the key parameter which controls the majority of variation in cancellous bone is its relative density. In order to facilitate the creation of a synthetic cancellous bone, it was first critical to assess the properties of the solid material ($\rho_{relative}$ = 100%). Once solid material properties are quantified it is possible to estimate the behavior of foams made from the solid materials.

There are several ways in which the mechanical properties of potential materials could be tested. Keeping with the need for a simple and repeatable test setup, four point bend testing was chosen. This testing requires the use of a four point bending jig, which is easily assembled, and a rectangular specimen geometry. Once in place, the test can be run quickly and effectively, allowing determination of the modulus of elasticity, yield stress, ultimate stress, and associated strains.

This mode of testing was chosen over tensile tests, diametral compression and three point bending for various reasons. Tensile testing was ruled out as it requires the use of “dog bone” shaped specimens that would be time consuming to manufacture. Diametral compression is mainly suitable for brittle ceramics, and while specimens are easy to manufacture, the results would be questionable due to the ductile nature of the materials being tested. Three point bending is similar in setup and analysis to four point bending. However, it places a singular point

load on the specimen, and is likely to induce premature fracture under the loading point. In contrast, four point bending evenly distributes the maximum load between the inner-most loading points. This spreads out the possible location in which failure may occur.

In all, twenty nine different materials were tested and compared for use in a cancellous bone model. Testing was carried out in accordance with ASTM D 6272-02, "Standard Test Method for Flexural Properties of Unreinforced and Reinforced Plastics and Electrical Insulating Materials by Four-Point Bending" [119].The support span was chosen as one half of the support span (Figure 20).

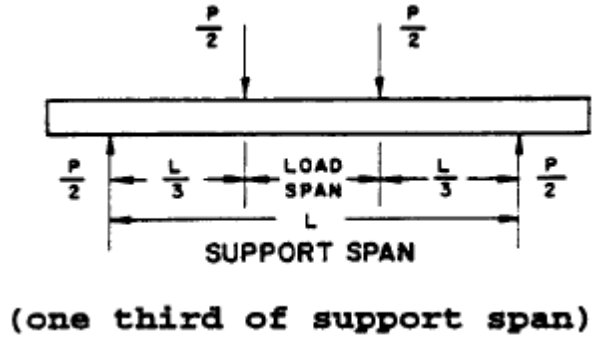

Figure 20: Diagram of loads on a four point bending specimen tested in accordance with ASTM D 6272-02 [119]. (Reprinted with permission of ASTM International©)

Loads were applied by supports positioned appropriately along the length of the inferior and superior test platens. Supports were cylindrical in shape, with a radius of 6.3 mm. The top span length (length between top supports) was 27.92mm. The bottom span length was 84.18mm. Both these values were measured with digital calipers (±.01mm) following jig assembly.

ASTM D 6272-02 specifies the use of an extensometer, or other deflection measurement device to be located at mid-span of the specimen. In this way the accurate measurement of maximum specimen deflection could be recorded. As such a device was not available; the

displacement of the superior loading platen with respect to the inferior platen was recorded. This was deemed acceptable since the purpose of this experiment was a comparison of different materials, not an assessment of exact material properties.

At least five (n=5) specimens of each material were prepared at Pacific Research Laboratories. Sheets of material were manufactured, and then placed in a CNC machine to reduce to their final dimensions. Ideal specimen geometry and dimensions are: L= 118 mm, d =5.80mm, and w=10.0mm.

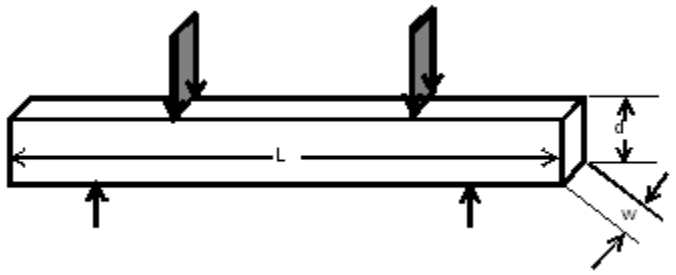

Figure 21: Ideal four point bending specimen used in this study. Loads from the test jig are illustrated with arrows. Specimen geometry fulfills the requirements of ASTM D 6272-02

Following shipment from Seattle to Lawrence, specimens were allowed to rest for at least 24 hours to facilitate acclimation to the laboratory environment. Prior to testing, each specimen dimension was measured at three locations along the dimension. Furthermore, the mass of each specimen was recorded to facilitate calculation of the solid material density for use in the predictive equations of foam theory.

For testing, the rate of crosshead motion was calculated following Equation 8 as 2.26 mm/min, or .0376 mm/sec. Specimens were placed on the loading platens, alignment checked, and then compressed to failure, or until 5% strain occurred. Compression was applied by an MTS Mini Bionix 858 (Eden Prairie, MN). Simultaneous with testing, platen displacement, and force were measured with the built in LVDT (±.01mm), and a 1.5 KN load cell (± .05N). Samples were

collected at 100 Hz. Following testing, stress and strain were calculated, and then used to calculate the material modulus of elasticity. These calculations were provided by ASTM D 6272-02 (Equation 9, Equation 10, Equation 11) [119].

$$R = \frac{.185\ Z\ L^2}{d}\ [\frac{mm}{min}]$$

Equation 8: Rate of crosshead motion (z=.01)

$$\sigma = \frac{P\ L}{w\ d^2}\ [MPa]$$

Equation 9: Maximum stress in a four point bending specimen

$$\varepsilon = 4.70\ \frac{Dd}{L}\ [unitless]$$

Equation 10: Maximum strain in a four point bending specimen

$$E = \frac{.21\ L^3\ m}{b\ d^3}\ [MPa]$$

Equation 11: Modulus of a four point bending specimen

P – load (N)

L – bottom span length [mm]

w – width of specimen [mm]

d – depth of specimen [mm]

D – center of deflection [mm]

m – slope of load –deflection curve [N/mm]

Yield strength and strain were calculated using the common .2% offset technique. This is done by locating the intersection of a line with slope equal to the modulus of elasticity that is offset by .2% (E-B = .2%, Figure 22), and the stress – strain curve. Ultimate strength and strain

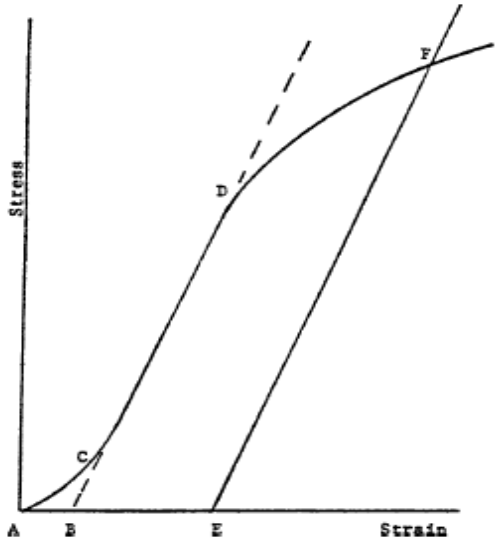

Figure 22: Initial portion of the stress - strain curve demonstrating calculation of yield properties with the .2% offset technique (E – B = .002) [119]. (Reprinted with permission of ASTM International©)

were calculated as the maximum stress, and strain at maximum stress. The ductile nature of each specimen was also quantified by analyzing the difference between the ultimate and yield strains. In extremely brittle structures, failure would occur immediately following yielding, leading to low post yield ductility.

2.3.3. Experimental Results and Analysis

Twenty nine different proprietary materials were evaluated in four point bending for potential use as a cancellous bone model. The modulus of elasticity, yield properties, ultimate properties, and post yield ductility were determined for each material. Post yield ductility was determined to be critically important by PRL, as they currently manufacture foam with acceptable stiffness and strength, but with very brittle failure. The twenty nine proprietary materials were variants of different matrices (epoxies and polyurethane resins), with various types and volume fractions of filler particulate (short fiber particles) [120]. The materials used were dictated by PRL, as they were readily available to the company, and their supply was ensured for the indefinite future.

As there was no uniform matrix or filler, it is not feasible to analyze the mechanical parameters as a function of different independent variables (i.e. density). However, as presented above, the dependence of modulus and strength on relative density squared means that there should exist a linear relationship between the two. Furthermore, there should be no relationship between modulus and strength with the yield strain. Plotting these relationships facilitates analysis of the upcoming results. Finally, it is worth recalling the objective of this study is to assess material properties in order to estimate potential foam performance. Performance of the final foam is not just a function of the material chosen, but the foam's relative density, which can be controlled while manufacturing. The modulus, and strength can be increased or decreased depending on density, however, the strain values are theoretically constant across most relative densities.

Limited variation was seen in the modulus of elasticity, it ranged from approximately 1 GPa to 6 GPa (Figure 23). As can be seen, there was limited variation within each material, demonstrating reliable processing by PRL, and testing at KU. Most coefficients of variance (COV = mean/std dev) were within 10% of the mean, with only 7 materials more variable. The

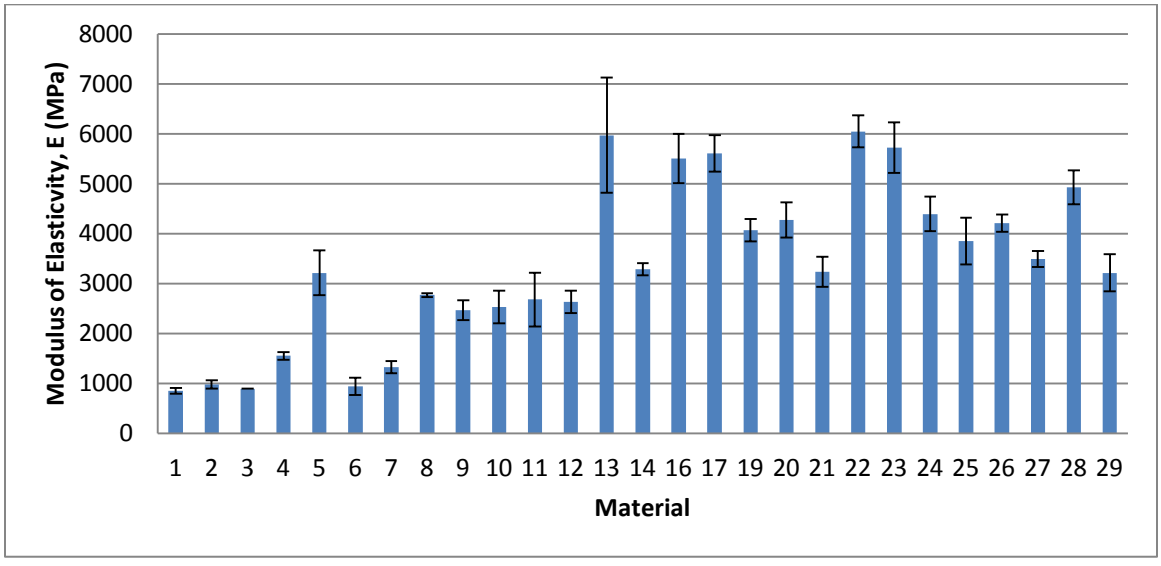

Figure 23: Modulus of Elasticity (mean ± std dev) for 29 four point bending materials

maximum reported COV was 20% in one material.

Values for yield stress ranged from approximately 5 to 55 MPa (Figure 24). Two materials possessed COVs of 18%, however all others were less than 14%. Yield strain values were also very consistent, ranging from approximately .75 to 2% (Figure 25). Furthermore, inter-specimen behavior was highly consistent, with most COV's under 10%, and only 6 materials

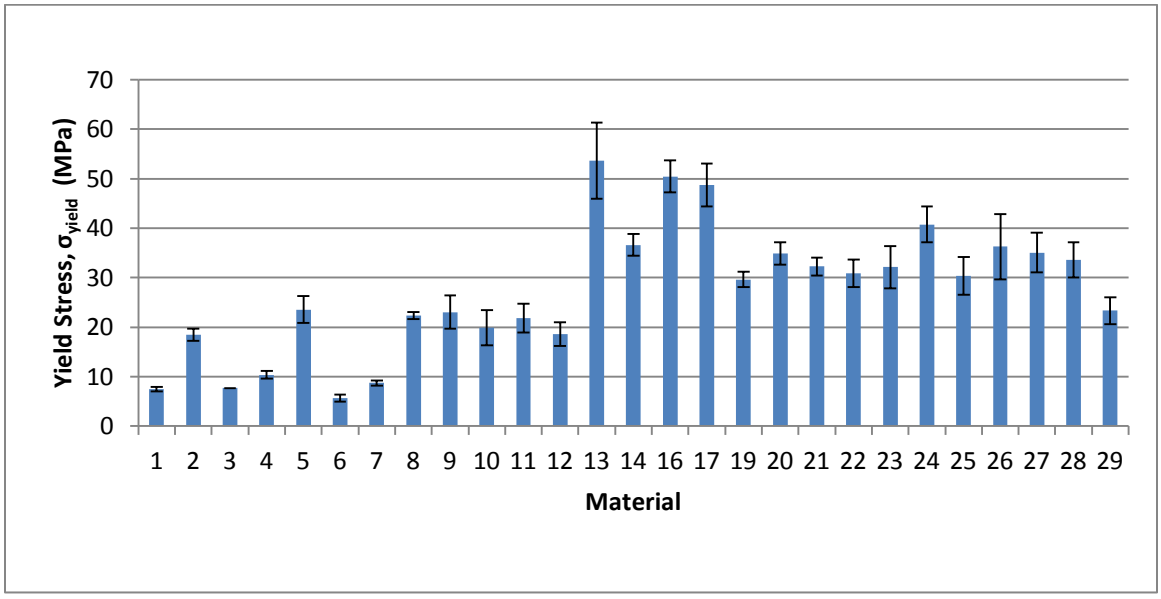

Figure 24: Yield stress (mean ± std dev) for 29 four point bending materials

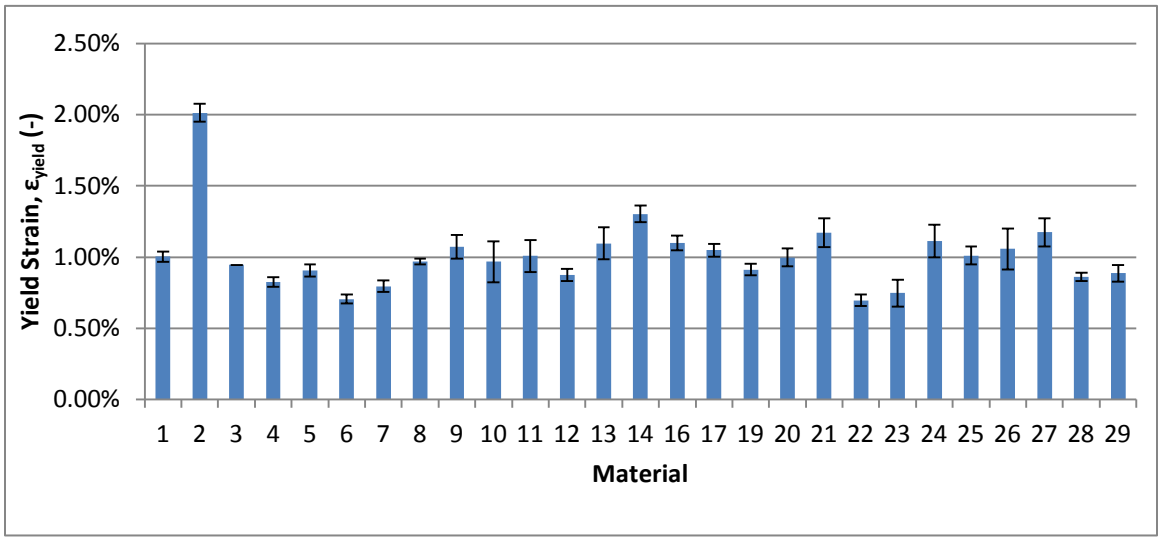

Figure 25: Yield strain (mean ± std dev) for 29 four point bending specimens

exhibiting higher variances.

Ultimate Stress behaved similarly to the modulus of elasticity. Limited range of values from 10 to 55 MPa were seen (Figure 26). COVs were higher, with 12 materials above 10%, and a high of 20%. The ultimate strain ranged from approximately .6% to 2.75% (Figure 27). COVs were fairly high, with 13 materials above 10%, and a high of 27%.

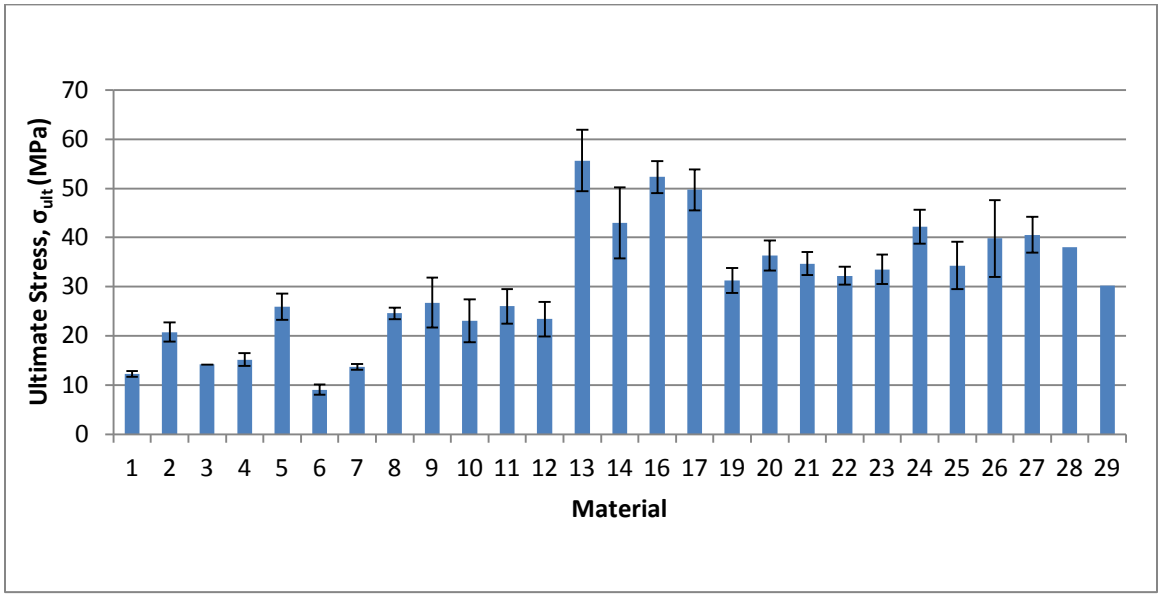

Figure 26: Ultimate stress (mean ± std dev) for 29 four point bending materials

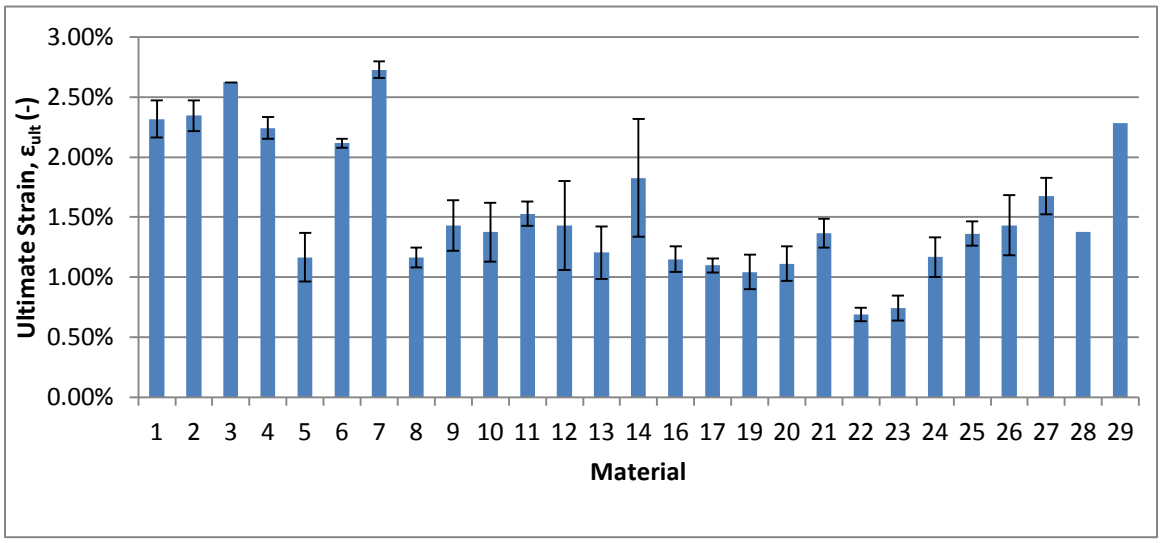

Figure 27: Ultimate strain (mean ± std dev) for 29 four point bending specimens

As discussed above, post yield ductility is one of the most important parameters. Values ranged from near 0%, extremely brittle with yield and failure occurring simultaneously, to just under 2% (Figure 28). This was the most variable parameter, with COVs for 23 materials above 10%, and a high of 358%. It is worth noting that most of the high COVs are from brittle materials, with means around zero. As the mean approaches zero, the COV becomes a less accurate measure of variability.

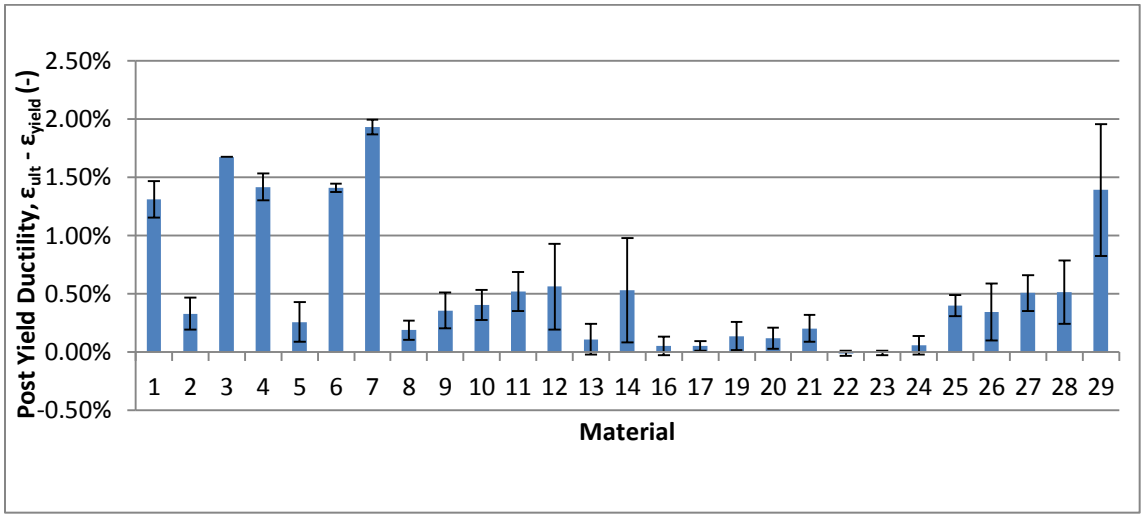

Figure 28: Post yield ductility (mean std dev) for 29 four point bending materials

As an assortment of different materials were tested, not just the same material at different densities, there is essentially no correlation between mechanical properties and density. In order to analyze the above results, it is useful to view properties with respect to a fixed variable. In this case, each variable is plotted with respect to the modulus of elasticity. Recall from above, increasing modulus should increase yield and ultimate stress, and have theoretically no effect on yield or ultimate strain.

There exists a positive correlation between yield stress and ultimate stress with the modulus of elasticity (Figure 29, Figure 30).There exists no correlation between yield strain and modulus of elasticity (Figure 31). There exists a negative correlation between ultimate strain and modulus of elasticity (Figure 32). As a result, post yield ductility, which depends on the previously reported strains, has a negative correlation with respect to modulus of elasticity (Figure 33).

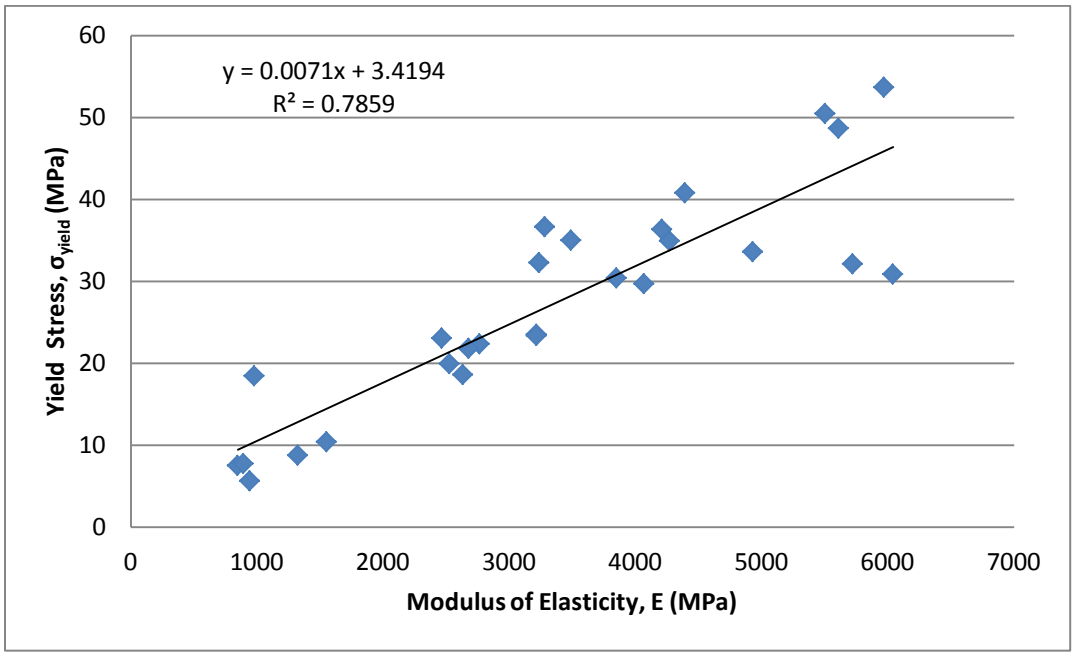

Figure 29: Correlation between yield stress and modulus of elasticity for 29 four point bending materials. The general trend is from low stiffness weak materials to high stiffness strong material

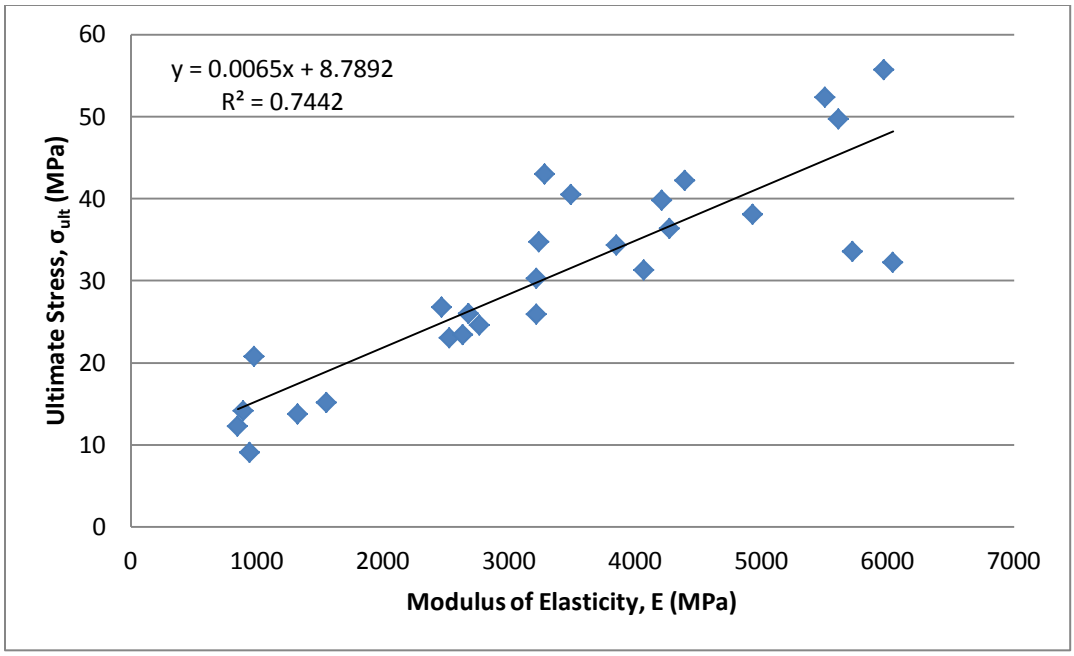

Figure 30: Correlation between ultimate stress and modulus of elasticity for 29 four point bending materials

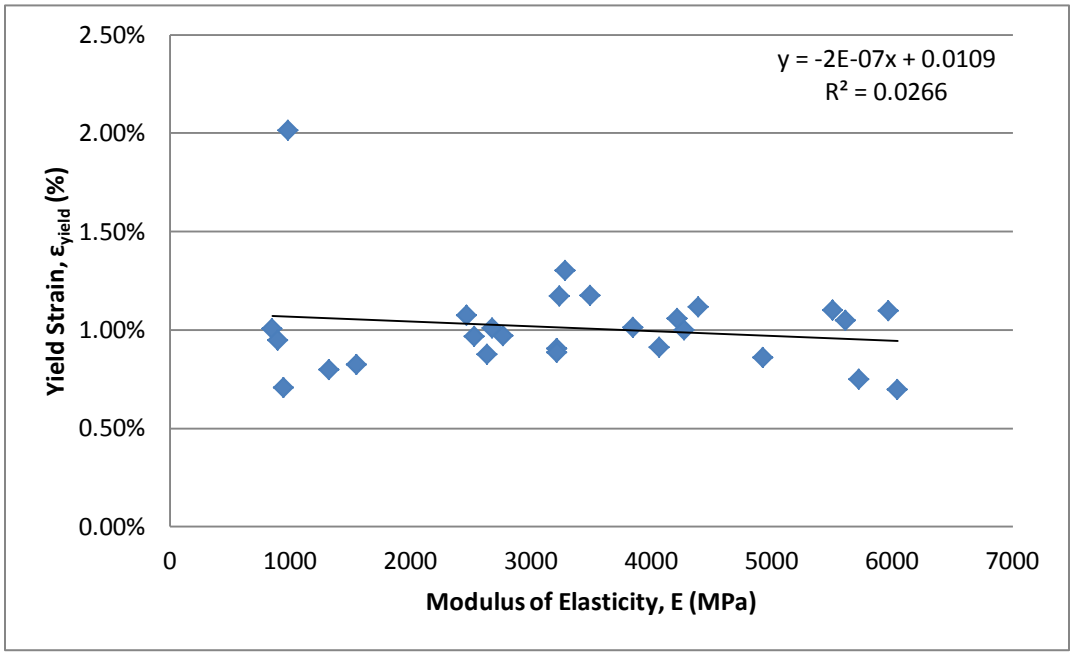

Figure 31: Correlation between yield strain and modulus of elasticity for 29 four point bending materials

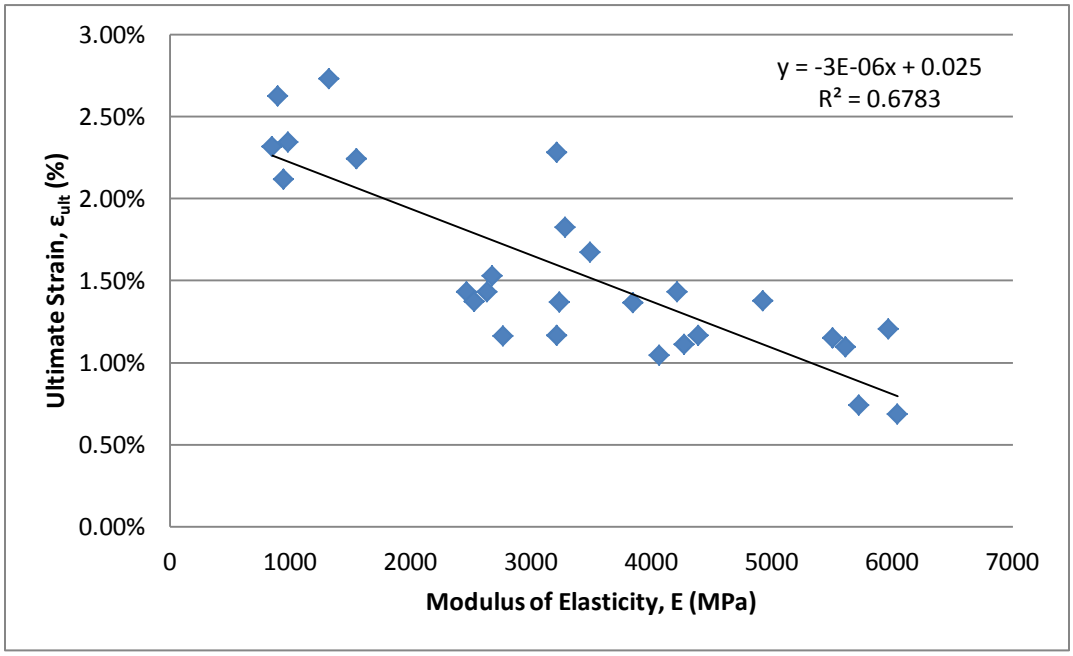

Figure 32: Correlation between ultimate strain and modulus of elasticity for 29 four point bending materials

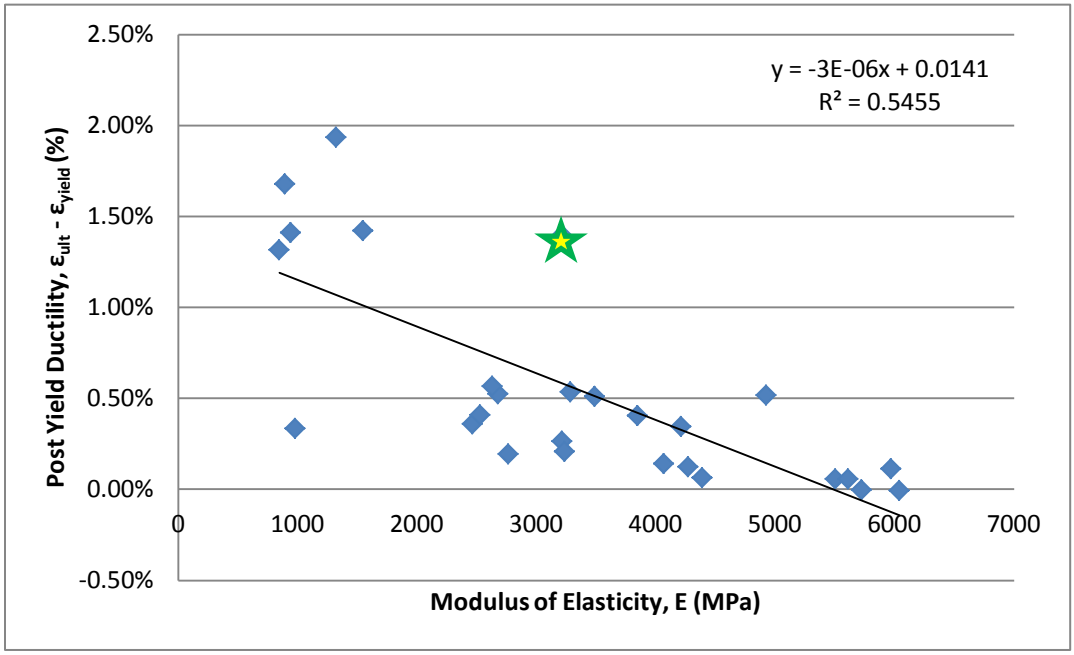

Figure 33: Correlation between post yield ductility and modulus of elasticity for 29 four point bending materials. Material 29 is highlighted by a star. This material exhibited increased post yield ductility, and a relatively high modulus of elasticity

2.3.4. Discussion

In most instances stiff, strong materials were extremely brittle, and would not be representative of human bone. However, one material (number 29), exhibited moderate strength (30.27 ± 3.27 MPa) and stiffness (3.2 ± .37 GPa), along with a markedly higher post yield ductility (1.39 ± .57%) than its competitors. This material is easily seen in Figure 33, highlighted by a star. As this was the only reasonably strong material that exhibited ductile behavior, it was used to manufacture a cancellous bone model.

These experimental results can be compared to the work of Gibson and Ashby by comparing their estimates based upon relative density. According to Gibson and Ashby, the modulus used to estimate 'solid' cancellous bone ($\frac{\rho_{apparent}}{\rho_{solid}}$ = 100%) is 12 GPa, with a corresponding strength of 136 MPa [93, 96]. These results are calculated by normalizing all densities to 2000 kg/m^3 (2 g/cm^3).

In order to obtain the same modulus of elasticity and strength with material 29, accurate morphology would need to be adjusted. By setting predictive equations equal to each other (Equation 12 a-c), the same modulus could be expected for relative densities of 1.93 times human relative density. As human vertebral bone typically falls in the range of 5-15% relative density, foams would need to manufactured with relative densities of approximately 9.65% - 28.95% [69, 98].

$$E = E_{G\&A}\left(\frac{\rho_{apparent}}{\rho_{solid}}\right)^{\mathbf{2}}_{G\&A} = E_{Exp}\left(\frac{\rho_{apparent}}{\rho_{solid}}\right)^{\mathbf{2}}_{Exp} \quad \textbf{(a)}$$

$$\left(\frac{\rho_{apparent}}{\rho_{solid}}\right)^{\mathbf{2}}_{Exp} = \frac{E_{G\&A}}{E_{Exp}} \left(\frac{\rho_{apparent}}{\rho_{solid}}\right)^{\mathbf{2}}_{G\&A} \quad \textbf{(b)}$$

$$\frac{\rho_{apparent}}{\rho_{solid}}_{Exp} = \sqrt{\frac{E_{G\&A}}{E_{Exp}}} \frac{\rho_{apparent}}{\rho_{solid}}_{G\&A} = \sqrt{\frac{12}{3.2}} \frac{\rho_{apparent}}{\rho_{solid}}_{G\&A} = 1.93 \frac{\rho_{apparent}}{\rho_{solid}}_{G\&A} \quad \textbf{(c)}$$

Equation 12 a-c: Foam theory comparing the modulus of elasticity reported in the literature and the collected experimental results

A similar process can be used to analyze relative density required to obtain reasonable strength. According to the required strength, relative densities 2.12 times greater than human values are needed. This analysis yields required apparent densities of 10.5 – 31.8% in order to obtain the appropriate yield strength. This corresponds very closely to estimates based on the modulus of elasticity.

Even though the required model's relative density will be nearly twice that of average vertebral cancellous bone, it is still within ranges reported by the literature, especially when taking additional anatomical sites (tibial metaphysis) into account. Furthermore, if more recent data and experimentally derived relationships are utilized, the expected performance of material 29 is drastically improved.

According to data from Kopperdahl and Keaveny, the relative density only needs to be 0.85 times that of human tissue in order to obtain an accurate modulus of elasticity. This holds for a power law relationship ($E=A\ \rho^B$) with A = 2.35 GPa, and B = 1.2. Furthermore, according to data from Morgan and Keaveny, the relative density only needs to be 1.1 times that of human tissue in order to obtain an accurate failure strength [69]. This holds for a power law relationship ($\sigma_{Ult}=A\ \rho^B$) with A = 37.1 MPa, and B = 1.74. Based on these estimates, it was determined that material 29 was acceptable to move forward with. The next steps required the creation of open-cell foam from material 29, and its subsequent characterization.

2.4.Mechanical Properties of Synthetic Cancellous Bone

2.4.1. Experimental Protocol - Synthetic Cancellous Bone Mechanical Test Methods

Unconfined compression tests were conducted in order to assess the performance of open-cell foam made from material 29. The manufacturing process was carried out by PRL, using a technique developed and patented by the company [55].

Six rectangular blocks of foam (130 x 180 x 40 mm) were manufactured on three separate days in order to assess not only foam properties, but inter-batch repeatability as well. Following shipping, blocks were allowed to acclimate to the laboratory environment for at least 24 hours post receipt. In order to obtain the most accurate results, the effect of specimen geometry, aspect ratio, and additional sources of potential variance were closely controlled.

The main protocol used in this study closely follows that of Keaveny et al., in order to enable direction comparison between the studies [69, 98]. A table saw with diamond blade was used to section off twelve rectangular specimens (20 x 20 x 40 mm) with a 2:1 aspect ratio from the center of each block. Six of those specimens (n=6) are being used in this study (Figure 34). Authors have shown this aspect ratio to produce repeatable and accurate results [97, 105]. This is a different geometry than that used by Keaveny (rectangular vs. cylindrical), however, these geometries with uniform aspect ratios were shown statistically similar by Linde et al. [97]. Specimens were numbered in the direction of processing in order to determine if the

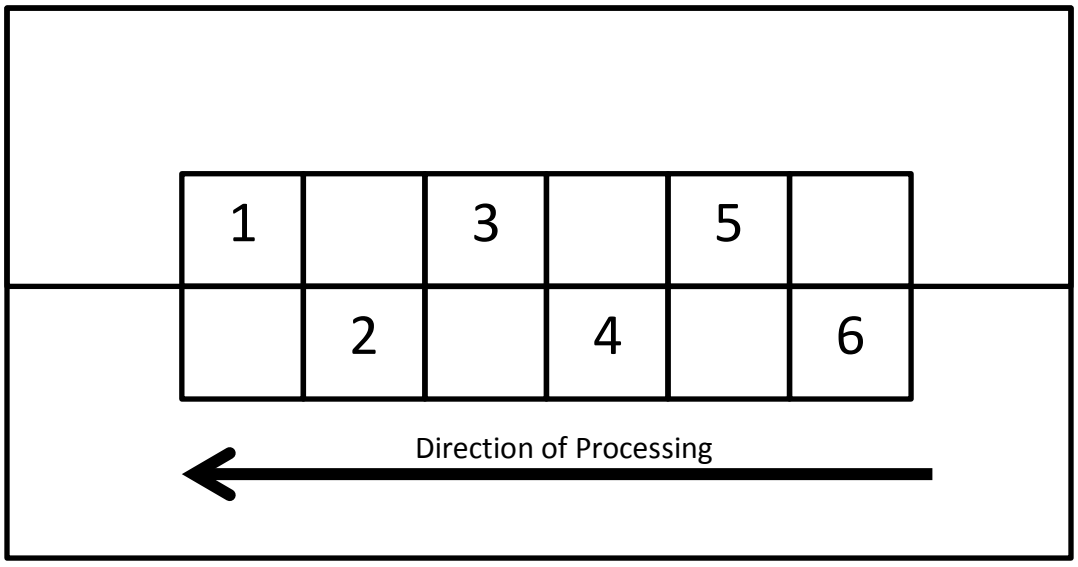

Figure 34: Diagram illustrating the location of each foam compression specimen in the large foam block received from PRL. The direction of processing was labeled by PRL to examine if the manufacturing process set up a gradient throughout the material. The six unlabeled specimens are being used in a different study

manufacturing process set up a density gradient through the length of the block. A density gradient could affect the mechanical properties, and would be undesirable. Direction of processing was labeled by PRL prior to shipping.

As previously mentioned, a key source of variation occurs if specimen ends are placed in direct contact with loading plates. To remediate this effect, each end was potted in 3.70 mm of Bondo, using a custom jig to maintain specimen alignment while curing. Testing was conducted one day following preparation, to allow Bondo to achieve maximum mechanical properties. Mechanical testing was conducted using an MTS 858 Mini Bionix Hydraulic Materials Testing Machine (Eden Prairie, MN). The machine was equipped with a 2.5 kN load cell, and self-aligning lower platen (**Figure 35**).

Figure 35: Experimental foam compression test setup. The lower platen is self-aligning, and the ends of each material were potted with filled polyester resin to prevent end artifacts.

The testing protocol was conducted as follows:

- Compress specimens to 5 N
- Cycle 5 times to .5% strain (≈.2mm) with a sine wave profile at 1 Hz
- Return to 5 N
- Compress to failure at (.05 mm/sec)
- Record applied load and platen displacement while compressing to failure

Analysis was conducted on several aspects of the collected data. First, blocks manufactured on the same day (n=6 x 2 blocks x 3 days) were analyzed to determine if they were statistically similar to each other. This was conducted by utilizing a two-tailed Student's T-test with 95% confidence ($H_0: \mu_1 = \mu_2, \alpha = .05$). Next, the three manufacturing days were compared to each other (n=12 x 3 days). As two blocks were manufactured each day, this step assumed those blocks were the same sample, thus doubling sample sizes from the previous analysis. Specimen parameters were calculated using a custom computer program (Matlab, Natick, MA). All statistical analysis was completed using SPSS 18.0 (SPSS, Inc., Chicago, IL).

2.4.2. Experimental Results and Analysis

Blocks manufactured on the same day were similar in some respects, while differing in several others. There was a significant difference in density between blocks A1 and A2 (Table 10). Logically, this difference is seen for the relative density as well. While densities were different, there was not a significant difference between most mechanical properties, and the null hypothesis ($H_0: \mu_0 = \mu$) was not rejected. The only variable this did not hold true for was post yield ductility, which was statistically different. Blocks B1 and B2 followed the same trend as blocks A1 and A2 (Table 11). There was a statistically significant difference between densities. This led to a difference in relative density, and post yield ductility. However null hypothesis was

not rejected for the remaining mechanical properties. Finally, blocks C1 and C2 had densities that did not statistically differ (Table 12). However, the modulus of elasticity, yield stress, and ultimate stress failed the null hypothesis and their differences were deemed statistically significant at 95% confidence.

Table 10: Multi-variate T-test comparing foam compression specimens from blocks A1 and A2 (Day 1). Statistical significance is reported for 95% confidence.

		t-test for Equality of Means		
		t	df	Sig. (2-tailed)
Density (gcc)	Equal variances assumed	5.485	8	.001
	Equal variances not assumed	5.602	7.038	.001
Relative Density (-)	Equal variances assumed	5.485	8	.001
	Equal variances not assumed	5.602	7.038	.001
Modulus (MPa)	Equal variances assumed	.430	8	.679
	Equal variances not assumed	.398	4.978	.707
Yield Stress (MPa)	Equal variances assumed	1.813	8	.107
	Equal variances not assumed	1.612	4.307	.177
Yield Strain (-)	Equal variances assumed	1.576	8	.154
	Equal variances not assumed	1.432	4.655	.216
Ult Stress (MPa)	Equal variances assumed	1.641	8	.139
	Equal variances not assumed	1.526	5.053	.187
Ult Strain (-)	Equal variances assumed	.561	8	.590
	Equal variances not assumed	.534	5.507	.614
Post Yield Ductility (-)	Equal variances assumed	-2.610	8	.031
	Equal variances not assumed	-2.296	4.149	.081

Table 11: Multi-variate T-test comparing foam compression specimens from blocks B1 and B2 (Day 2). Statistical significance is reported for 95% confidence.

		t-test for Equality of Means		
		t	df	Sig. (2-tailed)
Density (gcc)	Equal variances assumed	2.909	6	.027
	Equal variances not assumed	3.254	5.790	.018
Relative Density (-)	Equal variances assumed	2.909	6	.027
	Equal variances not assumed	3.254	5.790	.018
Modulus (MPa)	Equal variances assumed	1.465	6	.193
	Equal variances not assumed	1.783	5.765	.127
Yield Stress (MPa)	Equal variances assumed	.622	6	.557
	Equal variances not assumed	.583	3.569	.595
Yield Strain (-)	Equal variances assumed	-.088	6	.933
	Equal variances not assumed	-.080	3.341	.941
Ult Stress (MPa)	Equal variances assumed	.254	6	.808
	Equal variances not assumed	.241	3.705	.822
Ult Strain (-)	Equal variances assumed	-1.103	6	.312
	Equal variances not assumed	-1.057	3.818	.353
Post Yield Ductility (-)	Equal variances assumed	-4.567	6	.004
	Equal variances not assumed	-5.299	5.995	.002

Table 12: Multi-variate T-test comparing foam compression specimens from blocks C1 and C2 (Day 3). Statistical significance is reported for 95% confidence.

		t-test for Equality of Means		
		t	df	Sig. (2-tailed)
Density (gcc)	Equal variances assumed	1.850	7	.107
	Equal variances not assumed	1.713	4.189	.159
Relative Density (-)	Equal variances assumed	1.850	7	.107
	Equal variances not assumed	1.713	4.189	.159
Modulus (MPa)	Equal variances assumed	3.034	7	.019
	Equal variances not assumed	3.167	6.937	.016
Yield Stress (MPa)	Equal variances assumed	2.930	7	.022
	Equal variances not assumed	2.871	5.980	.029
Yield Strain (-)	Equal variances assumed	-.445	7	.670
	Equal variances not assumed	-.469	6.784	.654
Ult Stress (MPa)	Equal variances assumed	3.614	7	.009
	Equal variances not assumed	3.664	6.854	.008
Ult Strain (-)	Equal variances assumed	.377	7	.717
	Equal variances not assumed	.372	6.235	.722
Post Yield Ductility (-)	Equal variances assumed	1.258	7	.249
	Equal variances not assumed	1.283	6.936	.241

It is evident from the above results that the manufacturing process needs to be improved in order to reduce same day manufacturing variance. As manufacturing is still in its prototyping stages, this variance is expected to decrease.

One-way ANOVA was conducted to analyze the differences between multiple days of manufacturing (Appendix A: Foam Testing ANOVA Tables - Table 37). Material properties were the dependent variables, while the day of manufacturing was the factor across which they were analyzed. When analyzing across manufacturing days, only the ultimate strain and post yield

ductility showed statistical difference. A post hoc analysis (Scheffe) revealed that blocks made on days one and two were statistically similar, while day three differed. Day three had approximately .3% smaller ultimate strain, and .1% - .2% smaller post yield ductility. The large variation seen between same day manufacturing that was highlighted above actually served to increase the 'within groups' error, and therefore increase the likelihood that multiple days would produce statistically similar blocks.

As mentioned above, the direction of processing was carefully controlled and labeled by PRL prior to shipping. This allowed analysis to determine if there was a gradient along this direction, or if specimens taken from a block could be considered uniform regardless of their location. Similar to the previous section, one-way ANOVA was conducted with each material property as dependent variables, and the specimen number (location in block) as the factor (Appendix A: Foam Testing ANOVA Tables - Table 38). This analysis revealed no statistical difference between any material properties as a result of specimen location. This suggests that blocks can be considered uniform, and specimens removed from any of the areas tested. It should be noted that no specimens were used within 10 mm of any edge, where material properties are likely to change due to the manufacturing process.

Based on the above analysis, some material properties currently show high variance. However, it is expected that foam variance will decrease as manufacturing moves from prototyping to full scale production. Therefore, it seems reasonable to now analyze the average foam performance in order to facilitate comparison with the literature (Table 13).

Table 13: Mean, standard deviation, and range of values for the synthetic foam compression specimens (n=27).

Variables	Range	Minimum	Maximum	Mean	Std. Deviation
Density (gcc)	.15	.46	.61	.52	.04
RelativeDensity	.10	.31	.42	.36	.02
Modulus (MPa)	211.00	274.05	485.05	375.93	54.58
YieldStress (MPa)	2.22	2.89	5.11	3.81	.61
YieldStrain (%)	.99%	.98%	1.97%	1.43%	.26%
UltStress (MPa)	2.53	3.33	5.86	4.33	.68
UltStrain (%)	.80%	1.53%	2.33%	1.94%	.27%
PostYldDuctility (%)	.78%	.09%	.88%	.51%	.17%

2.4.3. Experimental Comparison to Human Bone

Each of the parameters previously recorded has been compared to human bone through an intensive literature review. The density of the chosen synthetic material is not intended to mimic that of human tissue. As such, it is unnecessary to compare the density of the synthetic material to that of human bone. The critical parameter when assessing morphology is the structure's relative density. As relative density was commonly not given in the literature concurrently with accurate mechanical values, it was derived from previous reports. This was conducted by dividing the given apparent densities by 2 g/cm^3 [93].

Table 14: Comparing synthetic open-cell foam to human vertebral cancellous bone reported in the literature - Relative Density - ρ*/ρs

Study	N	Mean	Std. Dev	Range	Minimum	Maximum
Current Study	27	35.61%	2.49%	10.18%	31.46%	41.64%
Morgan / Keaveny [69]	30	9.00%	2.50%	-	-	-
Kopperdahl / Keaveny [98]	22	8.50%	2.00%	7.50%	5.50%	13.00%
Banse [64]	63	8.70%	2.60%	12.50%	4.50%	17.00%

This study produced and analyzed foams that are morphologically dissimilar to vertebral cancellous bone (Table 14). However, a 35% relative density is not out of the range of human values. In fact, these are values that may be seen in long bones, certainly in the femoral neck [69]. A further note, as will be seen below, a reduced density will be used in future manufacturing due to elevated mechanical properties. This change will allow the synthetic model to become more morphologically similar to human vertebral cancellous bone.

The modulus of elasticity is a very close fit with the reported literature (Table 15). It falls within the range of reported values for all three studies. While easy to perform, a Student's T-test is not recommended for comparing multiple studies. This leads to an increased risk of type I errors. ANOVA generalizes the T-test to multiple samples, and can provide an analysis of whether or not means are statistically similar. As such, single factor ANOVA was used to analyze whether there was a statistical difference between the current study and the literature (Appendix A: Foam Testing ANOVA Tables - Table 39). This Analysis revealed statistically similar results. As such, the modulus of elasticity of the synthetic foam produced in this study can be considered equivalent to the human specimens reported on in the literature.

Table 15: Comparing synthetic open-cell foam to human vertebral cancellous bone reported in the literature - Modulus of Elasticity - E (MPa)

Study	n	Mean (MPa)	Std. Dev (MPa)	Range (MPa)	Minimum (MPa)	Maximum (MPa)
Current Study	27	376	55	211	274	485
Morgan / Keaveny [69]	30	344	148	785	90	875
Kopperdahl / Keaveny [98]	22	291	113	446	90	536
Banse [64]	63	352	145	598	127	725

The yield stress observed in the synthetic model is noticeably higher than the averages reported in the literature (Table 16). That said, it still falls within the range of values reported by Morgan and Keaveny. A difference in means was confirmed via single factor ANOVA as described above (Appendix A: Foam Testing ANOVA Tables - Table 40). The test F-value is higher than the F_{crit}, indicating significant difference of the means, and rejection of the null hypothesis.

Table 16: Comparing synthetic open-cell foam to human vertebral cancellous bone reported in the literature - Yield Stress - σ_{yield} (MPa)

Study	n	Mean (MPa)	Std. Dev (MPa)	Range (MPa)	Minimum (MPa)	Maximum (MPa)
Current Study	27	3.8122	0.61	2.21	2.89	5.11
Morgan / Keaveny	30	2.02	0.92	4.10	0.50	4.60
Kopperdahl / Keaveny	22	1.92	0.84	3.15	0.56	3.71

Yield strain is noticeably higher in the synthetic model compared to the literature (Table 17). This is partially due to a testing artifact. It has been shown by Keaveny, Gibson and Hayes that cancellous bone is fully linear, and does not exhibit a nonlinear toe region if strain is appropriately measured, with an extensometer [95, 112].

Table 17 Comparing synthetic open-cell foam to human vertebral cancellous bone reported in the literature - Yield Strain - ε_{yield}

Study	N	Mean	Std. Dev	Range	Minimum	Maximum
Current Study	27	1.43%	0.259%	0.99%	0.98%	1.97%
Morgan / Keaveny	30	0.77%	0.060%	-	-	-
Kopperdahl / Keaveny	22	0.84%	0.060%	0.20%	0.75%	0.95%

Additional work was conducted to correct yield strain values. This was done by extending the best fit curve of the linear region to the x-axis, and setting the intersection as the new origin. This can be visualized in Figure 22 on page 60 by subtracting (B-A) from all strain measurements. These corrected measurements demonstrate that the synthetic model compares much more closely with the literature than previously presented. While this assumption certainly needs to be verified by future work, it is currently accepted as a result of the synthetic bone being mechanically and morphologically similar to cancellous bone tested in previously reported studies. Once corrected, the mean synthetic bone value is slightly outside the range of reported values by Kopperdahl and Keaveny (Table 18). This discrepancy is confirmed by single factor ANOVA, which reports a significant difference between the means (Appendix A: Foam Testing ANOVA Tables - Table 41).

Table 18: Comparing synthetic open-cell foam to human vertebral cancellous bone reported in the literature - Yield Strain Corrected - ε_{yield}

Study	N	Mean	Std. Dev	Range	Minimum	Maximum
Current Study	27	1.12%	0.117%	0.470%	0.930%	1.400%
Morgan / Keaveny	30	0.77%	0.060%	-	-	-
Kopperdahl / Keaveny	22	0.84%	0.060%	0.20%	0.75%	0.95%

The ultimate stress calculated in this study is higher than the mean values presented in the literature (Table 19). It is however within the ranges presented by both Kopperdahl and Keaveny, and Banse for human vertebral cancellous bone. Single factor ANOVA was conducted to determine if the means were statistically similar. A cursory look at the ultimate stress comparison table is confirmed by the analysis of variance (Appendix A: Foam Testing ANOVA Tables - Table 42). A difference between the means was found statistically significant, and the null hypothesis rejected.

Table 19: Comparing synthetic open-cell foam to human vertebral cancellous bone reported in the literature - Ultimate Stress - σ_{ult} (MPa)

Study	n	Mean (MPa)	Std. Dev (MPa)	Range (MPa)	Minimum (MPa)	Maximum (MPa)
Current Study	27	4.33	0.68	2.53	3.33	5.86
Kopperdahl / Keaveny	22	2.23	0.95	3.63	0.70	4.33
Banse	63	2.37	1.14	5.57	0.60	6.17

In order to analyze ultimate strain, a procedure identical to that used for the analysis of yield strain was utilized. First the reported values were observed, and it was observed that the synthetic model's ultimate strain is substantially higher than the mean values presented in the literature (Table 20). After correcting the strain values for the initial nonlinear toe region, the model performs much closer to reported mean values from the literature (Table 21).

Table 20: Comparing synthetic open-cell foam to human vertebral cancellous bone reported in the literature - Ultimate Strain - ε_{ult}

Study	N	Mean	Std. Deviation	Range	Minimum	Maximum
Current Study	27	1.94%	0.27%	0.80%	1.53%	2.33%
Kopperdahl / Keaveny	22	1.45%	0.33%	1.34%	0.96%	2.30%
Banse	63	1.19%	0.26%	1.29%	0.72%	2.01%

The corrected mean value falls within the range of reported ultimate strains in both comparison studies. An analysis of variance and post hoc analysis revealed that the synthetic model is statistically similar to the work by Kopperdahl and Keaveny at 97.5% confidence (F_{crit} = 5.4). At 95% confidence, the results are statistically dissimilar. An ANOVA conducted between

the current study and that of Kopperdahl and Keaveny highlights this difference (Appendix A: Foam Testing ANOVA Tables - Table 43).

Table 21: Comparing synthetic open-cell foam to human vertebral cancellous bone reported in the literature - Ultimate Strain – Corrected ε_{ult}

Study	N	Mean	Std. Deviation	Range	Minimum	Maximum
Current Study	27	1.62%	0.19%	0.74%	1.27%	2.00%
Kopperdahl / Keaveny	22	1.45%	0.33%	1.34%	0.96%	2.30%
Banse	63	1.19%	0.26%	1.29%	0.72%	2.01%

The only study in the literature to report both ultimate and yield properties is by Kopperdahl and Keaveny. The post yield ductility of the model compares very well with the literature. Its mean value is within one standard deviation of the literature, and easily falls within the range of reported values (Table 22). A one-way ANOVA confirms these observations. At 95% confidence, the alternative hypothesis is rejected, and the means can be assumed statistically similar (Appendix A: Foam Testing ANOVA Tables - Table 44). As a general note, post yield ductility does not need to be corrected to account for the nonlinear toe region. As it is the difference between strains well away from the artifact, it is unaffected.

Table 22: Comparing synthetic open-cell foam to human vertebral cancellous bone reported in the literature - Post Yield Ductility - ε_{ult} - ε_{yield}

Study	N	Mean	Std. Dev	Range	Minimum	Maximum
Current Study	27	0.51%	0.17%	0.78%	0.09%	0.88%
Kopperdahl / Keaveny	22	0.61%	0.34%	1.14%	0.21%	1.35%

As demonstrated in the section on Foam Theory (pg. 52) the modulus of elasticity and strength are expected follow a power relation raised to the second power with respect to relative density. Furthermore, yield and ultimate strain should be constant with respect to relative density. Due to the limited range of relative densities checked, the exact relationship between relative density and mechanical properties is difficult to determine.

The following graphs for modulus of elasticity and strength are presented in similar fashion to Gibson and Ashby. Human properties are normalized with respect to tissue level material properties: density - 2 g/cm^3 [93], modulus of elasticity - 2350 MPa [98], and strength - 37.1 MPa [69].

The modulus of elasticity was related to relative density raised to the 1.23 power. This correlates very well with the results presented by Kopperdahl and Keaveny that suggest a relation to the 1.2 power (Figure 36). The main difference between the results is a scale factor denoted by the leading coefficient. The current study had a lead coefficient .57 times that of the

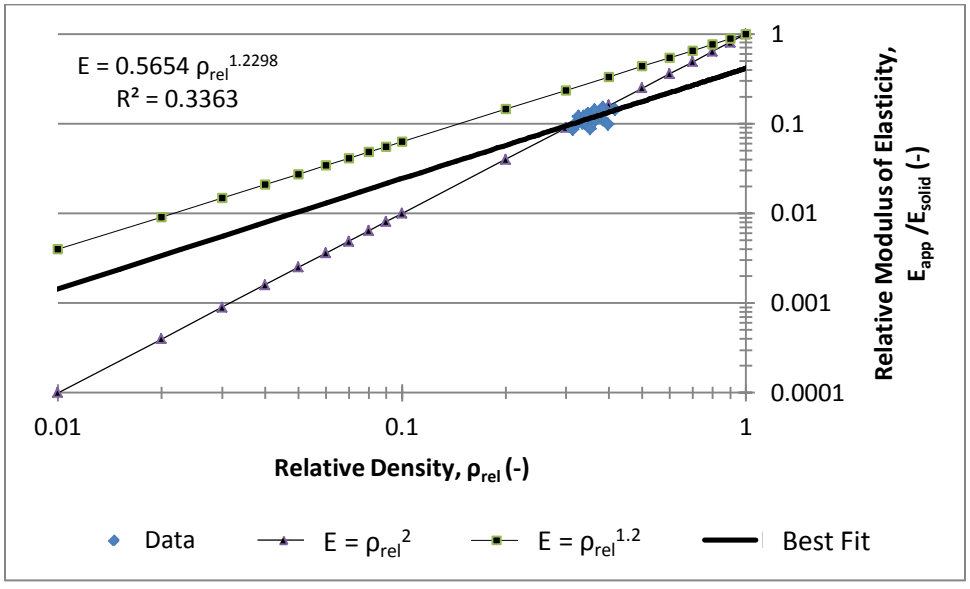

Figure 36: Normalized modulus of elasticity plotted against relative density. Literature moduli normalized with respect to 2.35 GPa. Literature apparent densities normalized with respect to 2 g/cm^3.

literature. Both of these studies differ from the theoretical relation to the second power as suggested in previous sections. It is unknown whether this model actually behaves as suggested, or if a larger range of relative densities should be tested in order to more accurately assess the relationship. The Pearson's correlation coefficient suggests a weak to moderate correlation.

Yield strength was related to relative density raised to the 1.39 power. This is lower than both theoretical results (second power) and the work of Morgan and Keaveny (raised to 1.74). Future study over a larger change in relative density is suggested to increase model accuracy. The Pearson's correlation coefficient suggests a weak to moderate correlation (Figure 37).

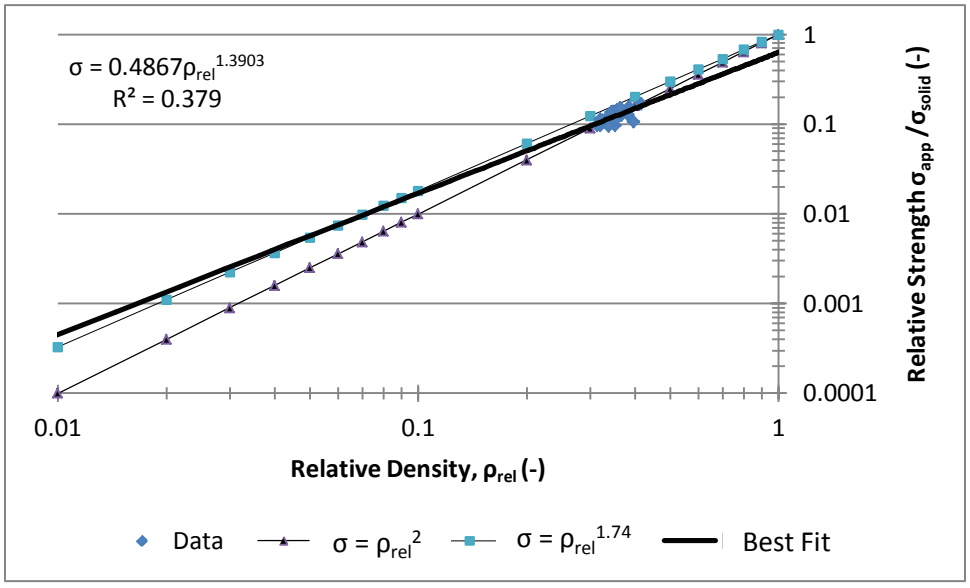

Figure 37: Normalized ultimate strength plotted against relative density. Literature strength normalized with respect to 37.1 MPa. Literature apparent densities normalized with respect to 2 g/cm^3.

Failure strain was related to relative density to the negative .12 power (Figure 38). This agrees well with theoretical analysis and the literature. Both sources suggest a weak to nonexistent relationship between these parameters, as outlined in the section on Foam Theory.

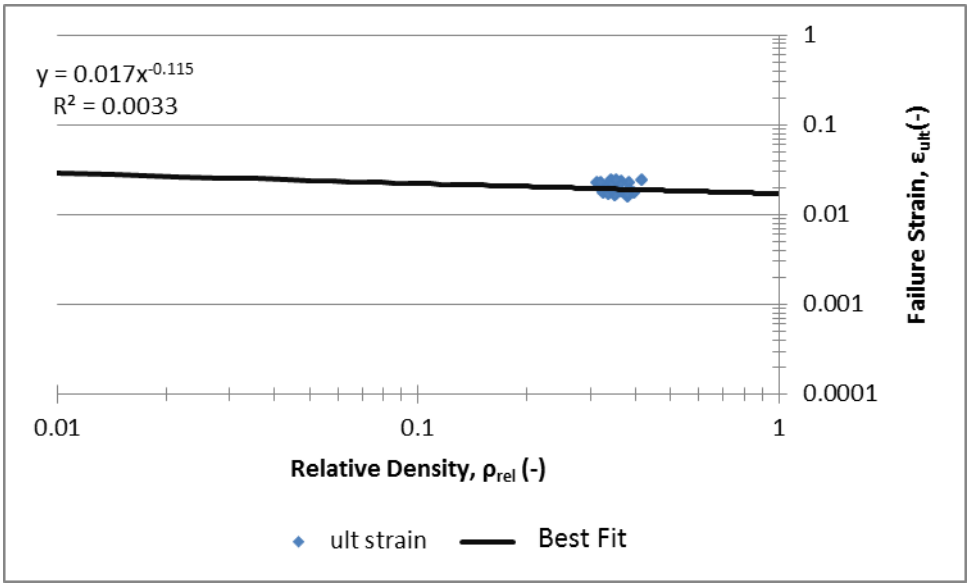

Figure 38: Failure strain plotted against relative density. Literature reports no relation with respect to failure strain. The synthetic model performs similarly, with a very low correlation coefficient.

2.4.1. Discussion

Overall it appears the synthetic cancellous bone developed by this study acts as a successful model of human cancellous bone. At the relative density studied, all of the mechanical and morphological properties are on the high end of values reported for vertebral cancellous bone. Future batches of this foam should utilize a lower relative density in order to become more mechanically and morphologically realistic (Table 23).

Analysis of Table 23 highlights the need to reduce relative density as a means of decreasing yield and ultimate stresses as well as for improved morphological accuracy. The key downside to this suggestion is that decreasing the relative density would also decrease the modulus of elasticity (strain should remain constant). However, it is worth re-highlighting a key discrepancy between our study, and the reported literature that is being compared to. Specimen strain in this study was recorded using platen displacement instead of an extensometer. The difference between these two techniques has been analyzed by Keaveny, Gibson and Hayes [112]. While yield and ultimate stress will be unaffected, our model most

Table 23: Summary of synthetic cancellous bone performance

Parameter	Comparison to Literature Mean		Comparison to Literature Range		Suggested Action
ρ^*/ρ_s	High	↑	Outside	↑	Reduce ρ^*/ρ_s
E (MPa)	Accurate	≈	Within	≈	
σ_{yield} (MPa)	High	↑	Within	≈	Reduce ρ^*/ρ_s
ε_{yield}	High	↑	Outside	↑	
σ_{ult} (MPa)	High	↑	Within	≈	Reduce ρ^*/ρ_s
ε_{ult}	High	↑	Within	≈	
$\varepsilon_{ult} - \varepsilon_{yield}$	Accurate	≈	Within	≈	NA

↑ - Indicates values are higher than the reported mean / range

≈ - Indicates values are approximately equal to the mean / in range

likely has increased stiffness, and decreased yield and ultimate strain. These changes likely hold true even over the corrected strain values discussed above. As can be seen in Figure 39, using an extensometer not only eliminates the nonlinear toe region (corrected for above), but also records stiffer performance.

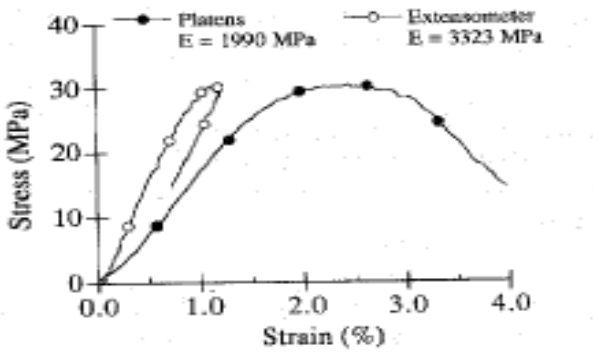

Figure 39: Comparison of strain measurement techniques on recorded specimen behavior [112]. Use of an extensometer results in stiffer specimen performance. (Reprinted with permission of Elsevier©)

If the material properties from this study were corrected for the use of an extensometer, there would be some slight changes in its comparison to the literature. Table 24 illustrates the expected performance of the synthetic cancellous bone described in this study if strain had been collected using an extensometer. The modulus, yield strength and ultimate strength are all higher than the reported literature for vertebral cancellous bone. There should be reductions to the yield and ultimate strains, as they are affected by measurement technique. Strain values are minimally dependent on specimen relative density as highlighted above. As a result, decreasing the relative density should only have positive effects on the final model performance. This work will be conducted in future studies.

Table 24: Summary of expected synthetic cancellous bone performance if strain had been recorded by an extensometer mounted to the specimen midsection

Parameter	Comparison to Literature Mean		Comparison to Literature Range		Suggested Action
ρ^*/ρ_s	High	↑	Outside	↑	Reduce ρ^*/ρ_s
E (MPa)	High	↑	Within	≈	Reduce ρ^*/ρ_s
σ_{yield} (MPa)	High	↑	Within	≈	Reduce ρ^*/ρ_s
ε_{yield}	High	↑	Within	≈	NA
σ_{ult} (MPa)	High	↑	Within	≈	Reduce ρ^*/ρ_s
ε_{ult}	High	↑	Within	≈	NA
$\varepsilon_{ult} - \varepsilon_{yield}$	Accurate	≈	Within	≈	NA

↑ - Indicates values are higher than the reported mean / range

≈ - Indicates values are approximately equal to the mean / in range

Chapter 3. – The Lumbar Spine

The following chapter discusses the overall performance of an analogue lumbar spine model. An introduction to the form and function of the lumbar spine is followed by a description of its mechanical properties. Included in this is a discussion of in-vivo and in-vitro testing, and the effects of specimen preparation and test setup on measured values. The chapter concludes with analysis of a model created to mimic the lumbar spine.

3.1.Form and Function

The composition and structure of the human lumbar spine has been covered in detail in Section 1.2: Spinal Anatomy. The following section covers the mechanical and sensory nature of the lumbar spine, as well as a description of the functional spinal unit.

3.1.1. Function: Support and Protection

The main biomechanically relevant functions of the human spinal column are the support of the human body, and protection of the spinal cord. The spinal column serves as the main component of the axial skeleton. It provides insertion sites for the skull, rib cage, and pelvis. These connections facilitate interaction between the components including load transfer. A reason why the lower back is so commonly injured is its role in load transfer. The majority of upper body weight is transferred through the lumbar spine. This makes regions with curvature out of alignment with applied loads subject to high shear forces and bending moments. The L5-S1 level is one such level, and a common source of LBP. The expected loads and motions of the lumbar spine will be covered in much further detail in section 3.2.1 - Biomechanics of the Lumbar Spine In-vivo.

The spinal cord primarily runs through the central vertebral foramen, branching out between the intervertebral foramen. The spinal cord is fairly compact above L1-L2. Below that

level it branches out into a structure referred to as the cauda equina. At the cauda equina, nerves branch out from the spinal cord through vertebral foramen, and openings in the pelvic bones. These nerves are responsible for communicating with the lower appendages. The bony structures of the lumbar spine provide openings through which the spinal cord and nerves may safely travel. Furthermore, the bony structures protect these elements from potentially harmful contact.

3.1.2. Function: Sensory

Hard tissues are not the only innervated structures of the lumbar spine. As previously mentioned, most researchers easily recognize the role of ligaments and soft tissues as sensory structures [82-85, 88]. The lumbar spine is innervated by the sinuvertebral nerve and posterior primary ramus [84]. The Sinuvertebral nerve originates from the anterior portion of the spinal nerve, distal to the spinal ganglion. This branch is shortly connected with a sympathetic branch of the ramus communicans (Figure 40) [82, 84]. This combined structure passes through the intervertebral foramen into the spinal canal. Impingement of this nerve as it passes through the foramen can be a large source of pain. This can also occur as a result of disc herniation. From the canal, the main filament moves cranially from the pedicle base to the posterior longitudinal ligament. At this point it branches into inferior, superior and transverse branches. The sinuvertebral nerve is also known to supply the vertebral body, neural laminae, adjacent to the intervertebral disc, posterior longitudinal ligament, internal vertebral plexus, epidural tissue and dura matter. Early studies presumed these nerves to mediate pain, thermal sensation and proprioception. The posterior primary ramus originates from the spinal nerve lateral to the intervertebral foramen [84]. It separates into medial and lateral branches. The medial branch descends posterior to the transverse process. This branch innervates the inferior articular capsule of the facet joint. It also sends fine nerves to the superior capsule of adjacent caudal

level. It then moves into the dorsal muscles, where it finally anastomoses with nerves from the adjacent levels. The lateral branch is composed of cutaneous nerves that reach distally to the greater trochanter.

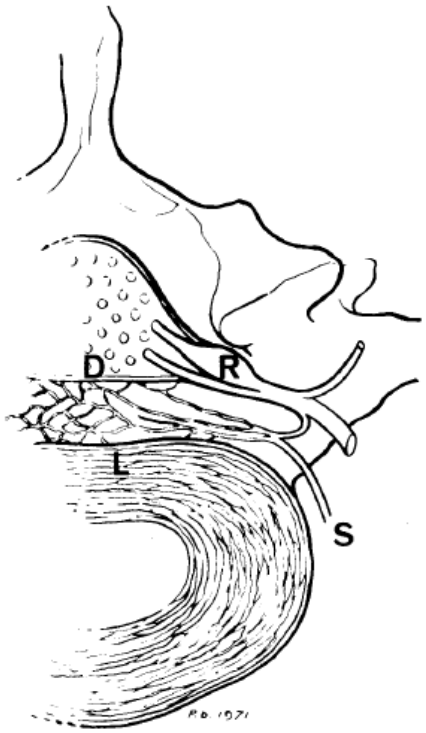

Figure 40: Cross section of the lumbar spine illustrating the sinuvertebral nerve. R-Root, S-Sympathetic, L-Annulus Fibrosus, D-Anterior Dura [84]. (Reprinted with permission of Wolters Kluwer Health©)

The soft tissues of the lumbar spine are widely innervated. The intervertebral disc has nerve endings located in the peripheral part of the annulus fibrosus. Nerve Fibers have been observed on the surface and into the outer fibers of the annulus. The nucleus pulposis appears to be devoid of nerve endings, and is therefore likely insensitive. Surface fibers have encapsulated endings, while the majority of fibers in the outer AF are un-encapsulated. These un-encapsulated fibers are likely sensitive to pain [82, 84, 88, 121].

The posterior longitudinal ligament is innervated by the sinuvertebral nerve. Fibers overlap medial lateral with the same nerves on the opposite side of the body. They also overlap

inferior and superior with branches from adjacent segments. The PLL contains a variety of encapsulated and un-encapsulated nerve endings. These fibers are the first to be impinged on by disc protrusion, and are therefore likely culprits for discogenic pain [82, 84, 85, 121].

The anterior longitudinal ligament is supplied by branches of the sympathetic nervous system. Similar to the PLL, fibers overlap from medial to lateral, and from adjacent levels. Both encapsulated and naked endings have been observed in this ligament [82, 84, 85].

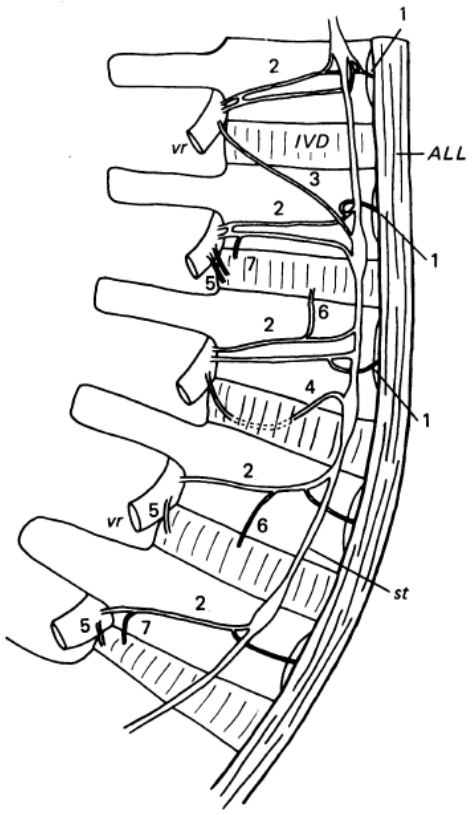

Figure 41: Innervation of the lumbar spine. ALL-Anterior Longitudinal Ligament, IVD-Intervertebral Disc, st-sympathetic trunk, vr-ventral rami, 1-nerves to ALL, 2-rami crossing vertebral bodies to psoas, 3-ramus communicans from fibers to psoas, 4-deep ramus comunicans, 5-branches to IVD from vr, 6-branches to lateral IVD, 7-branches to posterolateral IVD [82]. (Reprinted with permission of John Wiley and Sons, Inc.©)

The ligamentum flavum, interspinous and supraspinous ligaments are similarly innervated. The LF is supplied superficially by the overlying muscles, and deeply by nerves terminating in the posterior epidural space. Most researchers conclude that no fibers terminate

within these ligaments; instead they have limited superficial terminations. It has been suggested that they are only sensitive to chemical irritation [84, 85].

The innervation of the lumbar spine has far reaching clinical implications [82, 84]. Most nerves supply several adjacent levels and there is sufficient overlap between nerves. This may be responsible for the inability of patients and physicians to precisely locate the origin of pain generators. Additionally, spinal muscles, hard and soft tissues are all innervated. As a result, LBP can occur in all these potential locations. The dorsal and ventral rami supply the majority of these structures. Excess strain is a leading cause of nerve pain, along with possible fractures, mechanical irritation (impingement), hypertension, venous engorgement of the epidural veins, and various pathologies.

A large reason for the clinical success of spinal fusion is due to its ability to mediate a majority of these potential pain generators. It effectively limits motion (strain), restores disc height (mechanical irritation), and inflamed tissue can be removed (pathologic nerve fibers and soft tissue). In contrast, alternative such as intervertebral disc replacement restore disc height, and remove the majority of the IVD, but still allows motion. If pain isn't located within the IVD, or height restoration is ineffective at reducing nerve impingement, then while the procedure may be a surgical success, pain may continue.

3.1.3. The Functional Spinal Unit

Biomechanical analysis of the human spine is often conducted on a Functional Spinal Unit (FSU). An FSU "is the smallest functional spinal unit exhibiting the generic biomechanical characteristics of the spine" [20]. It is composed of two vertebrae, an intervertebral disc, and the associate ligaments (Figure 42).

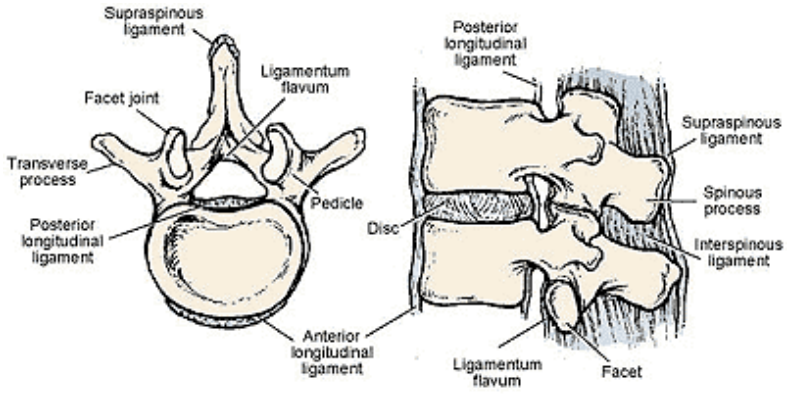

Figure 42: The functional spinal unit (FSU) and associated soft tissues. These tissue include all single and multilevel ligaments: ALL, PLL, LF, CL, TL, ISL, SSL [122]. (Reprinted with permission of ©2011 Spine Center, Hospital for Joint Diseases, New York University)

The FSU is viscoelastic, absorbs energy, moves with six degrees of freedom, has coupled motion, and relies on its hard and soft tissues for mechanical stability [17]. Furthermore, the FSU is often used in mechanical testing as it simplifies the test setup, is less expensive, and allows for more controlled experiments. Reducing the number of levels reduces the number of variables that can influence the experiment, simplifying analysis and possible sources of error. When using human spines, their costly nature drives researchers to utilize them as best as possible. By sectioning a full lumbar spine into several FSUs, several tests can be run, and comparisons made across multiple levels from the same individual.

3.2.Mechanical Properties of the Human Lumbar Spine

3.2.1. Biomechanics of the Lumbar Spine In-vivo

There have been very few in-vivo studies conducted that measure parameters common to in-vitro testing. This is due to the invasive nature of most measurements, and an inability to apply concentrated known loads or moments in-vivo.

Wilke et al. performed an in-vivo study by instrumenting an internal fixator to measure forces and moments in 3 orthogonal directions. While most test setups apply uniform moments

(discussed in Section 3.2.3), in-vivo the spine is subject to a combination of forces and moments from external loads and muscle contractions. The experimental setup from Wilke et al. was designed to measure these unknown loads [123]. Researchers instrumented bisegmental internal spinal fixation devices which were then implanted into 10 patients about to undergo anterior interbody fusion. During bending activities, researchers found a range of loads and moments (mean ± standard deviation) of 250N, and 3.5 Nm. However, these are in patients recovering from surgery, which are most likely not going through the same range of motions and loads to be expected from an intact healthy spine.

While loads and moments are extremely difficult to obtain in-vivo, several researchers have been able to collect intradiscal pressure measurements. Nachemson et al. performed an in-vivo study collecting intradiscal pressure in human subjects. They discovered that forces of at least 2.5 kN can be resisted by the lumbar IVD while a person is seated and holding a 22.7 kg weight [124]. Work on this study is supported by a later study conducted by Wilke et al. They discovered good correlation with Nachemson's results, even with their limited sample size (n=1) [125]. Other analyses have concluded that during walking, the range of axial force exerted on the spine is in the range of .2 to 2.5 times body weight [126].

While the measurement of in-vivo loads is extremely difficult and invasive, several imaging studies have been performed to reveal information about physiological ranges of motion. In the lumbar spine, ROM for flexion-extension typically falls between 9 and 14° [127]. Other studies have shown mean lumbar FSU motion from 6.3° to 12° for flexion-extension, and 5.7° to 12° for lateral bending [128]. An extensive study by Dvorak et al. reported level by level ROMs for intact healthy patients subject to flexion-extension and lateral bending [129].These subjects bent to their furthest extent, and were then aided by a clinician who applied a force allowing them to bend until discomfort was felt. This study therefore represents the maximum

expected ROM in non-traumatic circumstances for healthy individuals. ROM was found to increase moving caudally from the L1-L2 joint to L5-S1. These rotations averaged 11.9° - 17.0° between peak flexion and extension. In lateral bending, the range of averages motion was between 5.1° -12.4°. In lateral bending there was not a monotonic increase from one level to the next. Instead peak ROM was found in L2-L3, and L3-L4, with small ROMs in adjacent segments. A study by McGregor et al. dynamically analyzed the spine in-vivo. It analyzed the ROM for the full lumbar spine in flexion-extension, lateral bending and axial rotation [130]. Furthermore, it assessed the rate of motion, providing a range of physiologically relevant test parameters. Rates were collected for the whole lumbar spine, but an average FSU rate of motion can be calculated from this data assuming a uniform rate between levels. Flexion experience 13.8° of motion at 7.6°/sec, extension 5.5° at 6.2°/sec, lateral bending 7.66° at 7.4°/sec, and axial rotation 6.70° at 7.9°/sec. These values correspond well with the previously mentioned radiographic studies, and show rates of motion typical to physiologic motion.

3.2.2. Specimen Preparation

The effect of preparation on specimen properties has been investigated by several researchers. Specialized storage (less than -20°C) is required to preserve a specimen's mechanical properties [38]. Additionally, specimens can't be embalmed to preserve soft tissues as it affects the overall mechanical properties [15].These observations have been checked independently on intervertebral discs [131], the annulus fibrosis [132], cancellous bone [113], intervertebral joints [133], tendons [134], and ligament [135]. Furthermore, if accurate soft tissue properties are required, there is only a 20 hour window during which testing may occur. If a specimen is thawed, and left out of a freezer any longer the soft tissue is substantially degraded, and the results become unreliable [37]. Tests on multiple freeze-thaw cycles have determined that up to three cycles may be used before degradation of soft tissue mechanical

properties occurs [39]. Hard tissues can undergo several more freeze thaw cycles and still be viable. However defatting the specimens can lead to a 30% increase in stiffness, and 50% decrease in energy dissipation [113].

3.2.3. Mechanical Characterization

The human FSU and full segment both display a highly nonlinear sigmoid behavior between load and deflection (Figure 43). This behavior is composed of a neutral zone and an extension zone. This non-linear stiffness is critical to the performance of the human spine. Large deflections occur in the neutral zone with little applied load. While large loads are required to move the spine within the extension zone. There is also a noticeable hysteresis between loading

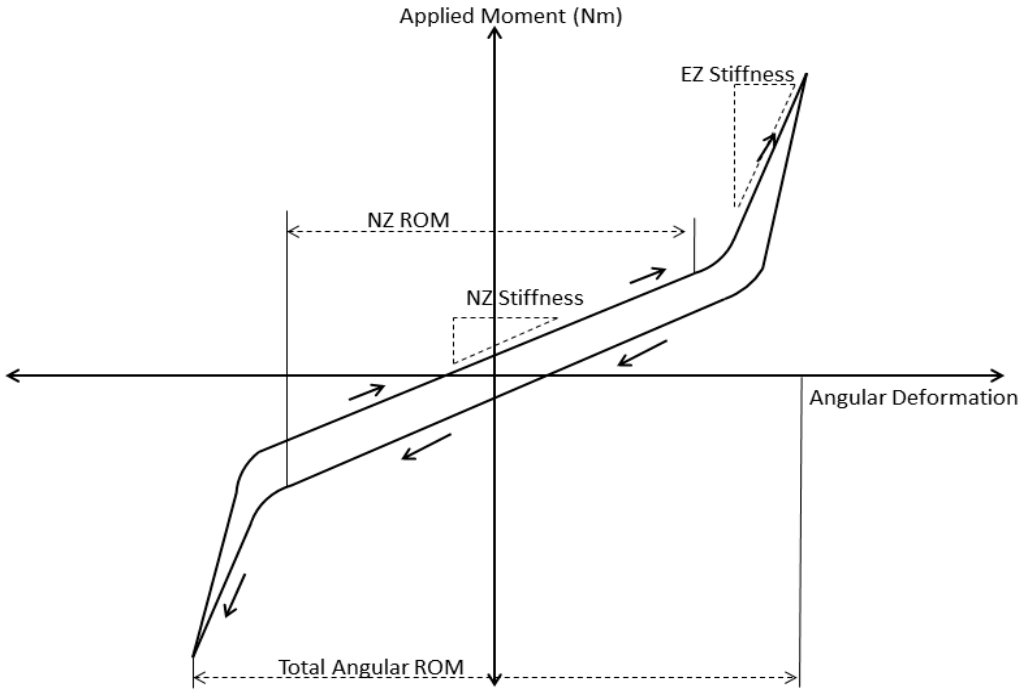

Figure 43: Typical sigmoid load-deflection behavior of the human spine. Highlighted are the neutral zone (NZ) stiffness and range of motion (ROM), as well as the extension zone (EZ) stiffness and total angular ROM. Directions of loading and unloading are indicated by arrows.

and unloading curves. This is due primarily to energy absorption by viscoelastic soft tissues. Deflection is symmetric in axial rotation and lateral bending. In flexion-extension there is a noticeable difference in extension zone stiffness between sides, with extension being stiffer.

This nonlinear behavior is a function of soft and hard tissue properties. In lateral bending and flexion, the facet joints have little to no contact with each other. As a result, behavior is dominated by soft tissue properties. As the soft tissues of the spine, including the ligaments, and annulus fibrosus all exhibit highly nonlinear behavior, the spine also exhibits nonlinear behavior. In extension and axial rotation, there is significant facet contact. As a result, these modes of bending tend to be stiffer, due to the inherently higher stiffness of bone. It is worth noting that the mechanical properties of this structure are dependent on strain rate. Viscoelastic materials are prone to stiffening under high loading rates, and reduced stiffness under low rates. Furthermore, this behavior is prone to creep if constant stress is applied, and stress relaxation if a constant displacement it held. Within physiological loading rates (.5°/sec – 5°/sec), there is little change in stiffness. However, creep should certainly be accounted for when using a discrete test setup. Measurement of specimen displacement following load application needs to occur after a consistent time interval in order for results to be valid.

3.2.4. Mechanical Test Methods

There are wide arrays of methods used to test the human spine. There are several choices to be made when initially setting up a test. Currently there is no standard testing protocol, and discrepancies exist between the setups of different labs. There is discrepancy over the use of FSUs or full lumbar segments, use of applied moments or eccentric forces, discrete or continuous loading, constrained or unconstrained test setups, and the validity of using follower loads to better simulate in-vivo conditions. Each of these choices affects the recorded mechanical properties of the specimen, and needs to be accounted for while testing. A useful

feature of the proposed spine model will be its ability to test across test setups. As its properties do not degrade over time, it will be feasible to discover the exact changes each test setup cause while utilizing the same specimen as its own control.

The use of an FSU or a full lumbar segment is a widely discussed topic in the spine community. Even though a multiple level segment allows for more accurate physiologically relevant motion, the FSU can provide a suitable alternative. That said, ligaments such as the supra/intra spinous ligament span multiple levels. Cutting it at one level may affect adjacent segments, and hinder FSU performance. A study by Kittler et al. provided a comparison of same segments in poly and single segment sheep specimens [136]. This study found that the range of motion (ROM) was increased in FSU's. Full segments generated 80% of FSU motion, while 3 vertebrae specimens had 95% of FSU motion. Furthermore, the neutral zone (NZ) ROM and amount of hysteresis decreased in FSUs. Even with all of these changes, the stiffness remained constant in most modes of bending at L3-L4, but increased for the L7-S1 segment. Dickey et al. performed a similar study on porcine segments [137]. Full lumbar segments were tested and then sectioned down into FSUs, with L3-L4 data recorded in all cases. In opposition to the findings of Kittler et al., Dickey's measure of the NZ ROM increased from multi-segment models to an FSU. They also showed that this was a function of cutting the ISL/SSL from adjacent segments, as discussed above. In agreement with Kittler et al., the overall ROM increased from multi-segment models to an FSU, and they found no significant difference in the stiffness of each specimen in either the neutral or extension zones. In summary, both authors found significant increases in the ROM in FSUs. This was paired with decreased hysteresis. The size of the neutral zone increased in one study and decreased in the other. The change in stiffness varied between loading modes. In general, there weren't statistically significant changes in segmental stiffness. This lends significance to presenting the stiffness of a spinal segment in the

results, as it appears somewhat independent of specimen length (number of segments tested). These authors have shown that an FSU can perform similarly to the same level in a full segment model.

It is also important to realize the difference between adjacent levels in the spine. Notably, the L5-S1 joint has been shown to behave quite differently from L1-L4 FSUs [138, 139]. This is primarily due to disc orientation as structure transitions from the spinal column to the pelvic girdle. Guan and Panjabi disagree on some changes from level to level, but overall were able to show increased ROM in L5-S1 in flexion and extension. Changes in flexion-extension are expected to arise as a result of changing soft tissue properties between L1-L4 and L5-S1. Notably, the ALL becomes softer by 2.5 times at L5-S1. This ligament experiences the highest strains in extension, and therefore can contribute greatly to its stiffness. Ligaments contributing to stiffness in lateral bending have shown invariant behavior. This mainly includes the ligamentum flavum and capsular ligaments. This work was verified by Yamamoto and Panjabi et al. (Figure 44) [140]. They quantitatively assessed the ROM for each level of the spine in each mode of bending. In agreement with the aforementioned studies, a large increase in ROM for flexion is seen when moving caudally down the spine. Extension experiences a sharp increase in movement below L3. Axial rotation is constant from L1-L4, but decreases below that. This is primarily due to the orientation of the facet joints. Lateral bending remains fairly constant through the lumbar spine.

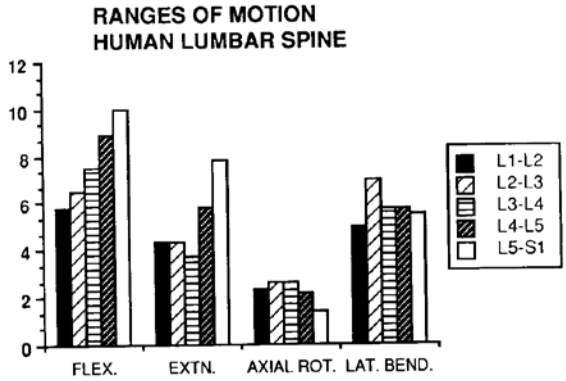

Figure 44: Graphical representation of mean ROM of the each level of the lumbar spine in each mode of bending [140]. (Reprinted with permission of Wolters Kluwer Health©)

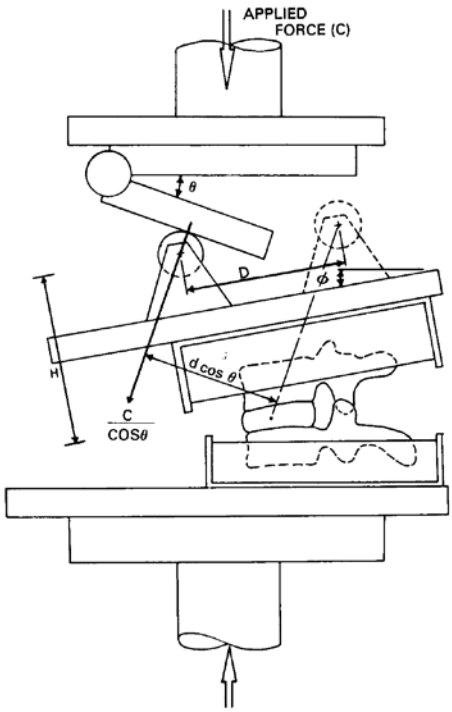

Figure 45: Example of a complex loading setup designed to simulate compression, shear and bending. This setups were often utilized as a simple compressive testing machine could be used to generate bending moments in the specimen [141]. (Reprinted with permission of Wolters Kluwer Health©)

Early studies used several methods of applying known loads or displacements to the spine. These studies routinely utilized eccentric forces, or complex loads to bend spine specimens (Figure 45). However, these setups are problematic, especially on multi-segment specimens. They cause an axial load, and an increasing bending moment along the specimen length. This practice has primarily been replaced with the use of pure moments [123]. In-vivo loading conditions are widely unknown, and a pure moment offers a simple uniform load that is easy to analyze.

There is an incredible array of reported methods for applying pure moments. Several authors hang opposing weights guided by pulleys. These weights act along the same length moment arm, but in opposite directions. More recent setups utilize hydraulic materials testing machines equipped with gimbals to apply pure moments. These setups are useful for testing FSU's, however as they are typically not equipped with a follower load, their accuracy can suffer on several segment specimens. Furthermore, these are typically constrained setups, whereby displacement of the inferior and superior specimen is rigidly controlled. This eliminates several degrees of freedom, restricting bending and translations to one plane. This drawback can be overcome with the use of an XY table, and orthogonal alignment of the bending gimbals to restore unconstrained motion (Figure 46) [142].

There is also no consensus on the magnitude of applied moments to use. These moments tend to be singular to the lab reporting on them. Similar to most testing parameters, they are unlikely to be changed, as researchers wish to enable comparison to all of their previous work. A brief review of the literature yielded the following magnitudes: ±3 Nm [143], ±3.75 Nm [123], ±4Nm[138, 144], ±6 Nm [145], ±6.5 Nm[33], ±6.6 Nm [146], ±6.9 Nm[147], ±7 Nm[148], ±7.5 Nm [139], ± 7.6 Nm [149], ±8 Nm [142], ±10 Nm[140, 150-152], ±10.6 Nm [153],

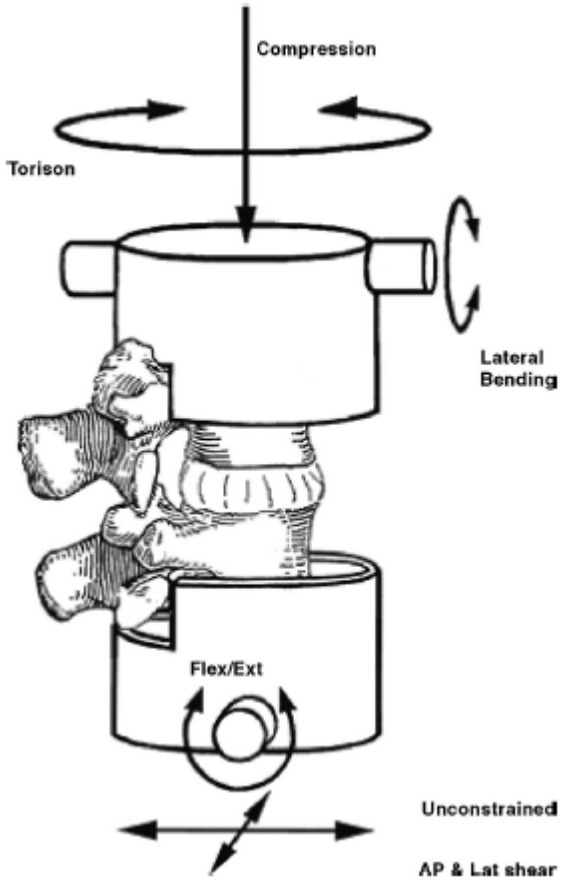

Figure 46: Graphical representation of an unconstrained method to test specimens in a servo-hydraulic materials testing machine [142]. (Reprinted with permission of Wolters Kluwer Health©)

±14 Nm [59], and ±15 Nm[154]. The majority of authors use loads above 6 Nm. This is in attempt to display the nonlinear behavior of the specimen, which only occurs at higher loads. At low loading magnitudes there is risk of not observing the whole nonlinear behavior of the spine. This may make it difficult to obtain accurate determination of the NZ stiffness or ROM, along with other relevant parameters. 10 Nm seems to be the most commonly used, and justifiable choice. As described by Yamamoto et al., the reason for this is that it is large enough to simulate a large range of physiological behavior, including capturing the nonlinearity, as well as being small enough to not risk damaging the specimen [140].

As touched on above, some authors hang discrete weights from their specimens to apply pure moments, while others use sophisticated servo-hydraulic machines. In discrete load setups, researchers apply known loads and allow the spine to reach equilibrium before recording displacement. This is often easy to setup, and to ensure that the loads being delivered are pure moments. This setup is widely used by researchers such as Goel, Schultz, Yamamoto, Panjabi, Markolf and others. However, it requires authors to wait after load application and allow creep to occur. This underestimates the in-vivo stiffness of the dynamic spine. Furthermore, different researchers wait different amount of time before recording data. Various authors have reported wait times of: immediately following load application [59], 10 seconds [149], 15 seconds [151, 153], 30 seconds [138-140], 60 seconds [59], 120 seconds [59], and 300 seconds [146]. This variation in recording time alters the measured properties owing to the viscoelastic nature of human tissue. Another key drawback to this setup is that researchers are unlikely to observe transition from the neutral zone to the extension zone. Typically authors collect only a few data points, resulting in a piecewise linear graph (Figure 47) [138].

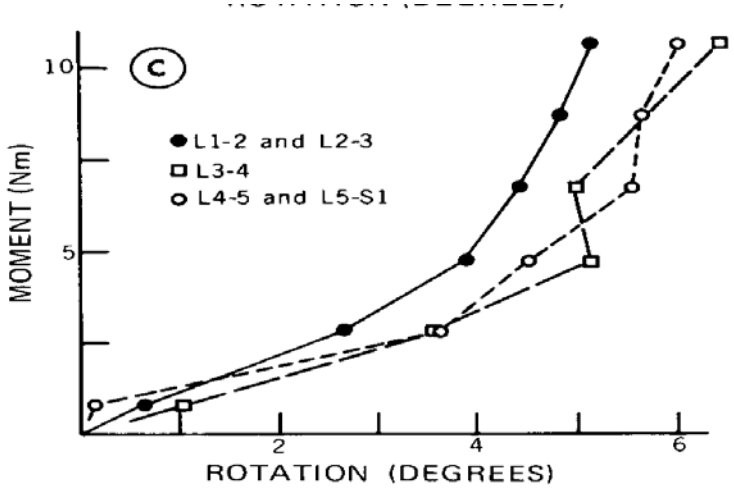

Figure 47: Load - displacement curve for lumbar FSUs in right lateral bending using discrete point loads. Results are grouped by segment level. Note the piece-wise linear form of the graph, and the difficulty in precisely locating the neutral zone boundaries [153]. (Reprinted with permission of Wolters Kluwer Health©)

Continuous loading is the alternative to hanging discrete weights. This is typically carried out on advanced electronic or servo-hydraulic test setups. Several researchers utilize a Materials Test Machine (MTS) in order to carry out loading, while others build custom machines that change from lab to lab. It has been shown that loading rates between .5°/sec and 5°/sec achieve similar results, and are also physiologically relevant [15]. Thus, within this range, the viscoelastic nature of the spine's soft tissues does not drastically affect performance. Continuous loading allows researchers to collect the exact load-displacement behavior of the specimen (Figure 48). This increases the accuracy in determining the neutral zone and extension zone size and stiffness, instead of measuring ROM at pre-defined arbitrary loads or displacements.

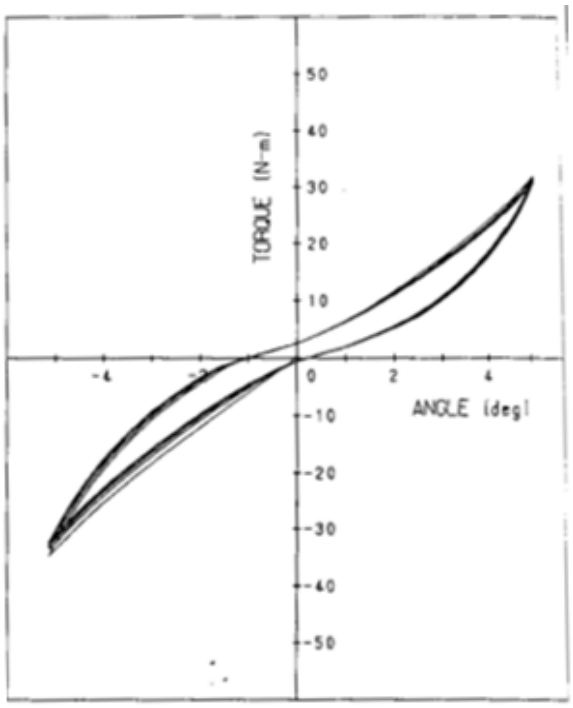

Figure 48: Load – displacement of a lumbar FSU in axial rotation tested on a continuous loading setup. Note how data exhibits the highly nonlinear behavior of an FSU, and identification of the neutral zone is clear [155]. (Reprinted with permission of Wolters Kluwer Health©)

Another key test condition briefly touched on above is the use of constrained or unconstrained setups. Unconstrained setups fix one end of the specimen, while allowing the other a full six degrees of freedom. Constrained setups are ones in which specimens have less than six full degrees of freedom. While boundary conditions are widely acknowledged to influence test results, there are few experiment studies that actually analyze this variable. Grassmann et al. conducted a study on its effect on axial rotation [156]. Lumbar FSUs were tested in axial rotation using both boundary conditions. Unconstrained testing utilized the application of pure moments, and three dimensional movements were collected with an optoelectronic camera system. Constrained specimens were loaded around a fixed axis. The axis was controlled to examine the effects of its location. This only required acquisition of angular rotation data. Axial rotation of the constrained setup always resulted in a larger ROM than the unconstrained setup. Furthermore, different loading axes produce different FSU behavior in the constrained specimen. This supports the use of unconstrained testing, where these effects do not require control. An additional analysis was conducted by Charriere et al. covering all modes of bending [157]. They found a large statistical difference between the two setups when testing out of the sagital plane of symmetry (i.e.in lateral bending and axial rotation). This is a result of the influence of coupled motion generating excess forces. In the extension zone the stiffness of constrained axial rotation was decreased by 26% in comparison to unconstrained testing. This change was magnified to a 53% reduction in lateral bending stiffness. In the neutral zone the only difference was a 6% reduction in the lateral bending ROM. The stiffness's in all modes were statistically similar. In flexion-extension the two setups produce similar results. It is worth noting that all of this work was carried out without the use of a follower load, which as will be seen shortly, heavily affects the biomechanics of the spine. Only five of nineteen studies on human lumbar specimens employed the use of constrained testing (constrained[144, 145, 155, 158,

159], unconstrained[33, 59, 123, 138-140, 142, 146, 148, 149, 151-153, 160]). Unconstrained motion is the gold standard, however depending on the nature of data to be collected, constrained testing can provide accurate results. This is mainly the case inside the neutral zone, and for flexion-extension, as reported above.

An additional experimental variable concerns the application of load or displacement control. It is suggested by Goel et al. that the applied loads should remain constant, and not depend on stiffness, and changes due to age, pathology, injury or instrumentation. These loads shouldn't constrain motion, as in-vivo there are a full six degrees of freedom. Researchers supporting this view believe it is easier to apply pure moments in load control [161]. Displacement control also has its proponents. In-vivo studies can provide the most accurate study of the human spine. While forces within the healthy spine are difficult to measure, imaging studies allow accurate assessment of spinal motion [161]. This motion can be represented in-vitro by controlling specimen displacement. In-vitro studies are capable of instrumenting the specimen to study the loads generated at these physiological displacements. Furthermore, tests within the specimen's neutral zone can experience large variance if conducted in load control. In this zone, very large displacements are possible with little to no change in applied load. For this reason, it is inappropriate to use load control in the neutral zone [162]. Also, if specimen failure occurs, the whole setup is much safer to operate in displacement control. At failure, there would be a drastic increase in motion under load control, leading to further specimen, or test machine damage. However, testing to a set displacement can provide difficult in extremely stiff specimens. If not monitored appropriately, specimen failure can occur as a result of excessively high loads. Overall, load and displacement control can generate extremely similar results. The variables previously discussed are more important than how the specimen is moved or loaded. Segment length, type of loading, and the boundary conditions

heavily influence specimen behavior. If a specimen moves 3° after the application of 6 Nm, it should also generate 6 Nm in response to being rotated 3° under the same test conditions.

One final experimental setup variable is worthy of consideration. That variable is the effect of utilizing a follower load. Compressive loading is routinely applied to specimens in order to replicate the effects of a specimen's body weight being transmitted through the lumbar spine. Research has shown that compressive loads affect the behavior of the spine [163-165]. A follower load is commonly used on full segment studies. A follower load differs from a mere compressive load in that it follows tangent to the curvature of the spine. The follower load is designed to deliver constant axial load through the length and curvature of the segment [163, 165, 166]. This is typically carried out by attaching cables bilaterally through eye hooks screwed into each vertebra. Cables are mounted in the top loading platen, and dead weights are hung from each. In this way, uniform symmetric load is applied to each vertebra. A study by Patwardhan et al. determined that muscles in the lumbar spine can activate in a way that mimics the follower loads. If certain muscles work synergistically, they deliver compressive loads in a direction tangent to the curvature of the spine [166]. The spinal column in-vitro has been shown unstable under loads much smaller than those expected in-vivo (100 N vs. 1200 N) when follower loads are not used [166]. Due to the finding that muscles and follower loads generate similar behavior, and that the spine is a stable structure under large compressive loads, it is likely that follower loads increase the physiological relevance of studies. In-vitro follower loads have been shown to decrease total ROM in lateral bending and axial rotation while simultaneously increasing the size of the neutral zone. This behavior holds true in both young and old specimens [163]. Other authors have shown that physiologically relevant follower loads significantly increase FSU neutral zone stiffness and that this effect is relevant to all six degrees of freedom [164, 167-169]. Theoretical models have shown that the spine is stable under

follower loads up to 1200 N [166]. Other authors have demonstrated that FSUs can hold up to 3-5 kN follower loads [170, 171]. Furthermore, physically active specimens have compressive failure loads over 10 kN [172]. The magnitude of what follower loads should be applied is rarely agreed upon between authors. Authors have reported using loads of: 0N [164], 182N [33], 200N [142], 250N [164], 280N [163], 350N [166], 400N [153], and 500N[164]. These are typically chosen to represent the weight of the body superior to the tested level.

3.2.5. Mechanical Properties

There is a wide array of data available on the intact properties of the human lumbar spine. Unfortunately, most of these studies typically only report on motion due to applied load, or to stiffness within specific regions (normally the neutral zone). As discussed above, there is a large diversity in test methods between labs. Factors such as follower loads and specimen boundary conditions have been shown to heavily influence specimen behavior. Presented below are several tables highlighting the measured values for specimen stiffness and neutral zone range of motion.

There is clearly a wide variety of reported values for NZ stiffness of the spine in flexion (Table 25). While the values presented by Gardner-Morse et al. seem unnaturally high, the remaining values suggest a range of approximately .50 Nm/° – 2 Nm/° to be physiologically relevant. Few authors present data for the EZ stiffness, however they seem fairly close to each other, and suggest a range of approximately 3 Nm/° - 4 Nm/°, but could easily be as high as 10 Nm/° [146]. Values for the NZ ROM are also concise, ranging from 1.5° - 2.2°.

Table 25: Literature review of the human lumbar spine tested in - Flexion

Authors	Constrained?	Follower Load	NZ Stiffness (Nm/°)	EZ Stiffness (Nm/°)	NZ ROM (°)
Busscher [144]	yes	0 N	.64 (.15)	3.03 (-)	2.2 (-)
Okawa [33]	no	182 N	-	3.70 (.99)	-
Wilke [173]	no	0 N	.90 (-)	-	1.7 (-)
Eysel [148]	no	0 N	.76 (.32)	-	-
Panjabi [174]	no	0 N	-	-	1.5 (-)
Markolf [59]	no	0 N	1.91 (.80)	-	-
Schmidt [146]	no	0 N	1.1 (6.12)	1.80 (7.58)	-
Gardner-Morse [160]	no	0 N	4.21 (.58)	-	-

The neutral zone stiffness for extension is slightly stiffer than that of flexion (Table 26). The literature suggests that an appropriate range of values falls between .5 Nm/° and 2.6 Nm/°. The extension zone stiffness is often much larger than is flexion counterpart. The data suggest a

Table 26: Literature review of the human lumbar spine tested in - Extension

Authors	Constrained?	Follower Load	NZ Stiffness (Nm/°)	EZ Stiffness (Nm/°)	NZ ROM (°)
Busscher [144]	yes	0 N	.64 (.15)	3.03 (-)	2.20 (-)
Okawa [33]	no	182 N	-	6.29 (2.45)	-
Wilke [173]	no	0 N	1.50 (-)	-	-
Eysel [148]	no	0 N	1.28 (.37)	-	-
Panjabi [174]	no	0 N	-	-	1.5
Markolf [59]	no	0 N	2.62 (-)	0.10 (-)	-
Schmidt [146]	no	0 N	1.60 (.83)	2.60 (1.45)	-
Gardner-Morse [160]	no	0 N	4.21 (.58)	-	-

range of 1 Nm/° - 8.5 Nm/° as physiologically relevant. The neutral zone ROM for extension is coupled with that of flexion, and already presented as 1.5° - 2.2°.

In lateral bending the neutral zone stiffness is similar to extension, ranging from .5 Nm/° to 3.5 Nm/° (Table 27). The extension zone stiffness likely ranges from 2 Nm/° - 7 Nm/°. The neutral zone ROM appears to range from 1.5° to 3°.

Table 27: Literature review of the human lumbar spine tested in - Lateral Bending

Authors	Constrained?	Follower Load	NZ Stiffness (Nm/°)	EZ Stiffness (Nm/°)	NZ ROM (°)
Busscher [144]	yes	0 N	.55 (.52)	5.0 (-)	2.0 (-)
Okawa [33]	no	182 N	-	5.83 (1.34)	-
Wilke [173]	no	0 N	0.50 (-)	-	2.9 (-)
Goel [143]	no	0 N	.87 (.27)	-	-
Eysel [148]	no	0 N	.99 (.24)	-	-
Gardner-Morse [160]	no	0 N	3.04 (.36)	-	-
Panjabi [174]	no	0 N	-	-	1.6 (-)
Markolf [59]	no	0 N	1.34 (.90)	-	-
Schmidt [146]	no	0 N	1.6 (.45)	2.30 (.47)	-

Axial rotation appears to be the stiffest mode of bending according to the three parameters listed below (Table 28). The neutral zone stiffness is commonly listed around 3 Nm/° in constrained test setups, but as high as 9 Nm/°-10 Nm/° in unconstrained testing. The extension zone stiffness is listed as ranging from 7.3 Nm/° - 13 Nm/°. Finally, axial rotation has the smallest NZ ROM, commonly listed below 1°, all the way down to .2°.

The wide variation present in the literature suggests not only a large variation from one spine to the next, but a significant influence of test setup upon property measurement. This

holds true for all modes of bending, and the variables influencing each study were discussed in detail above.

Table 28: Literature review of the human lumbar spine tested in - Axial Rotation

Authors	Constrained?	Follower Load	NZ Stiffness (Nm/°)	EZ Stiffness (Nm/°)	NZ ROM (°)
Busscher [144]	yes	0 N	2.63 (2.24)	13.0 (-)	1.0 (-)
Asano [155]	yes	0 N	3.13 (.22)	9.66 (.75)	-
Gardner-Morse [160]	no	0 N	9.84 (1.55)	-	-
Wilke [173]	no	0 N	1.10 (-)	-	0.2 (-)
Goel [143]	no	0 N	.33 (.13)	-	-
Panjabi [174]	no	0 N	-	-	0.7 (-)
Markolf [59]	no	0 N	9.64 (.7)	-	-
Schmidt [146]	no	0 N	9.20 (3.6)	8.4 (1.09)	-

3.3.Mechanical Properties of the Analogue Spine Model

3.3.1. Initial Status of the Analogue Spine Model

As laid out in the introduction, the mechanical properties of the Analogue Spine Model's soft tissues have already been quantified, and deemed similar to their human counterparts. This work was primarily carried out by LaPierre and Avidano et al. and then transferred to Pacific Research Laboratories for manufacture[57]. Unfortunately, during manufacturing unexpected interactions were occurring between components that resulted in stiffening of the model, as well as aberrant behavior in certain modes of testing. The first generation of models had several basic problems in need of improvement. Perhaps the most obvious initial flaw to the model was

the “stair-step” behavior inherent to the model in axial rotation. Furthermore, the overall stiffness of the model was not accurate enough in each mode of testing.

When tested in axial rotation, the “stair-step” behavior (Figure 49) consists of several large random displacements with no increase in load. Furthermore, these increases occur at the same angle for each of the 3 cycles shown in the figure. These discontinuities are not present in the human spine, and needed to be dealt with before the model could be sold.

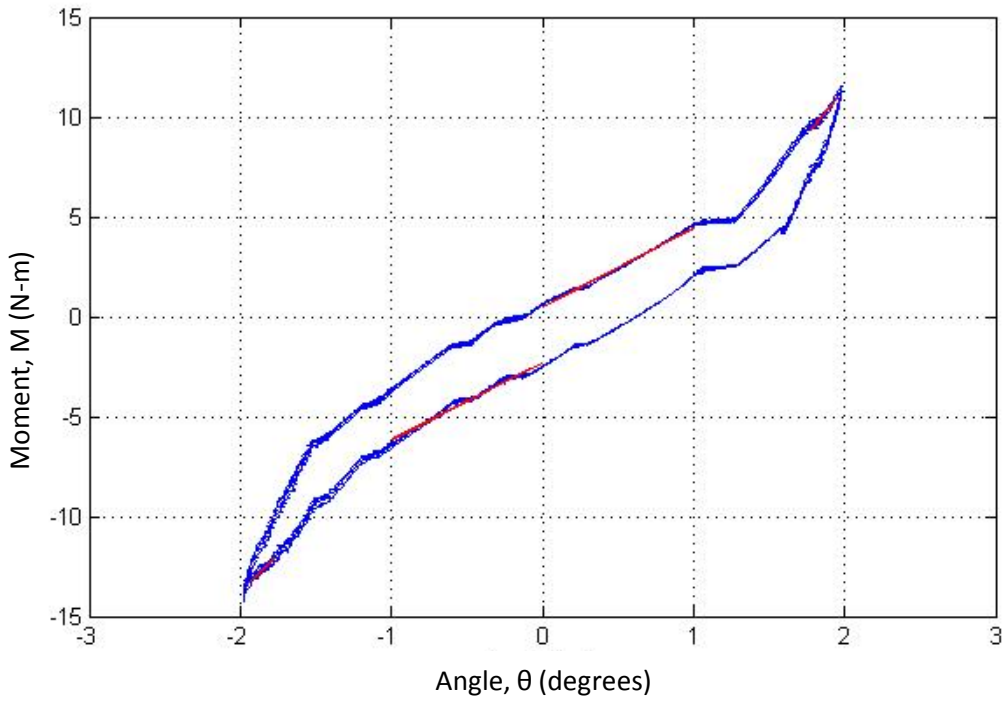

Figure 49: Initial FSU performance highlighting the “stair-step” behavior. This behavior was readily seen in axial rotation. Large displacements with no increase in moment would occur at the same angular displacement throughout each of the loading cycles.

The model initially manufactured by PRL after technology transfer was stiffer than expected. Several test FSUs were manufactured, each of which exhibited properties not desirable in the final production. The neutral zone is predominantly controlled by soft tissue properties, and was the focus of these initial studies (Table 29). Initial neutral zone stiffness’s are higher than those presented in the literature. The earliest specimens were not tested through a

full ROM to 15 Nm. As such, the extension zone values are lower than should be expected, as they were mostly measured in the transition from the neutral to extension zone. Due to this initial performance, a method of locating the elements and interactions causing each aberrant behavior and elevated NZ stiffness was developed.

Table 29: Initial Stiffness of the Analogue Spine Model in each mode of testing

Mode	NZ Stiffness (Nm/°)	EZ Stiffness (Nm/°)*
Flexion	2.52 (1.47)	3.13 (1.67)
Extension	2.87 (1.39)	5.42 (2.67)
Lateral Bending	1.77 (0.95)	3.27 (1.40)
Axial Rotation	3.38 (0.94)	7.63 (1.95)

3.3.2. Experimental Test Methods- Initial Analogue Spine Model Performance

As presented above, an FSU simplifies test setups by reducing the number of variables that need to be controlled. Furthermore, as shown by Guan et al. and Yamato et al., each segment from L1-L5 shows relatively consistent properties in flexion, extension, lateral bending and axial rotation [138, 140]. Thus, manufacturing and ensuring the accuracy of one segment will allow the creation of a full lumbar model. Once completed, slight changes in geometry from level to level should be sufficient to induce the necessary changes. Finally, the manufacture of FSUs occurs much more rapidly than full lumbar segments, and is more cost effective for small companies undertaking new product development.

FSUs were manufactured by Pacific Research Laboratories using a combination of technology transferred by the University of Kansas, and their own custom in-house manufacturing processes. FSUs are manufactured with two vertebrae, transverse ligaments,

supra/intra spinous ligament, capsular ligaments, ligamentum flavum, anterior and posterior longitudinal ligament and intervertebral disc.

Once received from PRL, specimens were allowed at least twenty four hours to acclimate to the laboratory environment. Three screws were placed vertically oriented in the superior L3 endplate, and inferior L4 endplate. Specimens were then embedded in a polyester resin (Bondo, 3M) to provide a rigid platform capable of being attached to the loading frame.

Testing was carried out using an MTS 858 Mini Bionix, with spine bending jigs (Figure 50) (Eden Prairie, MN). A bending moment was applied to each specimen in order to determine its load-deformation response. This moment was applied in displacement control. Prior to collecting data, specimens were broken in with 100 cycles of motion to ±1° in flexion-extension, lateral bending and axial rotation. Following break in, the ROM was found for each specimen independently. Specimens were rotated until subject to 15 Nm moments. Rotational

Figure 50: Experimental setup on MTS Mini Bionix with bending jigs. The specimen in this picture is oriented for testing FSU behavior in flexion-extension

displacement at this load was recorded and used as the end limits for testing. Loading was applied at .92°/sec. According to the test criteria laid out by Wilke et al., rates between .5°/sec and 5°/sec can be used without considerable effect on the results [15]. This low rate was utilized to facilitate more accurate comparison with discrete quasi-static studies. Specimens were subject to five cycles of bending between the ROM limits previously defined for each specimen. All testing was carried out with a 100 N preload. The load was applied with the axial piston of the MTS. While this is not a true follower load, in that it doesn't follow the curvature of the specimen, the use of an FSU decreases possible differences between the methods. Specimens were fixed such that the axis of rotation in torsion was located medially in the posterior 1/3rd of the centrum [156]. The axis of rotation in flexion, extension and lateral bending was in the same location, but translated cranially into the center of the IVD. Applied displacement and measured load were simultaneously recorded at 100 Hz using the built in LVDT and angular displacement / torque sensors on the MTS. Following testing of the intact specimen, a systematic dissection was performed to locate the source of aberrant specimen behavior and interactions causing increased specimen stiffness. After each dissection, specimens were tested to the ROM previously recorded. This dissection followed a specific protocol, with ligaments removed in a sequential order. After intact testing, the capsular ligaments were removed, followed by the transverse ligaments, supraspinsous / intraspinous ligament, ligamentum flavum, anterior longitudinal ligament and posterior longitudinal ligament. Finally, the wrap surrounding the intervertebral disc was removed.

Data was analyzed with a custom computer program created in Matlab (Mathworks, Natick, MA). The third loading cycle in each direction was analyzed to determine the specimen's performance. Variables of interest are the neutral zone stiffness, extension zone stiffness and neutral zone ROM (Figure 51). Neutral zone stiffness is calculated as the slope of the load-

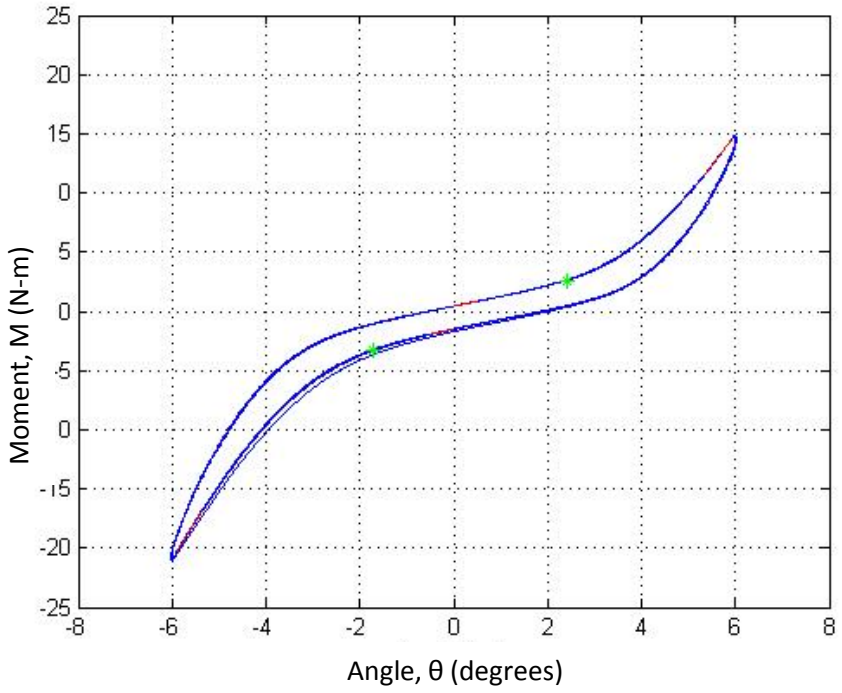

Figure 51: Typical FSU behavior in lateral bending illustrating NZ and EZ stiffness (red lines), along with NZ ROM (angular distance between green marks)

displacement curve between zero and one half degree in the loading direction. In all cases, it was verified that this fell within the linear neutral zone, and did not factor in the transition or extension zone. Extension zone stiffness was calculated as the slope of the top ten percent of the load-displacement curve. In all cases it was verified that this was entirely in the extension zone, and was not influenced by the transition zone. The neutral zone ROM was determined by using a threshold technique. A best fit line to the NZ was calculated, and extrapolated across the entire ROM. This line was offset by .25 Nm to ensure signal noise did not result in detection of a false positive. In each case, the intersection was plotted, and visually checked to ensure it accurately represented the beginning of the transition from the neutral zone to the extension zone.

3.3.4. Experimental Results - Initial Analogue Spine Model Performance

Fourteen FSUs were manufactured and tested according the methods described above. The source of the "stair-step" behavior in torsion was successfully located. It turned out to be a result of excess epoxy built up at a site requiring large ranges of motion. As a result, the epoxy would catch and slide on an opposing surface. This was uncovered by observing that the "stair-step" behavior persisted through the removal of each ligament, and was only solved after removal of the wrap surrounding the IVD. Glue at this interface was the source of the problem. This issue was mediated by adjusting the manufacturing technique, and is no longer an issue

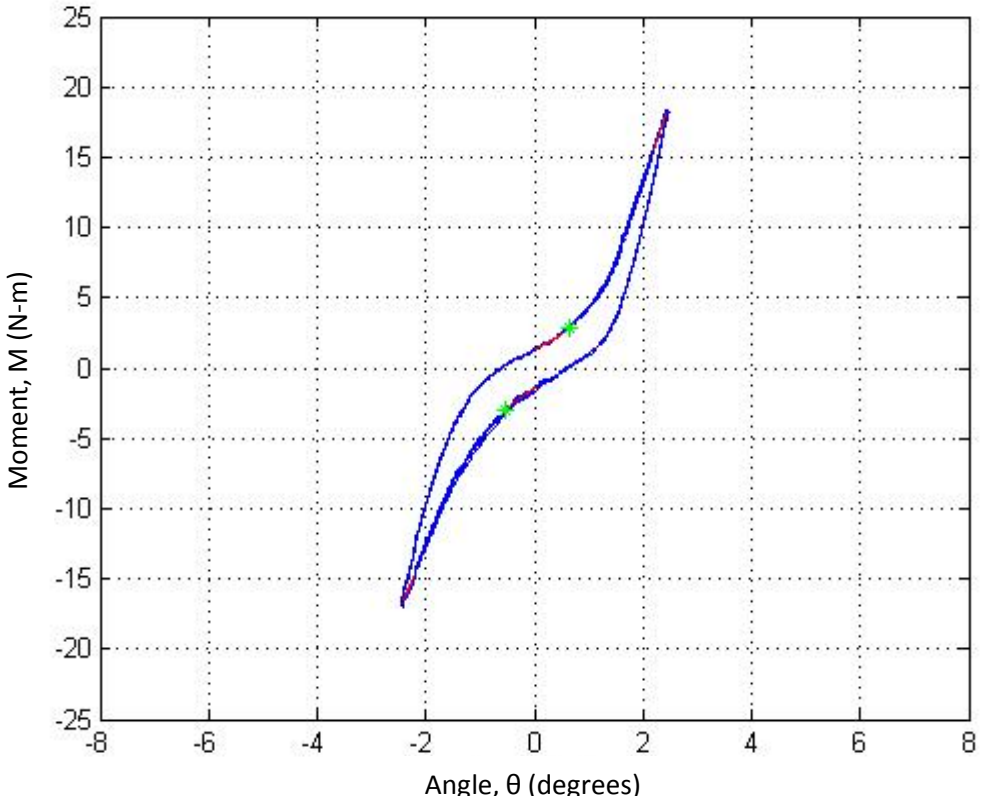

Figure 52: Typical FSU behavior in axial rotation after resolving "stair-step" behavior. NZ and EZ stiffness is highlighted with red lines. NZ ROM is the angular displacement between green marks.

(Figure 52).

During testing, the capsular ligaments and intervertebral disc / wrap were identified as having the largest impact on neutral zone stiffness in all modes of bending. Key changes were made to each of these structures in order to reduce the neutral zone stiffness of the final model. The injection molding jig responsible for the capsular ligaments was adjusted to result in ligaments with smaller cross sectional areas. This made the CL's more representative of human anatomy, and decreased their mechanical influence on overall stiffness. Several different IVD/wrap adjustments were made to reduce model stiffness. These consisted of changing the materials each component was made out of, as well as altering how each element was attached to each other, and the surrounding vertebral bodies. In the end, this structure had reduced stiffness, drastically impacting overall model performance.

3.3.5. Experimental Test Methods – Analogue Spine Model Repeatability Study

Following the above work, it was determined that the model was close to FSU performance reported in the literature. As such, a measure of variance within a set of uniform FSUs was needed. The purpose of this study was to determine the average FSU behavior, and ensure specimens could be manufactured in a repeatable manner.

Seven uniform FSUs were manufactured by Pacific Research Laboratories, and shipped to the University of Kansas for testing. Specimens were prepared and tested according to the protocol listed in the preceding section. The only difference between in specimen preparation is that PRL potted these FSUs following manufacture. They used a custom potting jig to ensure proper alignment, and embedded each end of the FSU in a polyester resin. Constrained bending tests were conducted utilizing an MTS 858 Mini Bionix with bending jigs. Five cycles of flexion /extension, lateral bending, and axial torsion were carried out with a preload of 100 N at .92 °/s

until a moment of approximately 15 Nm was achieved. By the third cycle, behavior was constant, and recorded for data analysis. The non-linear behavior of the model in the neutral zone and extension zone was quantified in each mode, and then compared to the literature to assess overall accuracy. Due to the large number of differences between studies in the literature and our experimental setup it is unreasonable to statistically compare the studies. Therefore, a quantitative comparison was performed, but checks of statistical significance were not.

3.3.6. Experimental Results and Analysis – Analogue Spine Model Repeatability Study

The performance of all seven FSUs has been analyzed. Below is a summary of the results for each specimen, along with the average FSU behavior and associated standard deviation of model performance. The key variables of interest are the neutral zone and extension zone stiffness's (Table 30), as well as the neutral zone ROM (Table 31).

Neutral zone stiffness's were highly symmetric about the origin. Stiffness in extension is only slightly stiffer than flexion in the neutral zone. Due to its anatomical geometric symmetry, lateral bending is anticipated to be symmetric, which is easily seen in the neutral zone. Symmetric behavior is achieved in the neutral zone for axial rotation as well. Lateral bending is the least stiff mode of bending, with values around .85 Nm/°, while axial rotation is the stiffest, with stiffness around 2.47 Nm/°. The coefficient of variation (COV = mean/std dev) is relatively low in the neutral zone. Flexion-extension was the most repeatable mode of testing, with a COV around 8%. Torsion was the least repeatable mode of testing, with a COV around 19%. Neutral zone stiffness is predominantly controlled by soft tissue properties, indicating work needs to be completed assuring the tissues controlling axial rotation are appropriately manufactured and assembled.

Extension zone stiffness is expected to be symmetric for lateral bending and axial rotation, but exhibit different values for flexion-extension. This performance was validated by

our study. Extension was nearly three times as stiff as flexion. Furthermore, lateral bending values were within 12% of each other, and axial rotation values within 20%. Flexion was the most variable mode of testing, with a COV of 20%. Torsion was the most repeatable mode of testing with a COV around 10%. Flexion's EZ stiffness is controlled by its soft tissues, while torsion's behavior is dominated by hard tissue interactions. This lends further credence to the idea that work needs to be completed refining soft tissue manufacturing.

Table 30: Neutral and extension zone stiffness of the Analogue Spine Model in all modes of testing.

	FSU 1	FSU 2	FSU 3	FSU 4	FSU 5	FSU 6	FSU 7	Ave.	Std Dev
NZ Stiffness - Nm/°									
Flexion	1.65	1.89	1.68	1.63	1.91	2.00	1.95	1.82	0.16
Extension	1.92	2.19	1.92	1.80	2.02	2.11	2.10	2.01	0.14
Right Bending	0.89	0.82	0.97	0.74	1.00	0.91	0.87	0.89	0.09
Left Bending	0.80	0.76	0.92	0.68	0.93	0.86	0.78	0.82	0.09
Right Rotation	2.35	3.23	2.56	1.64	2.66	2.38	2.41	2.46	0.47
Left Rotation	2.50	3.02	2.09	2.19	2.47	3.13	1.96	2.48	0.45
EZ Stiffness - Nm/°									
Flexion	3.78	2.32	3.60	2.41	3.64	3.25	2.61	3.09	0.63
Extension	10.00	9.66	9.79	7.79	7.69	9.85	9.30	9.15	0.99
Right Bending	6.23	3.97	5.89	4.60	6.17	5.88	6.54	5.61	0.95
Left Bending	5.16	5.03	4.97	4.03	5.43	4.92	5.35	4.98	0.46
Right Rotation	9.25	10.57	11.27	10.27	9.72	12.07	8.58	10.25	1.19
Left Rotation	10.64	11.36	13.57	13.10	12.66	12.53	11.90	12.25	1.02

Neutral zone range of motion ended up being one of the most variable aspects of the spine model. While lateral bending was consistent, with a COV of 8%, flexion-extension and axial rotation exhibited COV's of 17% and 19% respectively. While the NZ ROM for lateral bending is controlled almost entirely by soft tissue properties, each of the other modes are strongly influenced by the facet joints, and therefore, bony contact. Since each vertebra is injection molded, and can be produced repeatably, it is likely that variation in the experimental setup is responsible for some of this variation. Since a constrained test setup is utilized, this variation is

likely due to slight deviations in specimen alignment during preparation (potting) and testing. Misalignment during either of these stages will alter the axis of rotation, as well the gap distance between facets. This distance is a key factor controlling the NZ ROM.

Table 31: Neutral zone range of motion of the Analogue Spine Model in all modes of testing.

	FSU 1	FSU 2	FSU 3	FSU 4	FSU 5	FSU 6	FSU 7	Ave	Std Dev
NZ ROM - Deg (°)									
Flexion-Extension	4.64	6.48	5.11	7.11	5.27	5.47	6.92	5.86	0.97
Lateral Bending	4.18	4.17	4.29	4.98	4.03	4.22	4.04	4.27	0.33
Axial Rotation	1.82	1.72	1.29	1.27	1.45	1.92	1.20	1.52	0.29

3.3.7. Experimental Comparison of the ASM to Human Literature

Presented below in Table 32 to Table 35 are comparisons between the current study and the previously reported on literature. Before looking through the tables, there are two key reminders to point out. First off, follower loads have been shown to increase stiffness in all modes of testing. The majority of studies in the literature are conducted without preloads. This in in opposition to the current study which used a 100 N load. Second, constrained testing has been shown to result in lower stiffness's compared with testing using six degree of freedom systems.

In flexion (Table 32), the neutral zone and extension zone both have stiffness within the range of values reported by the literature. In extension (Table 33), the neutral zone stiffness is within the values reported by the literature. The extension zone stiffness however is nearly 30% higher than the value reported by Okawa et al. [33]. The neutral zone ROM for flexion-extension is unnaturally high. At 6.83°, it is over three times higher than the highest reported value. Only Busscher et al. used a reasonable method to measure the ROM. Most of the studies use discrete loads, and as such are not able to precisely detect the transition from neutral zone to extension zone. As a result, these studies don't directly analyze where the change occurs. Instead, these

Table 32: Literature review of the human lumbar spine and its comparison to the Analogue Spine Model tested in - Flexion

Authors	Constrained?	Follower Load	NZ Stiffness (Nm/°)	EZ Stiffness (Nm/°)	NZ ROM (°)
Current Study	yes	100 N	1.82 (.16)	3.09 (.63)	6.83 (1.07)
Busscher [144]	yes	0 N	.64 (.15)	3.03 (-)	2.2 (-)
Okawa [33]	no	182 N	-	3.70 (.99)	-
Wilke [173]	no	0 N	.90 (-)	-	1.7 (-)
Eysel [148]	no	0 N	.76 (.32)	-	-
Panjabi [174]	no	0 N	-	-	1.5 (-)
Markolf [59]	no	0 N	1.91 (.80)	-	-
Schmidt [146]	no	0 N	1.1 (6.12)	1.80 (7.58)	-
Gardner-Morse [160]	no	0 N	4.21 (.58)	-	-

studies observe the specimen's displacement upon removing all loads. This displacement is typically referred to as the neutral zone range of motion. However, this zone is actually a measure of specimen hysteresis, and should not be referred to as a range of motion. Inter-specimen variance is always lower in the current study than in the reported literature. This occurs slightly in the neutral zone, but by a larger margin in the extension zone.

Table 33: Literature review of the human lumbar spine and its comparison to the Analogue Spine Model tested in - Extension

Authors	Constrained?	Follower Load	NZ Stiffness (Nm/°)	EZ Stiffness (Nm/°)	NZ ROM (°)
Current Study	yes	100 N	2.01 (.14)	9.15 (.99)	6.83 (1.07)
Busscher [144]	yes	0 N	.64 (.15)	3.03 (-)	2.20 (-)
Okawa [33]	no	182 N	-	6.29 (2.45)	-
Wilke [173]	no	0 N	1.50 (-)	-	-
Eysel [148]	no	0 N	1.28 (.37)	-	-
Panjabi [174]	no	0 N	-	-	1.5
Markolf [59]	no	0 N	2.62 (-)	0.10 (-)	-
Schmidt [146]	no	0 N	1.60 (.83)	2.60 (1.45)	-
Gardner-Morse [160]	no	0 N	4.21 (.58)	-	-

Table 34: Literature review of the human lumbar spine and its comparison to the Analogue Spine Model tested in - Lateral Bending

Authors	Constrained?	Follower Load	NZ Stiffness (Nm/°)	EZ Stiffness (Nm/°)	NZ ROM (°)
Current Study	yes	100 N	.85 (.09)	5.30 (.71)	4.98 (.34)
Busscher [144]	yes	0 N	.55 (.52)	5.0 (-)	2.0 (-)
Okawa [33]	no	182 N	-	5.83 (1.34)	-
Wilke [173]	no	0 N	0.50 (-)	-	2.9 (-)
Goel [143]	no	0 N	.87 (.27)	-	-
Eysel [148]	no	0 N	.99 (.24)	-	-
Gardner-Morse [160]	no	0 N	3.04 (.36)	-	-
Panjabi [174]	no	0 N	-	-	1.6 (-)
Markolf [59]	no	0 N	1.34 (.90)	-	-
Schmidt [146]	no	0 N	1.6 (.45)	2.30 (.47)	-

In lateral bending (Table 34), the neutral and extension zone stiffness's fall within the values reported in the literature. Similar to flexion-extension, the neutral zone ROM is too high compared to the literature. Inter-specimen variance is lower in the current study than in the reported literature.

In axial rotation (Table 35), both neutral and extension zone stiffness's are within the reported literature. The neutral zone ROM in axial rotation is slightly less than twice as much as the value reported by Busscher et al. [144]. Inter-specimen variance in the current study is lower in the neutral zone than the reported literature. However, in the extension zone, it is slightly larger.

Table 35: Literature review of the human lumbar spine and its comparison to the Analogue Spine Model tested in - Axial Rotation

Authors	Constrained?	Follower Load	NZ Stiffness (Nm/°)	EZ Stiffness (Nm/°)	NZ ROM (°)
Current Study	yes	100 N	2.47 (.46)	11.25 (1.10)	1.78 (.28)
Busscher [144]	yes	0 N	2.63 (2.24)	13.0 (-)	1.0 (-)
Asano [155]	yes	0 N	3.13 (.22)	9.66 (.75)	-
Gardner-Morse [160]	no	0 N	9.84 (1.55)	-	-
Wilke [173]	no	0 N	1.10 (-)	-	0.2 (-)
Goel [143]	no	0 N	.33 (.13)	-	-
Panjabi [174]	no	0 N	-	-	0.7 (-)
Markolf [59]	no	0 N	9.64 (.7)	-	-
Schmidt [146]	no	0 N	9.20 (3.6)	8.4 (1.09)	-

3.3.8. Discussion

Overall, the Analogue Lumbar Spine Model has provided convincing evidence that it will be a reliable, repeatable model to test and analyze new medical devices and procedures. While the NZ ROM is too high in all modes of testing, the specimen stiffness is accurate is seven out of eight instances (Table 36).

While it would be ideal to include a full statistical comparison to a cadaveric study, so far a study in the literature appropriate for direct comparison has not been located. As was highlighted in the background information, factors such as use of a follower load, specimen boundary conditions (constrained vs. unconstrained), and type of loading (discrete vs. continuous), can all affect the measured specimen performance. There are therefore two ways to proceed with future comparisons. FSUs can be tested with conditions replicating the work done by Busscher et al. [144]. The setup in this study is very similar to the current one, except that they did not use a follower load. Alternatively, a cadaveric study can be performed using the same test setup utilized in the current study. This work is currently underway, and will allow a direct comparison to human specimens. Overall, the researchers anticipate using both approaches, to check the validity of the ASM across conditions expected in multiple laboratories. Work is currently underway to resolve the discrepancies highlighted in this study, while maintaining the overall accuracy of the model.

Once this work has been completed, a synthetic analogue lumbar spine model will have been created satisfying the needs of the spine community. This model will exhibit anatomical and mechanical accuracy. It will also enable device fatigue testing studies, as it is not limited to a 20 hour testing window. Integration of a cancellous core and synthetic bone marrow will increase the accuracy of studies relying on cement intrusion, and failure of the bone-device interface. This model greatly reduces inter-specimen variance, and is much easier to test with as

it contains no hazardous biological material. Finally, this model can be rapidly manufactured, and researchers will not be subject to the long wait times currently imposed on them if they wish to test cadaveric material.

Table 36: Summary of FSU performance compared to the literature

Mode of testing	Property	Comparison to Literature Range
Flexion	NZ Stiffness	≈
	EZ Stiffness	≈
	NZ ROM	↑
Extension	NZ Stiffness	≈
	EZ Stiffness	↑
	NZ ROM	↑
Lateral Bending	NZ Stiffness	≈
	EZ Stiffness	≈
	NZ ROM	↑
Axial Rotation	NZ Stiffness	≈
	EZ Stiffness	≈
	NZ ROM	↑
↑ - Indicates spine model values are higher than the reported literature **≈ - Indicates spine model values are approximately equal to the literature**		

Chapter 4. – Conclusions and Future Work

4.1.Synthetic Cancellous Bone

The open-celled synthetic foam developed in this thesis serves as an acceptable model for human vertebral cancellous bone. An understanding of Foam Theory reveals the dependence of mechanical properties on a cellular solid's relative density. The density tested in this study possessed mechanical stiffness and strength slightly higher than values reported in the literature. By simply reducing the density of this model, these parameters will lowered into a more accurate physiological range. Furthermore, this change in density should have no effect on the model's yield or ultimate strain. The values for each of these parameters are slightly higher than the reported literature. However, strain in this study was determined by measuring the displacement of the loading platens, instead of using an extensometer, as is done in the literature. The use of an extensometer has been reported to record stiffer specimen performance, and should therefore decrease yield and ultimate strain values such that they are closer to the literature. As a result of these observations, it can be concluded that the model developed in this study, with slight density adjustments, will provide researchers with a useful synthetic model of human vertebral cancellous bone.

It is anticipated that reducing the foam's relative density will result in a model well within values reported in the literature. Once this initial change is validated, there are several smaller studies to be conducted. The first study, the effect of a synthetic bone marrow on model performance serves to increase overall anatomical accuracy of the model. Vertebral cancellous bone is surrounded by marrow in both young and old persons. This marrow can effect cement intrusion and also the stiffness and ductility of the bone it surrounds. As such, a synthetic marrow is currently being developed. Prior to utilizing this marrow in the ASM, its effects on

bone samples will be checked to ensure no degradation of material properties occurs over time. The remaining studies are all commonly performed on bone samples and synthetic models. The following studies need to be completed as further validation of the cancellous bone model:

- Effect of synthetic bone marrow on model performance
- Screw Pullout
- Screw toggle
- Cement intrusion
- Vertebral Body Compression

4.2.Analogue Spine Model

The Analogue Spine Model analyzed in this report shows great potential as a substitute for cadaveric testing in the near future. Work performed on the Analogue Spine Model located the sources of aberrant behavior in axial rotation, and overly stiff neutral zone performance in all modes of bending. One identified, the elements responsible were adjusted, resulting in a spine that exhibited the expected sigmoid behavior, and appropriate stiffness. A repeatability study showed that the model has accurate neutral zone stiffness in all modes of bending. Furthermore, it has accurate extension zone stiffness in flexion, lateral bending and axial rotation. Only extension possessed an extension zone stiffness higher than the reported literature. The main deficiency of this model was the size of its neutral zone. The neutral zone range of motion was two to three times too high in all modes of bending.

Several additional studies have already been planned that will help validate the spine model. Concurrent with work reducing the neutral zone range of motion, an in-depth cadaveric

study will be performed. This study will assess the intact properties of cadaveric FSUs, as well as the specimen's response to systematic dissections. This dissection procedure will be repeated on the ASM to guarantee not only intact performance, but that surgical alterations may be performed on the model while maintaining accuracy. Further work, including built in sensors will be conducted as the first stage of the second generation ASM. Future studies validating the ASM include work on:

- Neutral Zone Range of Motion
- Intact Cadaveric Study
- Effect of soft tissues on cadaveric and model stability
- IVD Pressure Sensor / facet force sensor
- Fatigue studies

References

1. Deyo, R.A. and J.N. Weinstein, *Low back pain.* N Engl J Med, 2001. **344**(5): p. 363-70.
2. *National Institute of Neurological Disorders and Stroke: Low Back Pain Fact Sheet*. 2003 12/21/2009 [cited 2009; Available from: http://www.ninds.nih.gov/disorders/backpain/detail_backpain.htm#toc.
3. *Medtech insight: US Markets for Spinal Fusion Products*. 2005 [cited 2010 1/5/2010]; Available from: http://www.medtechinsight.com/ReportA303.html.
4. Quality, A.f.H.R.a. *National and regional estimates on hospital use for all patients from the HCUP Nationwide Inpatient Sample (NIS)*. 2010 [cited 2011 2/2/2011]; Available from: http://hcupnet.ahrq.gov/HCUPnet.jsp?Id=5930513CE6F971DD&Form=SelLAY&JS=Y&Action=%3E%3ENext%3E%3E&_LAY=Researcher.
5. Menze, M. *Spine*. 2009 [cited 2010 4/8/2010]; Available from: http://www.pearldiverinc.com/pdi/spine.jsp.
6. Hangai, M., et al., *Factors associated with lumbar intervertebral disc degeneration in the elderly.* The Spine Journal, 2008. **8**: p. 732-40.
7. Vogt, M.T., et al., *Influence of Smoking on the Health Status of Spinal Patients.* Spine, 2002. **27**(3): p. 313-19.
8. Lorenz, M., A. Patwardhan, and R. Vanderby, *Load-bearing characteristics of lumbar facets in normal and surgically altered spinal segments.* Spine, 1982. **8**(2): p. 122-30.
9. Shirazi-Adl, A., *Load-bearing role of facets in a lumbar segment under sagittal plane loadings.* The Journal of Biomechanics, 1987. **20**(6): p. 601-13.
10. Kauppila, L.I., *Atherosclerosis and disc degeneration / low-back pain -- a systematic review.* European Journal of Vascular and Endovascular Surgery, 2009. **37**(6): p. 661-70.
11. Jhawar, B.S., et al., *Cardiovascular risk factors for physician-diagnosed lumbar disc hernation.* Spine, 2006. **6**: p. 684-91.
12. Ozkaya, N. and M. Nordin, *Fundamentals of Biomechanics: Equilibrium, Motion, and Deformation*. 2nd ed, ed. D.L. Leger1999, New York: Springer Science + Business Media. 393.
13. Spine, O.I.-. *Spinal Anatomy - Overview*. [cited 2011 2/3/2011]; Available from: http://www.oispine.com/subject.php?pn=spinal-anatomy-018.
14. Oda, I., et al., *An In Vitro Human Cadaveric Study Investigating the Biomechanical Properties of the Thoracic Spine.* Spine, 2002. **27**(3): p. E64-E70.
15. Wilke, H., K. Wenger, and L. Claes, *Testing criteria for spinal implants: recommendations for the standardization of in vitro stability testing of spinal implants.* European Spine Journal, 1998. **7**(2): p. 148-154.
16. Resnick, D.K., S.J. Weller, and E.C. Benzel, *Biomechanics of the thoracolumbar spine.* Neurosurgery clinics of North America, 1997. **8**(4): p. 455-69.

17. Leone, A., et al., *Lumbar intervertebral instability: A Review.* Radiology, 2007. **245**(1): p. 62-77.
18. Silva, M.J., et al., *Direct and computed tomography thickness measurements of the human, lumbar vertebral shell and endplate.* Bone, 1994. **15**: p. 409-14.
19. Ferguson, S.J. and T. Steffen, *Biomechanics of the aging spine.* Eur Spine J, 2003. **12**(Suppl. 2): p. 97 - 103.
20. Sharma, M., N.A. Langrana, and J. Rodriguez, *Role of Ligaments and Facets in Lumbar Spinal Stability.* Spine, 1995. **20**(8): p. 887-900.
21. Rissanen, P., *Comparison of pathologic changes in intervertebral discs and interspinous ligaments of the lower part of the lumbar spine in the light of autopsy findings.* Acta Orthopaedica, 1964. **34**(1): p. 54-65.
22. Adams, M., *Biomechanics of back pain.* Acupuncture in Medicine, 2004. **22**(4): p. 178.
23. Neumann, D.A., *Kinesiology of the Musculoskeletal System: Foundations for Rehabilitation*2010: Mosby/Elsevier.
24. Boeree, N., *The case for disc replacement.* Ann R Coll Surg Engl, 2007. **89**: p. 6-11.
25. Kelly, M.P., J.M. Mok, and S. Berven, *Dynamic Constructs for Spinal Fusion: An Evidence-Based Review.* Orthopedic Clinics of North America, 2010. **41**(2): p. 203-215.
26. Turner, J.A., et al., *Patient outcomes after lumbar spinal fusions.* JAMA, 1992. **268**: p. 907-11.
27. Goffin, J., et al., *Long-term follow-up after interbody fusion of the cervical spine.* J Spinal Disord Tech, 2004. **17**: p. 79-85.
28. Harrop, J.S., et al., *Lumbar adjacent segment degeneration and disease after arthrodesis and total disc arthroplasty.* Spine, 2008. **33**(15): p. 1701-07.
29. Khan, S.N. and A.J. Stirling, *The case against disc replacement.* Ann R Coll Surg Engl, 2007. **89**: p. 6-11.
30. Resnick, D.K. and W.C. Watters, *Lumbar disc arthroplasty: a critical review.* Clinical Neurosurgery, 2007. **54**: p. 83-7.
31. Huang, R.C., et al., *Advantages and Disadvantages of Nonfusion Technology in Spine Surgery.* Othrop Clin N Am2005. **36**: p. 263-69.
32. Eidelson, S.G. *Laminotomy versus Laminectomy*. 2002 [cited 2011 2/2/2011]; Available from: http://www.spineuniverse.com/treatments/surgery/laminotomy-versus-laminectomy.
33. Okawa, A., et al., *A Cadaveric Study on the Stability of Lumbar Segment After Partial Laminotomy and Facetectomy with Intact Posterior Ligaments.* J. Spin. Dis., 1996. **9**(6): p. 518-26.
34. Abitbol, J.J. *Kyphoplasty and Vertebroplasy: Treatments for Spinal Compression Fractures*. [cited 2011 2/2/2011]; Available from: http://www.spineuniverse.com/treatments/surgery/kyphoplasty-vertebroplasty-treatments-spinal.
35. Graham, J., et al., *Effect of bone density on vertebral strength and stiffness after percutaneous vertebroplasty.* Spine, 2007. **32**(18): p. E505.

36. Busscher, I., et al., *In Vitro Biomechanical Characteristics of the Spine: A Comparison Between Human and Porcine Spinal Segments.* Spine, 2010. **35**(2): p. E35-E42.
37. Wilke, H., et al., *Spinal segment range of motion as a function of in vitro test conditions: effects of exposure period, accumulated cycles, angular-deformation rate, and moisture condition.* The Anatomical Record Part A: Discoveries in Molecular, Cellular, and Evolutionary Biology, 1998. **251**(1): p. 15-19.
38. Anderson, A.L., et al., *The Effect of Posterior Thoracic Spine Anatomical Structures on Motion Segment Flexion Stiffness.* Spine, 2009. **34**(5): p. 441.
39. Hongo, M., et al., *Effect of multiple freeze-thaw cycles on intervertebral dynamic motion characteristics in the porcine lumbar spine.* J. Biomechanics, 2008. **41**: p. 916-20.
40. Sheaa, M., et al., *Variation of stiffness and strength along the human cervical spine.* Journal of Biomechanics, 1991. **24**(2): p. 95-107.
41. McLain, R.F., T.A. Moseley, and S.A. Yerby, *Comparative morphometry of L4 vertebrae: comparison of large animal models for the human lumbar spine.* Spine, 2002. **27**: p. E200-6.
42. Cunningham, B.W., et al., *The effect of spinal destabilization and instrumentation on lumbar intradiscal pressure: an in vitro biomechanical analysis.* Spine, 1997. **22**(22): p. pp. 2655 - 63.
43. Wilke, H.J., A. Kettler, and L.E. Claes, *Are sheep spines a valid biomechanical model for human spines?* Spine, 1997. **22**: p. 2365-74.
44. McAfee, P.C., I.D. Farey, and C.E. Sutterlin, *The biomechanical and histomorphometric properties of anterior lumbar fusions: a canine model.* J. Spinal Disord., 1988. **1**: p. 101-10.
45. Gurr, K.R., P.C. McAfee, and K.E. Warden, *Roentgenographic and biomechanical analysis of lumbar fusions: a canine model.* J. Orthop. Res., 1989. **7**: p. 838-48.
46. McAfee, P.C., I.D. Farey, and C.E. Sutterlin, *The effect of spinal implant rigidity on vertebral bone density: A canine model.* Spine, 1991. **16**: p. S190-7.
47. Wilke, H.J., S.T. Krischak, and K.H. Wenger *Load-displacement properties of the thoracolumbar calf spine: experimental results and comparison to known human data.* Eur. Spine J., 1997. **6**: p. 129-37.
48. Dath, R., A.D. Ebinesan, and K.M. Porter, *Anatomical measurements of porcine lumbar vertebrae.* Clin. Biomech., 2007. **22**: p. 607-13.
49. ASTM, F. *2077-03, Test Methods For Intervertebral Body Fusion Devices*.
50. Friis, E.A., et al., *Mechanical Analogue Model of the Human Lumbar Spine; Development and Evaluation*, in *Spinal implants: are we evaluating them appropriately?*, M. Melkerson, S. Griffith, and J. Kirkpatrick, Editors. 2003, Astm Intl: West Conshohoken, PA.
51. Chong, A., et al., *Fracture toughness and fatigue crack propagation rate of short fiber reinforced epoxy composites for analogue cortical bone.* Journal of Biomechanical Engineering, 2007. **129**: p. 487.
52. Palissery, V., M. Taylor, and M. Browne, *Fatigue characterization of a polymer foam to use as a cancellous bone analog material in the assessment of*

orthopaedic devices. Journal of Materials Science: Materials in Medicine, 2004. **15**(1): p. 61-67.
53. Johnson, A.E. and T.S. Keller, *Mechanical properties of open-cell foam synthetic thoracic vertebrae.* J. Mat. Sci.: Mat. Med., 2008. **19**: p. 1317-23.
54. Chen, L., et al., *Pullout strength for cannulated pedicle screws with bone cement augmentation in severely osteoporotic bone: Influences of radial hole and pilot hole tapping.* Clinical Biomechanics, 2009. **24**(8): p. 613-618.
55. Miller, F. and A. Johnson, *Artificial Bones and Methods of Making Same*, 2008, US Patent App. 20,090/216,327.
56. Friis, E.A., J. James, and A. Johnson, *Development and Validation of Instrumented Synthetic Mechanical Analogue Lumbar Spine Models*, NIH.
57. LaPierre, L., *Control of the Mechanical Properties of the Synthetic Anterior Longitudinal Ligament and its Effect on the Mechanical Analogue Lumbar Spine Model*, in *Department of Mechancial Engineering*2009, University of Kansas: Lawrence, KS. p. 152.
58. Hirsch, C., *The reaction of intervertebral discs to compression forces.* The Journal of Bone and Joint Surgery, 1955. **37**(6): p. 1188.
59. Markolf, K.L., *Deformation of the thoracolumbar intervertebral joints in response to external loads.* J. Bone and Joint Surg., 1972. **54A**: p. 511-33.
60. Cowin, S. and J. Telega, *Bone mechanics handbook.* Applied Mechanics Reviews, 2003. **56**: p. B61.
61. Keaveny, T. and W. Hayes, *A 20-year perspective on the mechanical properties of trabecular bone.* Journal of Biomechanical Engineering, 1993. **115**: p. 534.
62. Hollister, S.J. *Bone Structure*. BME/ME 456 Biomechanics 2011 [cited 2011 2/8/2011]; Available from: http://www.engin.umich.edu/class/bme456/bonestructure/bonestructure.htm.
63. Liebschner, M. and T. Keller, *Hydraulic strengthening affects the stiffness and strength of cortical bone.* Annals of Biomedical Engineering, 2005. **33**(1): p. 26-38.
64. Banse, X., T.J. Sims, and A.J. Bailey, *Mechanical properties of adult vertebral cancellous bone: correlation with collagen intermolecular cross-links.* Journal of Bone and Mineral Researrch, 2002. **17**(9): p. pp. 1621-28.
65. Rho, J.Y., L. Kuhn-Spearing, and P. Zioupos, *Mechanical properties and the hierarchical structure of bone.* Medical Engineering & Physics, 1998. **20**(2): p. 92-102.
66. Smit, T., A. Odgaard, and E. Schneider, *Structure and function of vertebral trabecular bone.* Spine, 1997. **22**(24): p. 2823.
67. Schluter, K., *Form and structure of normal and pathological vertebra.* The spine in Research and Practice, 1965. **30**.
68. Goldstein, S., *The mechanical properties of trabecular bone: dependence on anatomic location and function.* Journal of Biomechanics, 1987. **20**(11-12): p. 1055-1061.
69. Morgan, E. and T. Keaveny, *Dependence of yield strain of human trabecular bone on anatomic site.* Journal of Biomechanics, 2001. **34**(5): p. 569.

70. Badiei, A., M. Bottema, and N. Fazzalari, *Influence of orthogonal overload on human vertebral trabecular bone mechanical properties.* Journal of Bone and Mineral Research, 2007. **22**(11): p. 1690-1699.
71. Mosekilde, L., *Age-related changes in bone mass, structure, and strength-effects of loading.* Zeitschrift für Rheumatologie, 2000. **59**(7): p. 1-9.
72. Mosekilde, L., L. Mosekilde, and C.C. Danielsen, *Biomechanical competence of vertebral trabecular bone in relation to ash density and age in normal individuals.* Bone, 1987. **8**(2): p. 79-85.
73. Mazess, R.B., *On aging bone loss.* Clin Orthop, 1982: p. 239-52.
74. Ochia, R. and R. Ching, *Hydraulic resistance and permeability in human lumbar vertebral bodies.* Journal of Biomechanical Engineering, 2002. **124**: p. 533.
75. Ochia, R.S. and R.P. Ching, *Rate Dependence of Hydraulic Resistance in Human Lumbar Vertebral Bodies.* Spine, 2006. **31**(22): p. 2569.
76. Hong, J.H. and S.H. Song, *Poroelastic behavior of trabecular bone: The effect of strain rate.* Journal of Mechanical Science and Technology, 1998. **12**(3): p. 421-428.
77. Hwa, H.J., *Could the intraosseous fluid in cancellous bone bear external load significantly within the elastic range?* Proceedings of the Institution of Mechanical Engineers, Part H: Journal of Engineering in Medicine, 2004. **218**(6): p. 375-379.
78. Klippel, J.H., *Osteoporosis - Pathology and Pathophysiology*, in *Primer on the rheumatic diseases*2008, Springer Verlag.
79. Hernandez, C. and T. Keaveny, *A biomechanical perspective on bone quality.* Bone, 2006. **39**(6): p. 1173-1181.
80. Tzelepi, V., et al., *Bone Anatomy, Physiology and Function.* Bone Metastases, 2009: p. 3-30.
81. Groen, G.J., B. Baljet, and J. Drukker, *Nerves and nerve plexuses of the human vertebral column.* American journal of anatomy, 1990. **188**(3): p. 282-296.
82. Bogduk, N., W. Tynan, and A. Wilson, *The nerve supply to the human lumbar intervertebral discs.* Journal of Anatomy, 1981. **132**(Pt 1): p. 39.
83. BOGDUK, N., *The innervation of the lumbar spine.* Spine, 1983. **8**(3): p. 286.
84. Edgar, M. and J. Ghadially, *Innervation of the lumbar spine.* Clinical Orthopaedics and Related Research, 1976. **115**: p. 35.
85. Jackson, H.C., *Nerve endings in the human lumbar spinal column and related structures.* The Journal of Bone and Joint Surgery, 1966. **48**(7): p. 1272.
86. Hurrell, D.J., *The nerve supply of bone.* Journal of Anatomy, 1937. **72**(Pt 1): p. 54.
87. Khurana, J.S. and F.F. Safadi, *Bone Structure, Development and Bone Biology.* Essentials in Bone and Soft-Tissue Pathology, 2010: p. 1-15.
88. Hirsch, C., B.E. Ingelmark, and M. Miller, *The anatomical basis for low back pain: Studies on the presence of sensory nerve endings in ligamentous, capsular and intervertebral disc structures in the human lumbar spine.* Acta Orthopaedica, 1963. **33**(1-4): p. 1-17.
89. Antonacci, M.D., D.R. Mody, and M.H. Heggeness, *Innervation of the human vertebral body: a histologic study.* Journal of Spinal Disorders & Techniques, 1998. **11**(6): p. 526.

90. Rice, J., S. Cowin, and J. Bowman, *On the dependence of the elasticity and strength of cancellous bone on apparent density.* Journal of Biomechanics, 1988. **21**(2): p. 155-168.
91. McBroom, R.J., et al., *Prediction of vertebral body compressive fracture using quantitative computed tomography.* J Bone and Joint Surg Am, 1985. **67**: p. 1206-1214.
92. Neumann, P., et al., *Aging, vertebral density, and disc degeneration alter the tensile stress-strain characteristics of the human anterior longitudinal ligament.* J Orthop Res, 1994. **12**: p. 103-12.
93. Gibson, L.J., *Biomechanics of cellular solids.* Journal of Biomechanics, 2005. **38**(3): p. 377-399.
94. Carter, D.R. and W.C. Hayes, *The compressive behavior of bone as a two-phase porous structure.* The Journal of Bone and Joint Surgery, 1977. **59**(7): p. 954.
95. Keaveny, T.M., et al., *Trabecular bone exhibits fully linear elastic behavior and yields at low strains.* Journal of Biomechanics, 1994. **27**(9): p. 1127-1129.
96. Gibson, L.J. and M.F. Ashby, *Cellular Solids: Stucture and Properties*. 1st ed1988, New York: Pergamon Press. 357.
97. Linde, F., I. Hvid, and F. Madsen, *The effect of specimen geometry on the mechanical behaviour of trabecular bone specimens.* Journal of Biomechanics, 1992. **25**(4): p. 359-368.
98. Kopperdahl, D.L. and T.M. Keaveny, *Yield strain behavior of trabecular bone.* Journal of Biomechanics, 1998. **31**: p. pp. 601-08.
99. Linde, F. and I. Hvid, *The effect of constraint on the mechanical behaviour of trabecular bone specimens.* Journal of Biomechanics, 1989. **22**(5): p. 485-490.
100. Linde, F. and I. Hvid, *Stiffness behaviour of trabecular bone specimens.* Journal of Biomechanics, 1987. **20**(1): p. 83-89.
101. Grote, H., et al., *Intervertebral variation in trabecular microarchitecture throughout the normal spine in relation to age.* Bone, 1995. **16**(3): p. 301-308.
102. Hou, F.J., et al., *Human vertebral body apparent and hard tissue stiffness.* Journal of Biomechanics, 1998. **31**(11): p. 1009.
103. Heaney, R., *The natural history of vertebral osteoporosis. Is low bone mass an epiphenomenon?* Bone, 1992. **13**: p. S23-S26.
104. Lindahl, O., *Mechanical properties of dried defatted spongy bone.* Acta Orthopaedica, 1976. **47**(1): p. 11-19.
105. Keaveny, T.M., et al., *Trabecular bone modulus and strength can depend on specimen geometry.* Journal of Biomechanics, 1993. **26**(8): p. 991-995.
106. Keller, T.S., *Predicting the compressive mechanical behavior of bone.* Journal of Biomechanics, 1994. **27**(9): p. 1159-1168.
107. T.H., H., T.S. Keller, and M.M. Panjabi, *A study of the compressive properties of lumbar vertebral trabeculae: effects of tissue characteristics.* Spine, 1987. **12**(1): p. 56.
108. McCalden, R.W. and J.A. McGeough, *Age-related changes in the compressive strength of cancellous bone. The relative importance of changes in density and trabecular architecture.* The Journal of Bone and Joint Surgery, 1997. **79**(3): p. 421.

109. Chalmers, J. and J. Weaver, *Cancellous Bone: Its Strength and Changes with Aging and an Evaluation of Some Methods for Measuring Its Mineral Content: II. An evaluation of some methods for measureing osteoporosis.* The Journal of Bone and Joint Surgery, 1966. **48**(2): p. 299.
110. Weaver, J. and J. Chalmers, *Cancellous bone: its strength and changes with aging and an evaluation of some methods for measuring its mineral content: I. Age changes in cancellous bone.* The Journal of Bone and Joint Surgery, 1966. **48**(2): p. 289.
111. Keaveny, T.M., et al., *Systematic and random errors in compression testing of trabecular bone.* Journal of Orthopaedic Research, 1997. **15**(1): p. 101-110.
112. Keaveny, T.M., et al., *Theoretical analysis of the experimental artifact in trabecular bone compressive modulus.* Journal of Biomechanics, 1993. **26**(4-5): p. 599-607.
113. Linde, F. and H. Sørensen, *The effect of different storage methods on the mechanical properties of trabecular bone.* Journal of Biomechanics, 1993. **26**(10): p. 1249-1252.
114. Gibson, L.J., *The mechanical behaviour of cancellous bone.* Journal of Biomechanics, 1985. **18**(5): p. 317-328.
115. Nazarian, A. and R. Müller, *Time-lapsed microstructural imaging of bone failure behavior.* Journal of Biomechanics, 2004. **37**(1): p. 55-65.
116. Müller, R. and G. Harry van Lenthe, *Trabecular bone failure at the microstructural level.* Current osteoporosis reports, 2006. **4**(2): p. 80-86.
117. Birnbaum, K., et al., *Material properties of trabecular bone structures.* Surgical and Radiologic Anatomy, 2002. **23**(6): p. 399-407.
118. Ciarelli, M., et al., *Evaluation of orthogonal mechanical properties and density of human trabecular bone from the major metaphyseal regions with materials testing and computed tomography.* Journal of Orthopaedic Research, 1991. **9**(5): p. 674-682.
119. ASTM, *Standard Test Method for Flexural Properties of Unreinforced and Reinforced Plastics and Electrical Insulating Materials by Four-Point Bending*, 2008. p. 1 - 9.
120. Johnson, A. and J. James, *Composite Open-Cell Rigid Foam*, 2011, Pacific Research Laboratories: Vashon.
121. Roofe, P.G., *Innervation of annulus fibrosus and posterior longitudinal ligament: fourth and fifth lumbar level.* Archives of Neurology & Psychiatry, 1940. **44**(1): p. 100.
122. Center, N.Y.U.H.f.J.D.S. *Spinal Motion*. 2011 [cited 2011 4/25/2011]; Available from: http://hjd.med.nyu.edu/spine/patient-education/spine-anatomy/spinal-motion.
123. Wilke, H.J., et al., *Is It Possible to Simulate Physiologic Loading Conditions by Applying Pure Moments?: A Comparison of In Vivo and In Vitro Load Components in an Internal Fixator.* Spine, 2001. **26**(6): p. 636.
124. Nachemson, A. and J.M. MORRIS, *In vivo measurements of intradiscal pressure: Discometry, a method for the determination of pressure in the lower lumbar discs.* The Journal of Bone and Joint Surgery, 1964. **46**(5): p. 1077.

125. Wilke, H.J., et al., *New in vivo measurements of pressures in the intervertebral disc in daily life.* Spine, 1999. **24**(8): p. 755.
126. Cappozzo, A., *Compressive loads in the lumbar vertebral column during normal level walking.* Journal of Orthopaedic Research, 1983. **1**(3): p. 292-301.
127. Mimura, M., et al., *Disc degeneration affects the multidirectional flexibility of the lumbar spine.* Spine, 1994. **19**(12): p. 1371.
128. Kim, Y.M., et al., *Nonfusion Method in Thoracolumbar and Lumbar Spinal Fractures.* Spine, 2010.
129. Dvorak, J., et al., *Functional radiographic diagnosis of the lumbar spine: flexion-extension and lateral bending.* Spine, 1991. **16**(5): p. 562.
130. McGregor, A.H., I.D. McCarthy, and S.P. Hughes, *Motion characteristics of the lumbar spine in the normal population.* Spine, 1995. **20**(22): p. 2421.
131. Gleizes, V., et al., *Effects of freezing on the biomechanics of the intervertebral disc.* Surgical and Radiologic Anatomy, 1998. **20**(6): p. 403-407.
132. Hirsch, C. and J. Galante, *Laboratory conditions for tensile tests in annulus fibrosus from human intervertebral discs.* Acta Orthopaedica, 1967. **38**(1): p. 148-162.
133. Smeathers, J. and D. Joanes, *Dynamic compressive properties of human lumbar intervertebral joints: a comparison between fresh and thawed specimens.* Journal of Biomechanics, 1988. **21**(5): p. 425-433.
134. Smith, C., I. Young, and J. Kearney, *Mechanical properties of tendons: changes with sterilization and preservation.* Journal of Biomechanical Engineering, 1996. **118**: p. 56.
135. Woo, S., et al., *Effects of postmortem storage by freezing on ligament tensile behavior.* Journal of Biomechanics, 1986. **19**(5): p. 399-404.
136. Kettler, A., et al., *Effects of specimen length on the monosegmental motion behavior of the lumbar spine.* Spine, 2000. **25**(5): p. 543.
137. Dickey, J. and D. Kerr, *Effect of specimen length: are the mechanics of individual motion segments comparable in functional spinal units and multisegment specimens?* Medical Engineering & Physics, 2003. **25**(3): p. 221-227.
138. Guan, Y., et al., *Moment-rotation responses of the human lumbosacral spinal column.* Journal of Biomechanics, 2007. **40**(9): p. 1975-1980.
139. Panjabi, M., et al., *Mechanical behavior of the human lumbar and lumbosacral spine as shown by three-dimensional load-displacement curves.* The Journal of Bone and Joint Surgery, 1994. **76**(3): p. 413.
140. Yamamoto, I., et al., *Three-dimensional movements of the whole lumbar spine and lumbosacral joint.* Spine, 1989. **14**(11): p. 1256.
141. Adams, M.A., W.C. Hutton, and J.R.R. Stott, *The resistance to flexion of the lumbar intervertebral joint.* Spine, 1980. **5**: p. 245-53.
142. Burton, D., et al., *Biomechanical Analysis of Posterior Fixation Techniques in a 360 [degrees] Arthrodesis Model.* Spine, 2005. **30**(24): p. 2765.
143. Goel, V., et al., *Kinematics of the whole lumbar spine: effect of discectomy.* Spine, 1985. **10**(6): p. 543.

144. Busscher, I., et al., *Biomechanical Characteristics of Different Regions of the Human Spine: An In Vitro Study on Multilevel Spinal Segments.* Spine, 2009. **34**(26): p. 2858.
145. Lu, W.W., et al., *Stability of the whole lumbar spine after multilevel fenestration and discectomy.* Spine, 1999. **24**(13): p. pp. 1277.
146. Schmidt, T., et al., *The stiffness of lumbar spinal motion segments with a high-intensity zone in the anulus fibrosus.* Spine, 1998. **23**(20): p. 2167-2173.
147. Goel, V.K., et al., *Mechanical properties of lumbar spinal motion segments as affected by partial disc removal.* Spine, 1986. **11**(10): p. 1008.
148. Eysel, P., et al., *Multi-segment ventral stabilization of the lumbar spine: a comparative biomechanical study.* Zeitschrift fÃžr OrthopÃ die und ihre Grenzgebiete. **133**(3): p. 242.
149. Balabaud, L., et al., *Biomechanical evaluation of a bipedicular spinal fixation system: a comparative stiffness test.* Spine, 2002. **27**(17): p. 1875.
150. Panjabi, M., et al. *Helical axes of motion change with lumbar vertebral level*. 1991.
151. Charles, Y.P., et al., *Influence of an Auxiliary Facet System on Lumbar Spine Biomechanics.* Spine, 2010.
152. Heuer, F., et al., *Stepwise reduction of functional spinal structures increase range of motion and change lordosis angle.* Journal of Biomechanics, 2007. **40**(2): p. 271-280.
153. Schultz, A., et al., *Mechanical Properties of Human Lumbar Spine Motion Segments Part I: Responses in Flexion, Extension, Lateral Bending and Torsion.* Journal of Biomechanical Engineering, 1979. **101**(1): p. 46-52.
154. Panjabi, M.P., V.K. Goel, and K. Takata, *Physiologic strains in the lumbar spinal ligaments.* Spine, 1982. **7**: p. 192-203.
155. Asano, S., et al., *The mechanical properties of the human L4-L5 functional spinal unit during cyclic loading: The structural effects of the posterior elements.* Spine, 1992. **17**(11): p. 1343-52.
156. Grassmann, S., et al., *Constrained testing conditions affect the axial rotation response of lumbar functional spinal units.* Spine, 1998. **23**(10): p. 1155.
157. Charriere, E., et al., *Compliance of the L5-S1 spinal unit: a comparative study between an unconstrained and a partially constrained system.* European Spine Journal, 2006. **15**(1): p. 74-81.
158. Brown, T., R.J. HANSEN, and A.J. YORRA, *Some mechanical tests on the lumbosacral spine with particular reference to the intervertebral discs: a preliminary report.* The Journal of Bone and Joint Surgery, 1957. **39**(5): p. 1135.
159. Farfan, H.F., et al., *The Effects of Torsion on the Lumbar Intervertebral Joints: The Role of Torsion in the Production of Disc Degeneration.* JB&JS, 1970. **52-A**(3): p. 468-97.
160. Gardner-Morse, M.G. and I.A.F. Stokes, *Structural behavior of human lumbar spinal motion segments.* Journal of Biomechanics, 2004. **37**(2): p. 205-212.
161. Goel, V.K., et al., *Controversy Biomechanical Testing of the Spine: Load-Controlled Versus Displacement-Controlled Analysis.* Spine, 1995. **20**(21): p. 2354.

162. Tian, L. and L.G. Gilbertson, *The study of control methods for the robotic testing system for human musculoskeletal joints.* Computer methods and programs in biomedicine, 2004. **74**(3): p. 211-220.
163. Rohlmann, A., et al., *Influence of a follower load on intradiscal pressure and intersegmental rotation of the lumbar spine.* Spine, 2001. **26**(24): p. E557.
164. Stokes, I.A.F. and M. Gardner-Morse, *Spinal stiffness increases with axial load: another stabilizing consequence of muscle action.* Journal of Electromyography and Kinesiology, 2003. **13**(4): p. 397-402.
165. Tawackoli, W., R. Marco, and M.A.K. Liebschner, *The effect of compressive axial preload on the flexibility of the thoracolumbar spine.* Spine, 2004. **29**(9): p. 988.
166. Patwardhan, A., K.P. Meade, and B. Lee, *A frontal plane model of the lumbar spine subjected to a follower load: implications for the role of muscles.* Journal of Biomechanical Engineering, 2001. **123**: p. 212.
167. Janevic, J., J. Ashton Miller, and A. Schultz, *Large compressive preloads decrease lumbar motion segment flexibility.* Journal of Orthopaedic Research, 1991. **9**(2): p. 228-236.
168. Gardner-Morse, M.G. and I.A. Stokes, *Physiological axial compressive preloads increase motion segment stiffness, linearity and hysteresis in all six degrees of freedom for small displacements about the neutral posture.* Journal of Orthopaedic Research, 2003. **21**(3): p. 547-552.
169. Edwards, W., et al., *Variation of lumbar spine stiffness with load.* Journal of Biomechanical Engineering, 1987. **109**: p. 35.
170. Hutton, W. and M. Adams, *Can the lumbar spine be crushed in heavy lifting?* Spine, 1982. **7**(6): p. 586.
171. Adams, M., et al., *Posture and the compressive strength of the lumbar spine.* Journal of Biomechanics, 1994. **27**(6): p. 791.
172. Porter, R., M. Adams, and W. Hutton, *Physical activity and the strength of the lumbar spine.* Spine, 1989. **14**(2): p. 201.
173. Wilke, H.J., et al., *Stability increase of the lumbar spine with different muscle groups: a biomechanical in vitro study.* Spine, 1995. **20**(2): p. 192.
174. Panjabi, M., *The stabilizing system of the spine. Part II. Neutral zone and instability hypothesis.* Journal of Spinal Disorders & Techniques, 1992. **5**(4): p. 390.

Appendix A: Foam Testing ANOVA Tables

Table 37: Multi-variate ANOVA comparing material properties across the days each block was manufactured

ANOVA

		Sum of Squares	df	Mean Square	F	Sig.
Density	Between Groups	.002	2	.001	.580	.568
	Within Groups	.033	24	.001		
	Total	.035	26			
RelativeDensity	Between Groups	.001	2	.000	.580	.568
	Within Groups	.015	24	.001		
	Total	.016	26			
Modulus	Between Groups	4564.376	2	2282.188	.752	.482
	Within Groups	72879.889	24	3036.662		
	Total	77444.265	26			
YieldStress	Between Groups	.224	2	.112	.281	.758
	Within Groups	9.580	24	.399		
	Total	9.805	26			
YieldStrain	Between Groups	.149	2	.074	1.116	.344
	Within Groups	1.597	24	.067		
	Total	1.746	26			
UltStress	Between Groups	.784	2	.392	.839	.445
	Within Groups	11.219	24	.467		
	Total	12.003	26			
UltStrain	Between Groups	.566	2	.283	5.384	.012
	Within Groups	1.261	24	.053		
	Total	1.826	26			
PostYldDuctility	Between Groups	.226	2	.113	5.393	.012
	Within Groups	.502	24	.021		
	Total	.728	26			

Table 38: Multi-variate ANOVA comparing material properties across specimen location

ANOVA

		Sum of Squares	df	Mean Square	F	Sig.
Density	Between Groups	.006	5	.001	.868	.519
	Within Groups	.029	21	.001		
	Total	.035	26			
RelativeDensity	Between Groups	.003	5	.001	.868	.519
	Within Groups	.013	21	.001		
	Total	.016	26			
Modulus	Between Groups	21983.816	5	4396.763	1.665	.187
	Within Groups	55460.449	21	2640.974		
	Total	77444.265	26			
YieldStress	Between Groups	2.653	5	.531	1.558	.215
	Within Groups	7.151	21	.341		
	Total	9.805	26			
YieldStrain	Between Groups	.372	5	.074	1.138	.371
	Within Groups	1.373	21	.065		
	Total	1.746	26			
UltStress	Between Groups	3.640	5	.728	1.828	.151
	Within Groups	8.363	21	.398		
	Total	12.003	26			
UltStrain	Between Groups	.124	5	.025	.306	.904
	Within Groups	1.702	21	.081		
	Total	1.826	26			
PostYldDuctility	Between Groups	.085	5	.017	.556	.733
	Within Groups	.643	21	.031		
	Total	.728	26			

Table 39: ANOVA Comparing synthetic open-cell foam to human vertebral cancellous bone reported in the literature - Modulus of Elasticity - E (MPa)

Source of Variation	SS	df	MS	F	P-value	F crit
Between Groups	93079.7	3	31026.6	1.9	0.14	2.7
Within Groups	2284359.3	138	16553.3			
cf	16941720.4					
Total	2377438.9	141				

Table 40: ANOVA Comparing synthetic open-cell foam to human vertebral cancellous bone reported in the literature - σ_{yield} (MPa)

Source of Variation	SS	df	MS	F	P-value	F crit
Between Groups	59.9	2.0	30.0	46.3	0.00	3.1
Within Groups	49.2	76.0	0.6			
cf	536.0					
Total	109.1	78.0				

Table 41: ANOVA Comparing synthetic open-cell foam to human vertebral cancellous bone reported in the literature –Corrected ε_{yield}

Source of Variation	SS	df	MS	F	P-value	F crit
Between Groups	0.019%	2.0	0.0	132.2	0.00	3.1
Within Groups	0.005%	76.0	0.0			
cf	0.652%					
Total	0.024%	78.0				

Table 42: ANOVA Comparing synthetic open-cell foam to human vertebral cancellous bone reported in the literature - σ_{ult} (MPa)

Source of Variation	SS	df	MS	F	P-value	F crit
Between Groups	82.3	2	41.1	40.2	0.00	3.1
Within Groups	111.5	109	1.0			
cf	888.0					
Total	193.8	111				

Table 43: ANOVA Comparing synthetic open-cell foam to human vertebral cancellous bone reported in the literature -Corrected ε_{ult}

Source of Variation	SS	df	MS	F	P-value	F crit
Between Groups	0.00%	1	0.004%	5.3	0.03	4.0
Within Groups	0.03%	47	0.001%			
cf	1.17%					
Total	0.04%	48				

Table 44: ANOVA Comparing synthetic open-cell foam to human vertebral cancellous bone reported in the literature - Post Yield Ductility - ε_{ult} - ε_{yield}

Source of Variation	SS	df	MS	F	P-value	F crit
Between Groups	0.00%	1	0.001%	2.0	0.16	4.0
Within Groups	0.03%	47	0.001%			
cf	0.15%					
Total	0.03%	48				